Stochastic Neural Field Models of Binocular Rivalry Waves

Matthew Alexander Webber

The Queen's College

University of Oxford

A thesis submitted for the degree of

Doctor of Philosophy

Trinity 2013

Abstract

Binocular rivalry is an interesting phenomenon where perception oscillates between different images presented to the two eyes. This thesis is primarily concerned with modelling travelling waves of visual perception during transitions between these perceptual states. In order to model this effect in such a way that we retain as much analytical insight into the mechanisms as possible we employed neural field theory. That is, rather than modelling individual neurons in a neural network we treat the cortical surface as a continuous medium and establish integro-differential equations for the activity of a neural population.

Our basic model which has been used by many previous authors both within and outside of neural field theory is to consider a one dimensional network of neurons for each eye. It is assumed that each network responds maximally to a particular feature of the underlying image, such as orientation. Recurrent connections within each network are taken to be excitatory and connections between the networks are taken to be inhibitory. In order for such a topology to exhibit the oscillations found in binocular rivalry there needs to be some form of slow adaptation which weakens the cross-connections under continued firing. By first considering a deterministic version of this model, we will show that, in fact, this slow adaptation also serves as a necessary "symmetry breaking" mechanism. Using this knowledge to make some mild assumptions we are then able to derive an expression for the shape of a travelling wave and its wave speed. We then go on to show that these predictions of our model are consistent not only with numerical simulations but also experimental evidence.

It will turn out that it is not acceptable to completely ignore noise as it is a fundamental part of the underlying biology. Since methods for analyzing stochastic neural fields did not exist before our work, we first adapt methods originally intended for reaction-diffusion PDE systems to a stochastic version of a simple neural field equation. By regarding the motion of a stochastic travelling wave as being made up of two distinct components, firstly, the drift-diffusion of its overall position, secondly, fast fluctuations in its shape

around some average front shape, we are able to derive a stochastic differential equation for the front position with respect to time. It is found that the front position undergoes a drift-diffusion process with constant coefficients. We then go on to show that our analysis agrees with numerical simulation. The original problem of stochastic binocular rivalry is then re-visited with this new toolkit and we are able to predict that the first passage time of a perceptual wave hitting a fixed barrier should be an inverse Gaussian distribution, a result which could potentially be experimentally tested.

We also consider the implications of our stochastic work on different types of neural field equation to those used for modelling binocular rivalry. In particular, for neural fields which support pulled fronts propagating into an unstable state, the stochastic version of such an equation has wave fronts which undergo subdiffusive motion as opposed to the standard diffusion in the binocular rivalry case.

Acknowledgements

I would like to begin by thanking my supervisor Paul Bressloff for his continued suggestions, advice, help, and support. I would also like to thank the Systems Biology Doctoral Training Centre, the EPSRC and OCCAM for their financial support throughout my DPhil. I would like to thank Alain Goriely for making formal matters run smoothly.

I thank my parents for their kindness, generosity and support. I also thank George Rowlands for his encouragement and many interesting discussions during my time as an undergraduate.

Statement of Originality

The original work contained in this thesis has already been published in papers co-authored by myself and Paul Bressloff [16, 17, 80]. For clarity this section contains specific information on how the work was divided between the two authors. Paul proposed the initial ideas and provided direction throughout the project. All simulations were coded and run by myself. The vast majority of theoretical results were first derived by myself, then checked by Paul. Once we were satisfied we had interesting results to publish, a first draft of a paper would be produced by myself and sent to Paul. The final version of the papers is then the result of several back-and-forth edits by the two authors.

Contents

List of Figures

Chapter 1

Introduction

Binocular rivalry is the phenomenon whereby perception switches back and forth between different images presented to the two eyes [8]. A superposition of the two different images is generally not seen provided they are sufficiently different, that is, the two images appear to compete for perceptual dominance. It is somewhat unique [8] compared to other phenomena in that it provides a basis for non-invasive experimentation, in most individuals, of some of the mechanisms underlying conscious visual awareness. It is thought that the neural mechanisms underlying binocular rivalry are related to effects, such as the oscillations caused by ambiguous figures[1], occurring in high level cortices of the brain which are currently poorly understood. As such it is possible that understanding binocular rivalry would have wider implications for the understanding of the macroscopic functioning of the human brain as a whole.

Though the majority of the time a single stimulus is dominant where it remains for a few seconds before a switch occurs the transition itself is not instantaneous. This transition takes the form of a travelling wave of visual perception and there have been several experimental studies confirming this in detail [81, 45, 44]. This work focuses on modelling travelling waves during binocular rivalry using a continuum field approach known as Neural Field Theory. Though previous studies have computationally examined neural network models of binocular rivalry, including the propagation of waves [81, 50], the approach used here offers several advantages. It is often possible to derive analytical solutions giving greater insights into the mechanisms underlying binocular rivalry and in the stochastic case providing general predictions of how systems should behave. In section 1.1 the experimental basis for binocular rivalry waves along with key differential equation models for the

[1] In the case of ambiguous figures this is due to the fact that the two phenomena share similar distributions of dominance times.

perceptual oscillations will be presented, section 1.2 introduces neural field theory along with the key mathematical techniques and assumptions, and finally section 1.3 provides an informal introduction to the stochastic calculus which will be necessary for much of this work.

1.1 Binocular Rivalry Waves

Before presenting the experimental evidence and network models of binocular rivalry, the functional architecture of the primary visual cortex (V1), thought to be the primary substrate of binocular rivalry, will be briefly explained.

1.1.1 Neural Basis of Binocular Rivalry

There is substantial experimental evidence that binocular rivalry occurs primarily in V1. By choosing images as rival stimuli which are processed in different areas of the brain (such as a house and a face) it has been shown that the suppressed stimulus produces little activity in its corresponding area of the brain, only the dominant stimulus evokes activity [74]. Furthermore both fMRI [73, 62, 49] and single neuron [51] approaches have shown substantial activity in the V1 cortex during the transition between rivalrous states. Though there are unresolved issues involving feedback to V1 from higher cortices it is generally agreed that V1 is very important for binocular rivalry. This evidence along with the fact that the psychophysical experiments considered in this work only involve oriented gratings (V1 responds strongly to sharp edges) fixes the focus on V1.

In order to motivate a model some of the properties of neurons in V1 [41, 42] will be reviewed. V1 is the first cortical area that images from the retina reach after passing through the lateral geniculate nucleus (LGN), which serves to relay information from the retina. V1 is split across the left and right hemispheres (see Fig. 1.1) such that the right half of the visual field is transmitted to the left hemisphere and the left half of the visual field is transmitted to the right hemisphere, with half of the information originating in each eye. The cortical surface of V1 is functionally two-dimensional with the third dimension providing redundancy. Neurons which are all performing a similar function can be regarded as a single unit known in the literature as a column. Most neurons in V1 respond preferentially to stimuli targeting either the left or right eye, which is known as *ocular dominance* and it has been suggested that neurons with different ocular dominance may inhibit one another if they have nearby receptive fields [46]. The exact mapping of image to cortex is known as the Retinotopic map (see Fig. 1.2), though for our purposes since we are only considering linear images in the centre of vision the map is trivial (linear) for our application, though it is useful to note

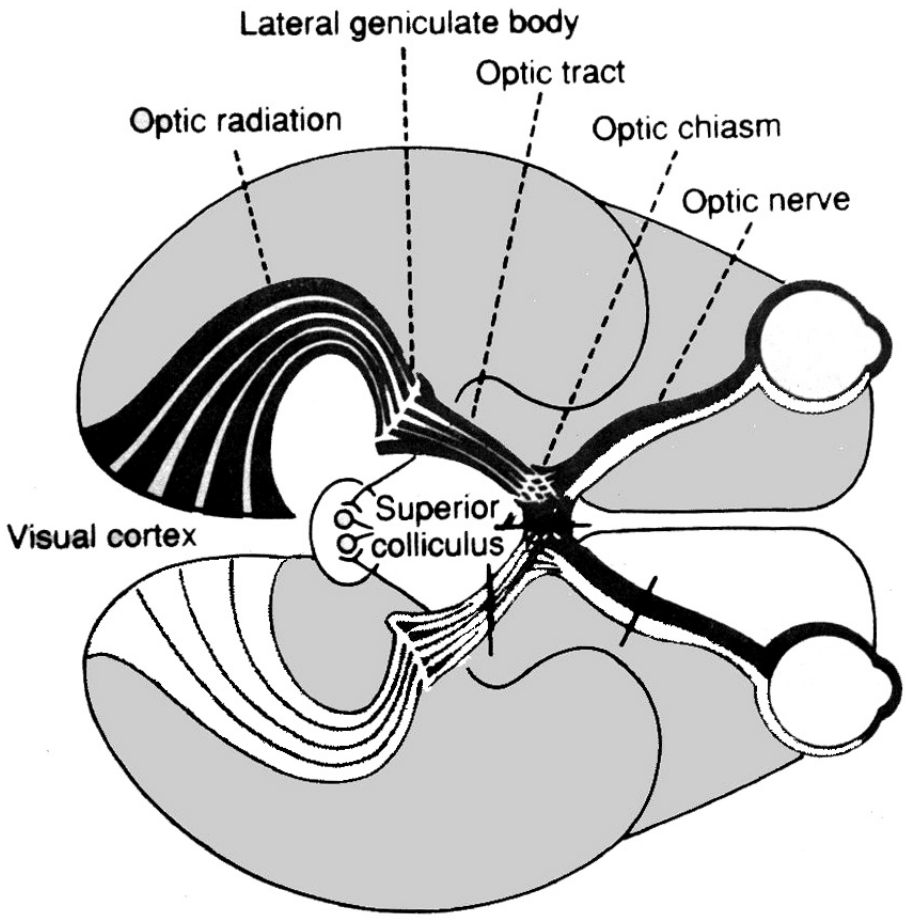

Figure 1.1: Schematic showing the path visual information from each eye takes while it is transmitted to the visual cortex (V1). The lateral geniculate nucleus serves as a relay for information from the retina. Figure is an adaptation from the original shown in [42]

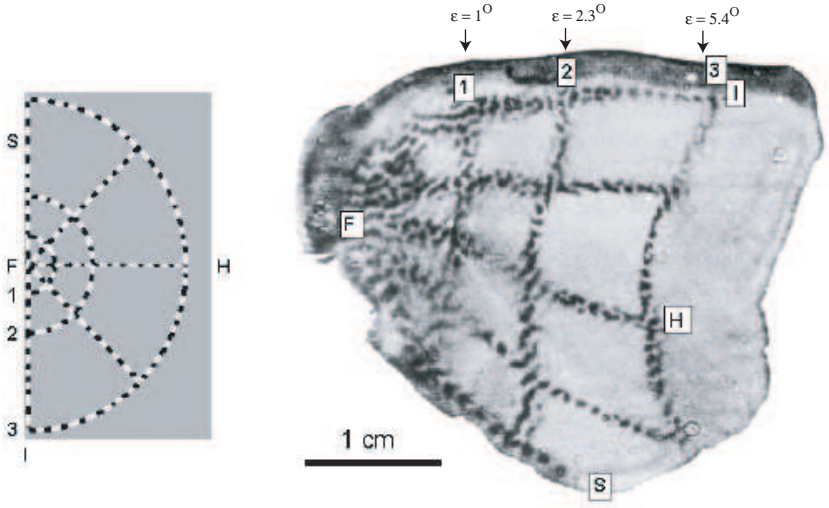

Figure 1.2: Shown to the right is an autoradiogram of the left visual cortex of a macaque shortly after being shown the image to the left. Radioactive tracer shows areas of high activity as darker regions. As can be seen, concentric circles are mapped to vertical lines and radial lines are mapped to horizontal lines (approximately). For this project the key fact is that neighbouring regions of an image invoke activity in neighbouring regions of V1 and we do not have to worry about the explicit form of the retinotopic map since we are considering linear images close to the centre of the visual field. Redrawn from [75]

that neurons with similar receptive fields are physically located near each other. Each neuron in V1 responds to light stimuli in a restricted region of the visual field called its *classical receptive field*; stimuli outside a neuron's receptive field do not directly affect its activity. These regions are usually rectangular in shape so that a neuron responds maximally to a particular orientation (see Fig. 1.3), this is known as a neuron's *orientation preference*, and the neuron will not respond if a stimulus is sufficiently different from its preferred orientation. Multielectrode recordings and optical imaging have established that for each point in the visual field there exists a corresponding set of neural columns spanning the entire spectrum of orientation preferences that are packed together as a unit in V1, known as a *hypercolumn* (see Fig. 1.4) [9, 76, 42]. Within each hypercolumn, neurons with sufficiently similar orientations tend to excite each other whereas those with sufficiently different orientations inhibit each other, and this serves to sharpen a particular neuron's orientation preference [6, 34]. Moreover, anatomical evidence suggests that inter-hypercolumn connections link neurons with similar orientation preferences [69, 3]. The functional relationship between stimulus feature preferences and synaptic connections within V1 thus suggests that V1 is a likely substrate of simple examples of binocular rivalry such as those involving sinusoidal grating stimuli.

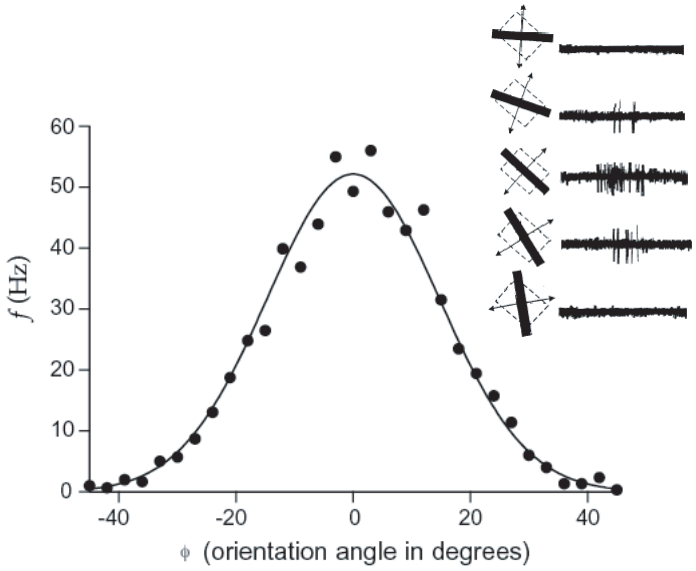

Figure 1.3: Shown here is the firing frequency of cat neurons when a black rectangle of various orientations is placed into its field of vision. As can clearly be seen, the neuron has a maximal firing rate for a rectangle with a particular orientation and no response for rectangles with a sufficiently different orientation.

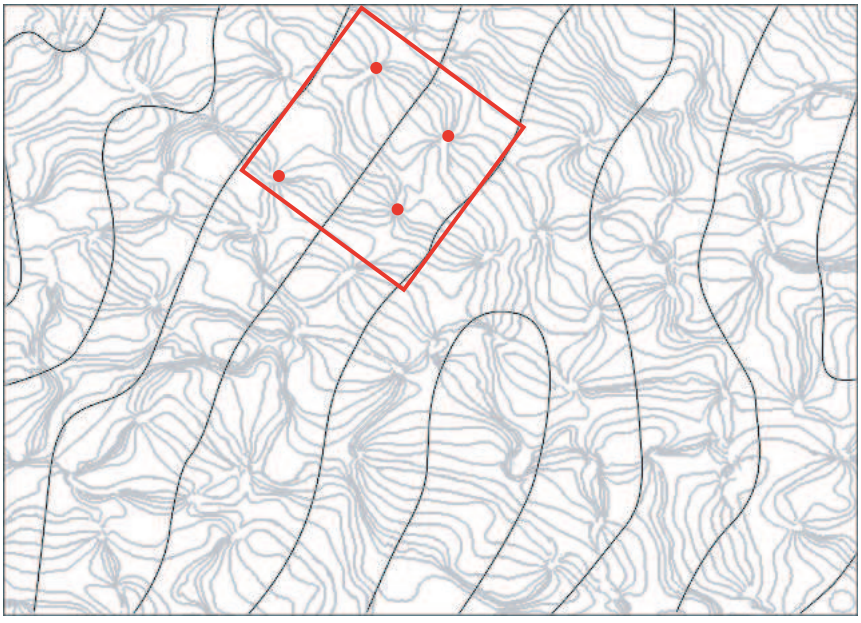

Figure 1.4: Shown are contours of orientation (light) and ocular dominance (dark) in a slice of primate V1, the red square shows a single hypercolumn - it contains all orientation preferences for both eyes for a single receptive field. The hypercolumn is approximately the fundamental tiling of the visual cortex (the reason for a hypercolumn containing two sets of orientation preference is that it is possible for multiple scales to exist in a receptive field and the visual system needs to be able to respond to this possibility though the exact nature of this is controversial).

1.1.2 Experimental Results

Psychophysical experiments have been able to observe and measure the speed of perceptual waves. Wilson *et. al.* [81] conducted experiments where the rival images consisted of a low contrast radial grating presented to one eye and a high contrast spiral grating presented to the other. The images were restricted to an annular region centred on the observer's centre of vision, effectively making wave propagation be one dimensional on a circle. They found that switches in perceptual dominance could be evoked by the experimenter at will by replacing a small part of the suppressed stimulus with a high contrast version of itself. The observer then presses a button when his or her perception changes in a target area.

Recently Kang *et. al.* [44, 45] have developed a new psychophysical method for studying binocular rivalry waves that involves periodic perturbations of the rival images. An observer tracks rivalry within a small, central region of spatially extended rectangular grating patterns, while alternating contrast triggers are presented repetitively in the periphery of the rival patterns. The basic experimental set up is illustrated in Fig. 1.5. A number of interesting results have been obtained from these studies. First, over a range of trigger frequencies, the switching between rival percepts within the central regions is entrained to the triggering events. Moreover, the optimal triggering frequency depends on the natural frequency of spontaneous switching (in the absence of triggers). Second, the latency between triggering event and perceptual switching increases approximately linearly with the distance between the triggering site and the central region being tracked by the observer, consistent with the propagation of a traveling front with constant wave speed. Third, the speed of the traveling wave across observers covaries with the spontaneous switching rate. These observations are sufficiently broad and qualitative that we expect any sensible model of binocular rivalry waves to be consistent with them.

1.1.3 Network model of binocular rivalry

Before considering effects such as travelling waves we will first focus on the switching mechanism itself by neglecting spatial effects. Suppose, for the sake of illustration, that a horizontally oriented grating is presented to the left eye and a vertically oriented grating is presented to the right eye. This triggers rivalry due to the combination of orientation and eye specific cross-inhibition in V1. During left eye stimulus dominance, it is assumed that a group of the left eye neurons that respond to horizontal orientations are firing persistently, while right eye neurons are suppressed by cross-inhibitory connections. Of course, there may still be some low rate firing of the right eye neurons, but

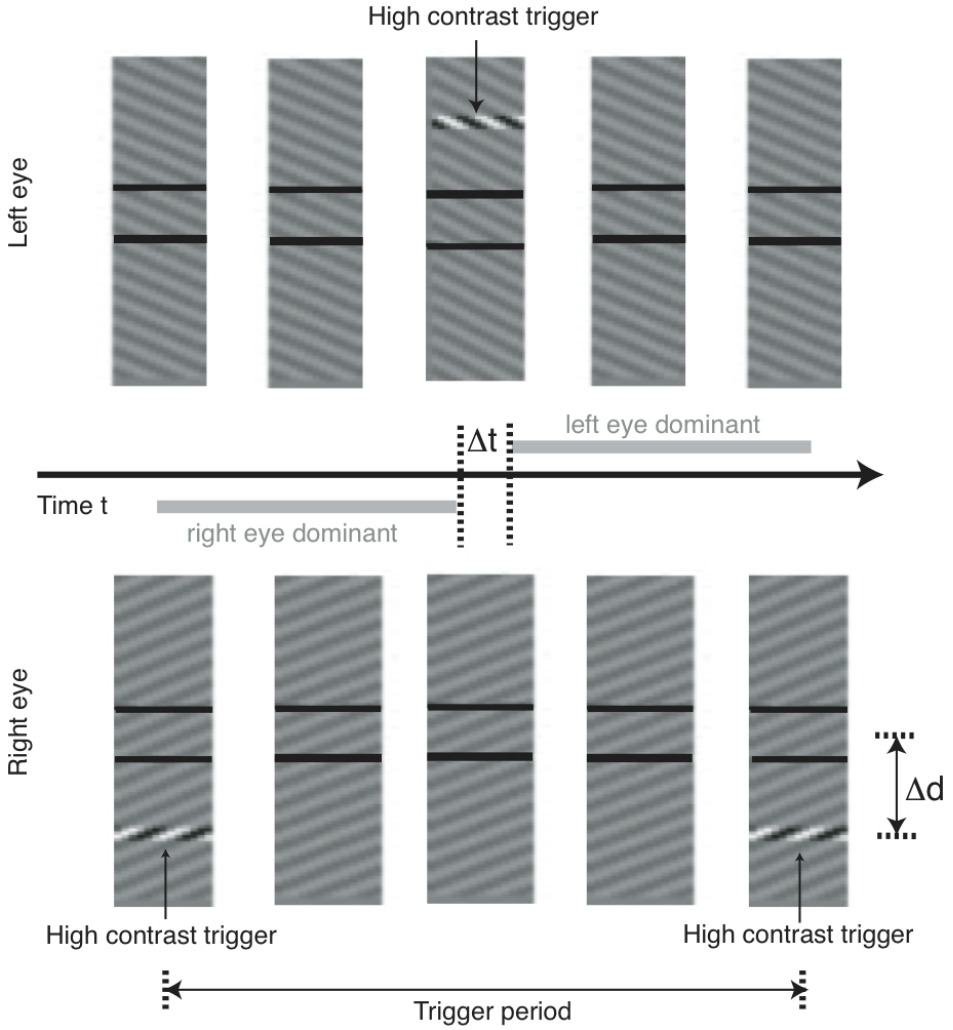

Figure 1.5: Schematic diagram illustrating experimental protocol used to study binocular rivalry waves [44]. High contrast triggers are presented periodically in antiphase within the upper extended region of one grating pattern and within the lower region of the rival pattern. Subject simply reports perceptual alternations in rival dominance within the central monitoring region indicated by the horizontal black lines on each pattern. The monitoring region is a distance Δd from the trigger region, which can be adjusted. If Δt is the latency between the triggering event and the subsequent observation of a perceptual switch, then the speed c of the wave is given by the slope of the plot $\Delta d = c\Delta t$.

it will be less than the firing rate of the left eye, horizontally tuned neurons [8]. Following this, some slow adaptive process causes a switch so that right eye, vertical orientation neurons fire persistently, suppressing the left eye neurons resulting in a repetitive cycle of perceptual dominance between the left and right eye stimuli. The competitive network architecture of reciprocal inhibition paired with slow adaptation (Fig. 1.6) has been used extensively to model oscillations in binocular rivalry [37, 70, 81, 48, 72, 67, 68, 47]. (In some versions of the model, recurrent excitation is omitted). In most cases a firing rate model appears sufficient to capture the elevation in neuronal spiking associated with the dominant stimulus.

It remains an open question as to which slow adaptive process is most responsible for the eventual switching of one stimulus dominance to the other [67]. Both spike frequency adaptation and synaptic depression have been proposed as possible substrates for this slow adaptive process. For the purpose of this example we will assume synaptic depression and leave the discussion of these two effects to sections 1.2.5 and 1.2.6. Synaptic depression is the process by which synaptic resources such as neurotransmitters, vesicles, and scaffolding proteins are exhausted due to their continuous use [79, 20]. If inhibitory synapses remain repeatedly active, due to one eye's neurons suppressing the others, eventually most of those synapses' resources will be used up, the effect of inhibition will be weakened and the suppressed population will escape [48, 67, 47]. It is worth noting that the specific choice of slow adaptation does not qualitatively effect our results in any way.

Let $u(t) \in \mathbb{R}$ and $v(t) \in \mathbb{R}$ denote the activity of the left and right eye populations at time t. The rate-based equations for a competitive network model with synaptic depression can be constructed

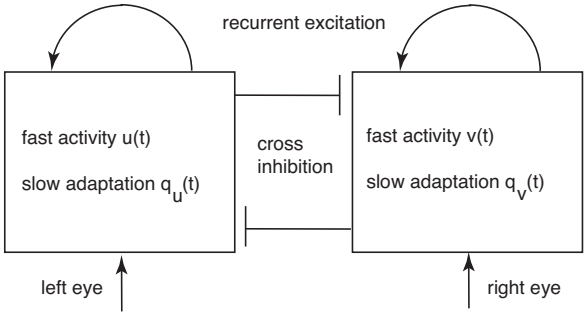

Figure 1.6: Schematic diagram of a competitive network architecture for rivalry oscillations [48, 81, 67], consisting of two homogeneous populations of cells, one driven by left eye stimuli and the other by right eye stimuli. Recurrent connections within each population are assumed to be excitatory, whereas connections between the two populations are inhibitory (cross-inhibition). Each network is described by two variables, a fast activity variable and a slow adaptation variable.

as follows:

$$\tau \frac{du(t)}{dt} = -u(t) + I_u(t) + \overline{w}_e q_u(t) f(u(t)) - \overline{w}_i q_v(t) f(v(t)) \tag{1.1}$$

$$\tau_s \frac{dq_u(t)}{dt} = 1 - q_u(t) - \beta q_u(t) f(u(t)) \tag{1.2}$$

and

$$\tau \frac{dv(t)}{dt} = -v(t) + I_v(t) + \overline{w}_e q_v(t) f(v(t)) - \overline{w}_i q_u(t) f(u(t)) \tag{1.3}$$

$$\tau_s \frac{dq_v(t)}{dt} = 1 - q_v(t) - \beta q_v(t) f(v(t)), \tag{1.4}$$

where the positive constants $\overline{w}_e$ and $\overline{w}_i$ denote the strengths of recurrent excitatory and cross-inhibitory connections, and I_u, I_v denote the input stimuli from the left and right eyes. The nonlinear function f represents the mean firing rate of a local population and is usually taken to be a smooth, bounded monotonic function such as a sigmoid

$$f(u) = \frac{1}{1 + e^{-\eta(u-\kappa)}}, \tag{1.5}$$

with gain η and threshold κ. The variables q_u, q_v are taken to be synaptic depression variables representing the fraction of baseline synaptic resources that are available to the neuron for firing. These synaptic resources are depleted under continuous firing at a rate proportional to $\beta q f$ and recover under no firing exponentially with time constant τ_s, $\tau_s \gg \tau$ (see section 1.2.5). Previous authors (e.g. [47]) have explicitly analyzed the existence and stability of fixed point solutions of equations (1.1) and (1.4) in the high gain limit $\eta \to \infty$ of (1.5) for which f becomes a Heaviside function

$$f(u) = H(u-\kappa) = \begin{cases} 0 & \text{if } u < \kappa \\ 1 & \text{if } u > \kappa. \end{cases} \tag{1.6}$$

This choice of rate function will be used throughout this work since it proves particularly useful when analyzing traveling wave solutions of continuum neural fields [2, 60, 25]. Denoting a homogeneous

fixed point by (U^*, V^*, Q_u^*, Q_v^*), we have for $I_u = I_v = I$ with I constant,

$$\begin{aligned} U^* &= Q_u^* \overline{w}_e H(U^* - \kappa) - Q_v^* \overline{w}_i H(V^* - \kappa) + I \\ V^* &= Q_v^* \overline{w}_e H(V^* - \kappa) - Q_u^* \overline{w}_i H(U^* - \kappa) + I \\ Q_u^* &= \tfrac{1}{1+\beta H(U^* - \kappa)}, \quad Q_v^* = \tfrac{1}{1+\beta H(V^* - \kappa)}. \end{aligned}$$

There are four possible homogeneous fixed points. First, there is the *off state* $U^* = V^* = I$, which occurs when $I < \kappa$, that is, the input is not strong enough to activate either population. Second there is the *on-state* or *fusion state*, where both populations are simultaneously active:

$$\begin{aligned} (U^*, V^*) &= \left(\tfrac{\overline{w}_e - \overline{w}_i}{1+\beta} + I, \tfrac{\overline{w}_e - \overline{w}_i}{1+\beta} + I \right), \\ (Q_u^*, Q_v^*) &= \left(\tfrac{1}{1+\beta}, \tfrac{1}{1+\beta} \right), \end{aligned}$$

and occurs when $I > \kappa - (\overline{w}_e - \overline{w}_i)/(1+\beta)$. This case is more likely for very strong depression (β large), since cross inhibition will be weak, or when the local connections are strong and excitation-dominated. Finally there are two *winner-take-all* (WTA) states in which one population dominates the other: the left eye dominant state

$$\begin{aligned} (U^*, V^*) &= \left(\tfrac{\overline{w}_e}{1+\beta} + I, I - \tfrac{\overline{w}_i}{1+\beta} \right), \\ (Q_u^*, Q_v^*) &= \left(\tfrac{1}{1+\beta}, 1 \right) \end{aligned}$$

and the right eye dominant state

$$\begin{aligned} (U^*, V^*) &= \left(I - \tfrac{\overline{w}_i}{1+\beta}, \tfrac{\overline{w}_e}{1+\beta} + I \right), \\ (Q_u^*, Q_v^*) &= \left(1, \tfrac{1}{1+\beta} \right) \end{aligned}$$

The WTA states exist provided that

$$I > \kappa - \frac{\overline{w}_e}{1+\beta}, \quad I < \kappa + \frac{\overline{w}_i}{1+\beta}. \tag{1.7}$$

This will occur in the presence of weak depression (β small) and strong cross-inhibition such that depression cannot exhaust the dominant hold one population has on the other. The stability of these fixed points is straightforward to analyze by considering the general Jacobian of (1.1) and (1.4) with

$f(x) = H(x - \kappa)$. It is a straightforward calculation (for $\tau = 1$) to show

$$J(u, v, q_u, q_v) = \begin{pmatrix} -1 & 0 & \overline{w}_e H(u-\kappa) & \overline{w}_i H(v-\kappa) \\ 0 & -1 & \overline{w}_i H(u-\kappa) & \overline{w}_e H(v-\kappa) \\ 0 & 0 & -(\tau_s + \frac{\beta}{\tau_s}) H(u-\kappa) & 0 \\ 0 & 0 & 0 & -(\tau_s + \frac{\beta}{\tau_s}) H(v-\kappa) \end{pmatrix}. \tag{1.8}$$

The eigenvalues are

$$\lambda = -1, -(\tau_s + \frac{\beta}{\tau_s}) H(u-\kappa), -(\tau_s + \frac{\beta}{\tau_s}) H(v-\kappa) \tag{1.9}$$

which are always negative regardless of u and v. Hence all four fixed points are stable. It can also be shown that equations (1.1)–(1.4) also support spatially homogeneous limit cycle oscillations in which there is periodic switching between left and right eye dominance consistent with binocular rivalry [47]. It follows from (1.9) that such oscillations cannot arise via a standard Hopf bifurcation. Instead bistable regimes where a rivalry state coexists with a fusion state are found, as illustrated in Fig. 1.7. (Such behaviour persists in the case of smooth sigmoid firing rate functions, at least for sufficiently high gain [47]).

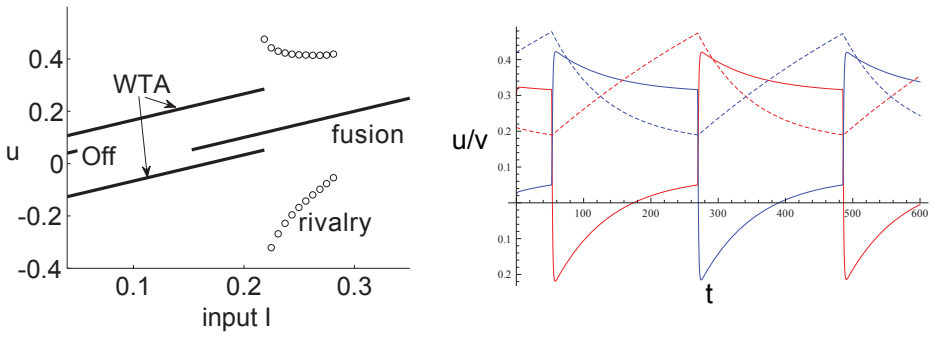

Figure 1.7: (a) Bifurcation diagram showing homogeneous solutions for the left population activity u as a function of the input amplitude I. Solid lines represent stable states, whereas circles represent the maximum and minimum of rivalry oscillations. It can be seen that there are regions of off/WTA bistability, WTA/fusion bistability, and fusion/rivalry bistability. Parameters are $\tau_s = 500$, $\kappa = 0.05$, $\beta = 5$, $\overline{w}_e = 0.4$ and $\overline{w}_i = 1$. Reproduced with permission from [47]. (b) Homogeneous oscillatory solution in which there is spontaneous periodic switching between left and right eye dominance. Plot against time of the left eye neural activity u (solid red), the right eye neural activity v (solid blue) together with the corresponding depression variables q_u (dashed red) and q_v (dashed blue).

This basic model of reciprocal inhibition paired with a slow adaptive process has often been used to phenomenologically model the neural substrate of binocular rivalry oscillations [37, 70, 81, 48, 67, 68, 47]. However, travelling waves are a spatial effect and we require a way to deal with the additional dimension over which the wave travels. Neural field equations are a very good approach

to this problem and we will introduce them in the next section.

1.2 Neural Field Theory

Neural field theory is a popular [22] modelling approach which provides a coarse-grained continuum approximation to neural tissue. Even a single neuron is a complex object, made up of many connected components some of which display a high degree of stochastic behaviour. Understanding their properties is an entire field in its own right and no complete model currently exists. Neural field theory equations are based upon assumptions on how these neurons behave on a macroscopic scale. It has been argued [82] that since neural tissue can be regarded as functionally two dimensional with the third dimension essentially providing redundancy, rather than considering individual neurons it is sensible to consider interacting populations of neurons instead. As highlighted in a recent review [14], there has not yet been a rigorous multiscale derivation of neural field theory equations from any respected biophysical model of how single neurons behave, such as Hodgkin-Huxley. Nevertheless, by making plausible assumptions, neural field equations have been used to model a wide variety of diverse phenomena such as visual hallucinations [15], EEG waves [57], working memory [32] and of course binocular rivalry [17, 47]. In this section a brief overview of some of the most common methods used in neural field theory will be reviewed with a particular emphasis on travelling waves.

1.2.1 1-D Neural field equation for a single field

There are two primary ways to model neural populations [14]. The first, originally popularised by Wilson and Cowan [82] considers equations where the average firing rate (spike train/action potential generation) is the dependent variable. The other, popularized by Amari [2] takes the average membrane potential (voltage) as the dependent variable. Both approaches have their merits but for most of this thesis we will work with the average membrane potential.

The following is a heuristic justification of one of the first neural field equations whose travelling wave properties were studied by Amari [2]. This is adapted from the justifications of neural field equations presented in [82, 2, 14]. Consider a line where at each point x we consider the population of neurons in a small region dx, we write $u(x,t)$ for the average membrane potential in this population. It is often assumed that for a population with average electrical activity $u(x,t)$ its neurons have a mean-field approximate firing rate $f(u(x,t))$ where f is a smooth, increasing, bounded function (such as a sigmoid) [14, 60]. Thus, it is assumed that on average, neurons begin to generate action potentials above a threshold. These action potentials are electrical activity which is sent by the

neuron (via its axon) to the inputs of other neurons (via synapses). In the mean field sense we see this as neuronal populations producing a constant level of activity which is received by other neuronal populations. Let $w(x, y, t)$ be the strength of connection between neuronal populations at positions x and y at time t. It is assumed that these do not change with time which is approximately true for largely crystallised cortices such as the primary visual cortex. For the sake of mathematical illustration, though not true in general (see section 1.1.1), it is further assumed that the strength of synaptic connection depends only on distance, that is, $w(x, y) = w(x - y)$. That is, a population at position y of size dy drives a population at x of size dx with magnitude

$$w(x - y)f(u(y, t))dy. \tag{1.10}$$

The population at x is then receiving input from many sources. It can be assumed that the neuron is a linear machine which simply sums over all input activity [14, 2, 15, 17, 25, 47, 52, 82]. Proceeding under this assumption, we can write, for the total input activity $\Psi(x, t)$ received by neurons in a small region around x at time t as

$$\Psi(x, t) = \int_{-\infty}^{\infty} w(x - y)f(u(y, t))dy. \tag{1.11}$$

It is further assumed that input activity linearly increases the membrane potential and then undergoes exponential decay with constant τ, this can be justified by considering equations for the potential of a single neuron [14]. Incorporating this gives an equation for $u(x, t)$,

$$u(x, t) = \int_{-\infty}^{t} \Psi(x, t - s)H(s)e^{-\tau(t-s)}ds \tag{1.12}$$

where $H(x)$ is the Heaviside step function. Identifying $H(s)e^{-\tau s}$ as the Green's function of a linear operator, the above equation is also commonly written as

$$\tau\frac{\partial u(x, t)}{\partial t} + u(x, t) = \int_{-\infty}^{\infty} w(x - y)f(u(y, t))dy + I(x, t) \tag{1.13}$$

where $I(x, t)$ represents an external input to the neurons at x (such as a stimulus). If instead we wish to model the average firing rate $a(x, t)$ the analysis is very similar. We assume that for a given average input firing rate to neurons at x at position t

$$\Phi(x, t) = \int_{-\infty}^{\infty} w(x - y)a(y, t)dy \tag{1.14}$$

a proportion given by $F(\Phi(x,t))$ will receive above threshold excitation, where as before F is a bounded monotone function such as a sigmoid. Thus the analogue of equation (1.13) becomes

$$\tau\frac{\partial a(x,t)}{\partial t} + a(x,t) = F\left(\int_{-\infty}^{\infty} w(x-y)a(y,t)dy\right). \tag{1.15}$$

Amari pioneered the study of neural field equations from an analytical as opposed to a computational standpoint. In order to proceed with his original method it is necessary to take a specific form for the firing rate function f. As previously mentioned, a common [2, 15, 14, 25, 47] choice for f is a sigmoid

$$f(x) = \frac{1}{1+e^{-\gamma(x-\kappa)}} \tag{1.16}$$

where γ is the gain and κ is the threshold. For the sake of mathematical tractability we will assume that $\gamma \to \infty$ so that

$$f(x) = H(x-\kappa) \tag{1.17}$$

where H is the Heaviside step function. This approximation allows explicit solutions to be constructed in many cases where analysis would otherwise be difficult or impossible. One can then easily verify this approximation by numerically simulating equations with the sigmoid function in place of the Heaviside (such as [17]). It is also sensible to take an explicit form for $w(x)$, provided such a choice represents a falling off with distance. Choices which have previously been used successfully [14] include the exponential weight function

$$w(x) = \frac{1}{2\sigma}e^{-\frac{|x|}{\sigma}} \tag{1.18}$$

the Gaussian weighting function

$$w(x) = \frac{1}{\sqrt{2\pi\sigma^2}}e^{-\frac{x^2}{2\sigma}} \tag{1.19}$$

and the so-called Mexican hat function [21]

$$w(x) = (1-|x|)\frac{e^{-|x|}}{4}. \tag{1.20}$$

The exact form used depends on the particular application, where it is the general shape that is of biological relevance. All these forms have been used previously in the literature and there is no accepted standard. As we shall later see, in the work presented in this thesis, the differences between choice of weighting kernel and gain of the sigmoid function have minimal effect, thus the

exact form used tends to be the one with the highest mathematical convenience. It will be convenient to introduce the notation

$$W(x) = \int_{-\infty}^{x} w(y)dy \tag{1.21}$$

to denote the integral of the kernel w.

1.2.2 Equilibrium Solutions

Following the original treatment by Amari [2], for equation (1.13) in equilibrium we have $\frac{\partial u}{\partial t} = 0$. For simplicity we fix the time scale by setting $\tau = 1$ and assume the input $I(x,t) = I$ is constant, equation (1.13) becomes

$$u(x,t) = \int_{-\infty}^{\infty} w(x-y)H(u(y,t)-\kappa)dy + I. \tag{1.22}$$

To find homogeneous fixed point solutions, we need to solve the equation $U = W(\infty)H(U-\kappa) + I$. This has solutions $U_+ = W(\infty) + I$ which can only exist when $W(\infty) + I > \kappa$ and $U_- = I$ which can only exist when $I < \kappa$. If we now consider localized excitations defined by activity on an interval, that is, define $O(u) = \{x : u(x,t) > \kappa\}$ and consider the situation where $O(u) = (a_1, a_2)$. It is sufficient to only consider the interval $(0, a)$ due to equation (1.22) being invariant to a shift in the x-axis. This reduces equation (1.22) to

(1.23)

$$u(x,t) = \int_{0}^{a} w(x-y)dy + I(x) \tag{1.24}$$

for which we can immediately write down the solution

$$u(x,t) = W(x) - W(x-a) + I(x). \tag{1.25}$$

In order for such a solution to exist it is necessary, owing to the fact that u is a continuous function, for $u(0,t) = u(a,t) = \kappa$. We have $\kappa = W(a) - W(0) + I = W(0) - W(-a) + I$, easily solved using $W(a) = -W(-a)$ to give $W(a) = \kappa - I$. A localized excitation will only exist whenever this equation has a solution for $a > 0$. By considering an explicit form of w such as an exponential weighting as in Amari [2] it is straightforward to enumerate over parameter regions where such solutions will exist. This is not particularly illuminating and so will be omitted.

1.2.3 Constructing a Travelling Wave

The standard approach for finding travelling wave solutions with a constant profile is to introduce the coordinate $\varepsilon = x - ct$ and seek solutions of the form $U(\varepsilon) = u(x,t)$. Substituting this into equation (1.13) with $f(x) = H(x-\kappa)$, $I(x) = I$ a constant and $\tau = 1$ gives us

$$-cU'(\varepsilon) + U(\varepsilon) = \int_{-\infty}^{\infty} w(\varepsilon - \varepsilon') f(U(\varepsilon'))d\varepsilon' + I. \tag{1.26}$$

The analysis is now very similar to the equilibrium case. Proceeding along the lines of Amari [2], assuming a Heaviside firing rate. We first consider front-like solutions which tend to U_+ as $\varepsilon \to -\infty$ and U_- as $\varepsilon \to \infty$. Such a solution need only cross the threshold κ once which we may assume occurs at the origin by homogeneity, that is, $U(0) = \kappa$. Naturally it is the case that $U(\varepsilon) > \kappa$ for $\varepsilon < 0$ and equation (1.26) becomes the Ordinary Differential Equation (ODE)

$$-cU'(\varepsilon) + U(\varepsilon) = \int_{-\infty}^{0} w(\varepsilon - \varepsilon')d\varepsilon' + I = \int_{\varepsilon}^{\infty} w(y)dy + I \tag{1.27}$$

$$\tag{1.28}$$

which can readily be solved by integrating factor. Explicitly, if we multiply both sides by $e^{-\frac{\varepsilon}{c}}$ and integrate we obtain the solution

$$U(\varepsilon) = e^{\frac{\varepsilon}{c}} \left[C_0 - \frac{1}{c} \int_0^{\varepsilon} e^{-\frac{y}{c}} \left(W(\infty) - W(y) + I \right) dy \right] \tag{1.29}$$

with C_0 a constant. Since for a travelling front we we require U to be bounded as $\varepsilon \to \infty$, the bracketed term must tend to zero. For $c > 0$, this implies

$$C_0 = \frac{1}{c} \int_0^{\infty} e^{-\frac{y}{c}} \left(W(\infty) - W(y) + I \right) dy \tag{1.30}$$

$$\tag{1.31}$$

for $c < 0$ requiring boundedness as $\varepsilon \to -\infty$ gives

$$C_0 = \frac{1}{-c} \int_0^{\infty} e^{-\frac{y}{-c}} \left(W(\infty) - W(y) + I \right) dy. \tag{1.32}$$

We also have an implicit equation for c, from the threshold condition $U(0) = \kappa$. Substituting equation (1.30) into equation (1.29) gives the solution a more compact form,

$$U(\varepsilon) = \frac{1}{|c|}\int_{\varepsilon}^{\infty} e^{-\frac{y-\varepsilon}{|c|}} \left(W(\infty) - W((sgn(c)y) + I\right) dy \tag{1.33}$$

$$\kappa = \frac{1}{|c|}\int_{0}^{\infty} e^{-\frac{y}{|c|}} \left(W(\infty) - W(sgn(c)y) + I\right) dy. \tag{1.34}$$

$$\tag{1.35}$$

Equation (1.37) and equation (1.34) give both the explicit form of the wave front and the implicit equation for the wave speed c respectively. In the case of exponential weighting function one does not even need to rely on computer simulation to find c and it is a matter of algebra to show

$$c = \begin{cases} c_+(\kappa) = \frac{1}{2\kappa}(1 - 2\sigma\kappa) & \kappa < \frac{1}{2} \\ c_-(\kappa) = \frac{\sigma}{2}\frac{1-2\kappa}{1-\kappa} & \kappa \in (\frac{1}{2}, 1) \end{cases} \tag{1.36}$$

is the unique speed of the travelling front. The front travels to the right when $0 < \kappa < 0.5$ and travels to the left when $0.5 < \kappa < 1$. The uniqueness persists for any symmetric weighting function.

1.2.4 Stability

Recently techniques for analyzing stability of travelling wave solutions which are already established for partial differential equations (PDEs) have been adapted to neural fields [83]. The so-called Evans function approach involves the construction of a function whose zeroes give the point spectrum of linear perturbations. The general method, following the excellent review [25], for neural fields is to consider a perturbation to the stationary solution. Though previously shown in [25] for neural field equations written in integral form, for the sake of consistency results here will be derived using the differential form for the field equations. Proceeding in this manner for equation (1.13) we set $\varepsilon = x - ct$, write U_0 for the solution to equation (1.26) and assume that $U(\varepsilon, t) = U_0(\varepsilon) + U_1(\varepsilon, t)$ where $U_1(\varepsilon, t)$ is the deviation from the equilibrium solution. Substituting into equation (1.13) and expanding gives

$$\frac{\partial U_1}{\partial t} - c\frac{\partial U_0}{\partial \varepsilon} - c\frac{\partial U_1}{\partial \varepsilon} + U_0(\varepsilon) + U_1(\varepsilon, t) = \int_{-\infty}^{\infty} w(\varepsilon - \varepsilon') f(U_0(\varepsilon') + U_1(\varepsilon', t)) d\varepsilon' + I. \tag{1.37}$$

Taking f, as usual, to be Heaviside, and exploiting the fact that it appears inside an integral, we can approximate $f(U_0(\varepsilon',t)+U_1(\varepsilon',t))$ as $f(U_0(\varepsilon'))+U_1(\varepsilon',t)\delta(U_0(\varepsilon')-\kappa)$ since the Heaviside has the delta measure as its Radon-Nikodym derivative. Substituting this back into equation (1.37) and using equation (1.26) to eliminate terms gives the linear operator equation

$$\frac{\partial U_1}{\partial t} = LU_1 \tag{1.38}$$

where L is a linear operator on the ε component only and is given explicitly by

$$LU_1 = c\frac{\partial U_1}{\partial \varepsilon} - U_1 + \int_{-\infty}^{\infty} w(\varepsilon-\varepsilon')U_1(\varepsilon',t)\delta(U_0(\varepsilon')-\kappa)d\varepsilon'. \tag{1.39}$$

Seeking solutions of the form $U_1(\varepsilon,t)=q(\varepsilon)e^{\lambda t}$, reduces equation (1.38) to the eigenvalue equation

$$c\frac{\partial q}{\partial \varepsilon} - q + \int_{-\infty}^{\infty} w(\varepsilon-\varepsilon')q(\varepsilon')\delta(U_0(\varepsilon')-\kappa)d\varepsilon' = \lambda q. \tag{1.40}$$

Using well-known properties of the delta function, in particular that $\delta(U_0(\varepsilon')-\kappa)=\frac{\delta(\varepsilon')}{|U_0'(0)|}$, this is equivalent to

$$c\frac{\partial q}{\partial \varepsilon} - q + \frac{w(\varepsilon)q(0)}{|U_0'(0)|} = \lambda q \tag{1.41}$$

which is again an ODE which is readily solved via integrating factor, with general solution

$$q(\varepsilon) = e^{\frac{(1+\lambda)\varepsilon}{c}}\left[C_1 - \int_0^{\varepsilon} e^{-\frac{(1+\lambda)y}{c}}\frac{w(y)q(0)}{|U_0'(0)|}dy\right]. \tag{1.42}$$

Since $U_1(\varepsilon,0)=q(\varepsilon)$ we may assume that $q(\varepsilon)$ is a small perturbation, in particular it should be bounded as $\varepsilon\to\infty$, this condition fixes C_1 giving the general solution

$$q(\varepsilon) = e^{\frac{(1+\lambda)\varepsilon}{c}}\left[\int_{\varepsilon}^{\infty} e^{-\frac{(1+\lambda)y}{c}}\frac{w(y)q(0)}{|U_0'(0)|}dy\right]. \tag{1.43}$$

It is obvious that for such a solution to exist we require $\lambda > -1$ thus $(-\infty,-1)$ is the continuous spectrum of the operator. To find the point spectrum we substitute $\varepsilon=0$ into the above to give a consistency condition which may implicitly be solved for λ. $\lambda=0$ is obviously an eigenvalue representing translational invariance. If $\lambda<0$ for all other eigenvalues it can be said that any such perturbation will eventually die out and the wave is said to be linearly stable. It is then assumed, though unfortunately not yet proved for the case of general neural fields that linear implies global stability.

1.2.5 Synaptic depression

Real neurons require cellular resources such as neurotransmitters and vesicles in order to transmit signals across a synapse. Under continued firing these resources can become depleted resulting in reduced firing efficiency, an effect known as synaptic depression. This effect can be modelled phenomenologically as follows [14]. Let $q(x,t)$ be the firing efficiency of neurons in a population centred on x at time t, that is, $q(x,t) \in (0,1]$ and $q(x,t) = 1$ when the cell has a saturated amount of synaptic resources. By definition, this modifies the firing rate function so that

$$f(x) \to q(x,t)f(x). \tag{1.44}$$

It has been shown that a reasonable phenomenological model for the firing efficiency [1], $q(x,t)$, is given by the equation

$$\tau_s \frac{\partial q(x,t)}{\partial t} + q(x,t) = 1 - \beta f(u(x,t))q(x,t) \tag{1.45}$$

where β is known as the strength of synaptic depression and τ_s is the time scale of synaptic depression (generally between $500ms$ and $1s$). This simple model captures the main effects - under continued firing the firing efficiency decreases exponentially to the level $\frac{1}{1+\beta} < 1$ whereas if the neurons are not firing the efficiency increases back to nominal levels. Though this kind of biological feature is often ignored for the sake of modelling it will turn out that synaptic depression or another process which results in a slow adaptation of the firing rate with time is essential for binocular rivalry waves.

1.2.6 Spike frequency adaptation

An alternative form of slow adaptation assumes that the output firing rate of a neuron can change with continued firing. Once again, it is assumed that this modulates synaptic responses over time in order to bring the system back to some form of resting state [24]. There are several ways to model spike frequency adaptation, for example, it can take the form of an additional voltage [24] which serves to lower $u(x,t)$ or it can be seen that the firing threshold κ is a variable which changes with time [54]. As an example of the former consider the equations

$$\tau \frac{\partial u(x,t)}{\partial t} + u(x,t) = \int_{-\infty}^{\infty} w(x-y)f(u(y,t))dy - gz(x,t), \tag{1.46}$$

$$\frac{\partial z(x,t)}{\partial t} = -z(x,t) + \beta f(u(x,t)). \tag{1.47}$$

In this case the variable z is seen to be an additional feedback voltage which is zero in the case where neurons are not firing but increases to some constant level under repeated firing. This has the effect of lowering $u(x,t)$ directly and can be seen as an alternative way to model slow adaptation.

1.3 Stochastic Calculus

Prior to the commencement of this doctorate there does not appear to have been much work on the effects of noise on travelling front propagation in neural field equations. One notable exception is a study by Brackley and Turner [10], who consider a specific model of a neural field with a fluctuating threshold. Waves in stochastic neural fields are also briefly considered by Coombes *et. al.* [23], although their main emphasis is the effects of quenched noise. This said, there have been studies which attempt to present plausible stochastic neural field equations. Furthermore, front propagation in spatially extended stochastic systems has been studied in a number of other cases. Much of the work presented in this thesis will rely on stochastic calculus to model the effects of noise. To this end in this section stochastic calculus will be introduced informally, more detail can be found in several books such as Gardiner [39].

1.3.1 Ito Calculus

The following is an informal introduction to stochastic calculus along the lines of Jacobs [43]. Suppose we divide the interval $[0,T]$ into N equal chunks and set $t_n = n\Delta t$ where $\Delta t = \frac{T}{N}$. Consider the stochastic difference equation

$$X_{t_{n+1}} = X_{t_n} + \Delta X_{t_n} \tag{1.48}$$

where the ΔX_{t_n} are independent identically distributed Gaussian r.v.s with mean zero and variance $\sigma^2 = \Delta t$. Taking $X_{t_0} = X_0 = 0$ this difference equation has the solution

$$X_{t_j} = \sum_{n=0}^{j-1} \Delta X_{t_n}. \tag{1.49}$$

This sum can in fact be computed using basic properties of the Gaussian distribution - the sum of a finite number of Gaussian r.v.s with zero mean is also Gaussian with mean zero and the variance is given by adding up all the composite variances. That is, $X_{t_n} \sim N(0, n\Delta t)$. We can now construct a

continuous time version of this process by taking the limit as $N \to \infty$. Explicitly for equation (1.49)

$$X(T) = \lim_{N\to\infty} \sum_{n=0}^{N-1} \Delta X_{t_n} \tag{1.50}$$

which looks suspiciously like an integral except the infinitesimal is a stochastic quantity. In fact this is a definition of an Ito integral and we shall write

$$X(T) = \lim_{N\to\infty} \sum_{n=0}^{N-1} \Delta X_{t_n} \equiv \int_0^T dW_t \equiv W(T) \tag{1.51}$$

where it is understood that the limit is in the mean-square sense. Throughout this work when we use limits of sequences of r.v.s we are strictly speaking always taking the limit in the mean-variance sense. Thus $W(T)$ is a Gaussian r.v. with mean zero and variance T. It is known in the literature as a Wiener process and is one of the most fundamental objects in stochastic calculus.

Suppose instead that we had started with the stochastic difference equation

$$X_{t_{n+1}} - X_{t_n} = f(t_n)\Delta X_{t_n} \tag{1.52}$$

where $f(t)$ is a deterministic function of time. This modified equation has solution given by

$$X_{t_j} = \sum_{n=0}^{j-1} f(t_n)\Delta X_{t_n}. \tag{1.53}$$

Again this looks suspiciously like an integral and we shall define it as such

$$X(T) = \lim_{N\to\infty} \sum_{n=0}^{N-1} f(t_n)\Delta X_{t_n} \equiv \int_0^T f(t)dW_t. \tag{1.54}$$

Now since we know that multiplying a Gaussian by a number merely changes the variance the object $f(t_n)\Delta X_{t_n}$ is still a Gaussian r.v. except now it has mean zero but variance $(f(t_n))^2 \Delta t$, thus the final distribution will have mean zero and variance given by

$$\sum_{n=0}^{N-1} (f(t_n))^2 \Delta t \tag{1.55}$$

which in the continuous limit becomes the integral

$$\int_0^T (f(t))^2 dt. \tag{1.56}$$

Writing this in another way we have that

$$\langle \int_0^T f(s)dW_t \int_0^T f(s)dW_s \rangle = \int_0^T (f(t))^2 \, dt \tag{1.57}$$

which can be captured by the rule

$$\langle dW_t dW_s \rangle = \delta(t-s)dt. \tag{1.58}$$

Note that we have introduced the "angle bracket" notation where we take $\langle x \rangle$ to mean the expected value of x. To be more precise,

$$\langle x \rangle = \int t f(t) dt \tag{1.59}$$

where $f(t)$ is the probability density function of the random variable x. Suppose that we wanted to consider an expansion in terms of the Wiener increment ΔW_{t_n}. Specifically consider the object $(\Delta W_{t_n})^2$. This trivially has mean Δt and it can be shown using the formulas for higher order moments of Gaussian distributions that all higher moments of $(\Delta W_{t_n})^2$ are order $(\Delta t)^2$ or higher. Writing this another way we have

$$(\Delta W_{t_n})^2 = \Delta t + o(\Delta t). \tag{1.60}$$

Consider the sum

$$\sum_{n=0}^{N-1} (\Delta W_{t_n})^2 = \sum_{n=0}^{N-1} (\Delta t + o(\Delta t)) \, . \tag{1.61}$$

Taking the limit $N \to \infty$ will give

$$\lim_{N\to\infty} \sum_{n=0}^{N-1} (\Delta W_{t_n})^2 = T + \lim_{N\to\infty} \sum_{n=0}^{N-1} g(N) = T + \lim_{N\to\infty} N g(N) \tag{1.62}$$

where $g(N)$ is $o(\Delta t) = o(\frac{1}{N})$. Hence the second term is identically zero by definition. Since these increments are only found inside integrals, this is sometimes written as $dW^2 = dt$ and is known as Ito's rule. This is a somewhat surprising but very useful result since it states that dW^2 is essentially a deterministic quantity.

1.3.2 Ito's Lemma

Suppose that X_t obeys the stochastic differential equation

$$dX_t = a(X_t, t)dt + b(X_t, t)dW_t \tag{1.63}$$

which we take to be short-hand for the integral equation

$$X_T = \int_0^T a(X_t, t)dt + \int_0^T b(X_t, t)dW_t \tag{1.64}$$

where the second integral is defined as

$$\int_0^T b(X_t, t)dW_t \equiv lim_{N\to\infty} \sum_{n=0}^{N-1} b(X_{t_n}, t_n)\Delta W_{t_n} \tag{1.65}$$

with terms defined as in the previous section. Let f be a continuous function and define a new process $Y_t = f(X_t)$. What stochastic differential equation will this new process obey? Taylor expanding gives

$$df(X_t) = f(X_t + dX_t) - f(X_t) = f'(X_t)dX_t + \frac{1}{2}f''(X_t)dX_t^2 + o(dX_t^2). \tag{1.66}$$

The crucial difference here compared with the deterministic case is the dX_t^2 term since our calculation above implies it cannot be discarded as a higher order term. Specifically

$$dX_t^2 = (a(X_t, t)dt + b(X_t, t)dW_t)^2 = (b(X_t, t))^2\, dt + o(dt). \tag{1.67}$$

Putting this all together we have

$$\begin{aligned} df(X_t) &= f'(X_t)(a(X_t, t)dt + b(X_t, t)dW_t) + \frac{1}{2}f''(X_t)\,(b(X_t, t))^2\, dt \\ &= \left(f'(X_t)a(X_t, t) + \frac{1}{2}f''(X_t)\,(b(X_t, t))^2\right) dt + b(X_t, t)dW_t \end{aligned}$$

which is a result known as Ito's Lemma. This is an extremely powerful result for one dimensional processes much like the chain rule for ordinary calculus. For example, the drift-diffusion process is defined by the stochastic differential equation

$$dX_t = vdt + DdW_t \tag{1.68}$$

which we can solve using Ito's Lemma. Consider the stochastic process $Y_t = X_t - vt$. Ito's Lemma tells us that $dY = -vdt + vdt + DdW_t = DdW_t$, hence $Y_t = DW_t$ by definition and the solution to the equation for X_t must be

$$X_t = vt + DW_t \tag{1.69}$$

that is, X_t is normally distributed with mean vt and variance D^2t (this result can also be readily obtained via direct integration).

It is also possible to solve more complicated stochastic equations using Ito's Lemma. A process which shall be encountered later is the Ornstein-Uhlenbeck process defined by the stochastic differential equation

$$dX_t = a(b - X_t)dt + \sigma dW_t \tag{1.70}$$

which represents a mean reverting process via the $b - X_t$ term. Of course, its non-stochastic counterpart is trivial to solve and represents a variable which tends to b exponentially from whatever the initial condition was. Taking $b = 0$ for simplicity and making the change of variables $X_t = e^{-at}Z_t$ (inspired by the deterministic case) then applying Ito's Lemma gives the stochastic differential equation

$$dZ_t = \sigma e^{at} dW_t. \tag{1.71}$$

From section 1.3.1 we know that Z_t will be a Gaussian r.v. with variance given by $\int \sigma^2 e^{2at} dt$. Putting this all together the distribution for the Ornstein-Uhlenbeck process is a Gaussian with mean given by

$$X_0 e^{-at} \tag{1.72}$$

and variance

$$\frac{\sigma^2}{2a}(1 - e^{-2at}). \tag{1.73}$$

1.3.3 Fokker-Planck Equation

Using Ito's lemma it is possible to derive a PDE for the density $p(X_t, t)$ of a process evolving under the SDE

$$dX_t = a(X_t, t)dt + b(X_t, t)dW_t. \tag{1.74}$$

Consider, for an arbitrary function f,

$$\begin{aligned}\langle df(X_t)\rangle &= \left(f'(X_t)a(X_t,t) + \frac{1}{2}f''(X_t)\left(b(X_t,t)\right)^2\right)dt + b(X_t,t)\langle dW_t\rangle \\ &= \langle\left(f'(X_t)a(X_t,t) + \frac{1}{2}f''(X_t)\left(b(X_t,t)\right)^2\right)\rangle dt\end{aligned}$$

since $\langle dW_t\rangle$ must be zero given that each Wiener increment is Gaussian with mean zero. Differentiating the above expression (remember that it is simply short-hand for an integral equation) gives

$$\begin{aligned}\frac{d}{dt}\langle f(X_t)\rangle &= \int\left(f'(y)a(y,t) + \frac{1}{2}f''(y)\left(b(y,t)\right)^2\right)p(y,t)dy \\ &= \int f(y)\left[-\frac{\partial}{\partial y}(a(y,t)p(y,t)) + \frac{1}{2}\frac{\partial^2}{\partial y^2}(b(y,t)^2p(y,t))\right]dy.\end{aligned}$$

However, one also has, by definition, that

$$\frac{d}{dt}\langle f(X_t)\rangle = \frac{d}{dt}\int f(y)p(y,t)dy = \int f(y)\frac{\partial}{\partial t}p(y,t)dy. \tag{1.75}$$

Since f is an arbitrary function subtracting the two expressions for $\frac{d}{dt}\langle f(X_t)\rangle$ gives the Fokker-Planck equation for the density

$$\frac{\partial}{\partial t}p(y,t) = -\frac{\partial}{\partial y}(a(y,t)p(y,t)) + \frac{1}{2}\frac{\partial^2}{\partial y^2}(b(y,t)^2p(y,t)). \tag{1.76}$$

1.3.4 Stratonovich Noise

It turns out that there are many ways to define a stochastic integral driven by Wiener increments. For instance, an alternative definition of a stochastic integral is the Stratonovich integral

$$\oint_0^T b(X(t),t)dW(t) = \lim_{N\to\infty}\sum_{n=0}^{N-1} b\left(\frac{X_{n+1}+X_n}{2}, t_n\right)\Delta W_n. \tag{1.77}$$

If this was a definition of a deterministic Riemann integral (i.e. $\Delta W_n \to \Delta t$) we would find the two definitions to be equivalent. However this is not the case for stochastic integrals. Expanding

$$b\left(\frac{X_{n+1}+X_n}{2}, t_n\right) = b_n + \frac{\Delta X_n}{2}\frac{\partial b_n}{\partial x} + \frac{1}{2}\left(\frac{\Delta X_n}{2}\right)^2\frac{\partial^2 b_n}{\partial x^2} + \dots \tag{1.78}$$

Substituting for ΔX_n and dropping terms that are higher order than Δt shows that

$$b\left(\frac{X_{n+1}+X_n}{2}, t_n\right) = b_n + \left(\frac{a_n}{2}\frac{\partial b_n}{\partial x} + \frac{b_n^2}{8}\frac{\partial^2 b_n}{\partial x^2}\right)\Delta t + \left(\frac{b_n}{2}\frac{\partial b_n}{\partial x}\right)\Delta W_n. \tag{1.79}$$

where for short $b_n = b(X_n, t_n)$. Now substituting this back into the definition of the stratonovich integral gives us

$$\begin{aligned}
\oint_0^T b(X(t),t)dW(t) &= \lim_{N\to\infty}\sum_{n=0}^{N-1} b\left(\frac{X_{n+1}+X_n}{2}, t_n\right)\Delta W_n \\
&= \lim_{N\to\infty}\left[\sum_{n=0}^{N-1} b_n\Delta W_n + \sum_{n=0}^{N-1}\left(\frac{a_n}{2}\frac{\partial b_n}{\partial x} + \frac{b_n^2}{8}\frac{\partial^2 b_n}{\partial x^2}\right)\Delta t\Delta W_n + \sum_{n=0}^{N-1}\left(\frac{b_n}{2}\frac{\partial b_n}{\partial x}\right)\Delta W_n^2\right] \\
&= \lim_{N\to\infty}\left[\sum_{n=0}^{N-1} b_n\Delta W_n + \sum_{n=0}^{N-1}\left(\frac{a_n}{2}\frac{\partial b_n}{\partial x} + \frac{b_n^2}{8}\frac{\partial^2 b_n}{\partial x^2}\right)\Delta t\Delta W_n + \sum_{n=0}^{N-1}\left(\frac{b_n}{2}\frac{\partial b_n}{\partial x}\right)\Delta t\right].
\end{aligned}$$

The first term is now an Ito integral, but there is a correction given by the third term. The second term is zero since $\langle \Delta t\Delta W_n\rangle = 0$ and higher moments are given by $\langle(\Delta t\Delta W_n)^m\rangle = \Delta t^m\langle\Delta W_n\rangle^m$ which is zero or $o(\Delta t)$ by standard results on moments of Gaussian r.v.'s. Putting this all together we have

$$\oint_0^T b(X(t),t)dW(t) = \int_0^T b(X(t),t)dW(t) + \frac{1}{2}\int_0^T \frac{\partial b(X(t),t)}{\partial x} b(X(t),t)dt. \tag{1.80}$$

For a wide class of functions b these two definitions of stochastic integral will not be equivalent. In particular in the case of multiplicative noise the correction term will be nonzero and one has to decide which type of stochastic integral is best for the application at hand.

1.4 Stochastic Neural Fields

So far our neural field equations have been deterministic. However, the underlying biology is in fact extremely noisy. Experiment has shown that the spike trains of individual neurons follow a Poisson process, that is, neurons do not fire at regular intervals but instead the time between firings follows a Poisson distribution [71]. This noise largely arises from the mechanism by which neurons are able to establish a resting membrane potential and generate action potentials. Ion channels are biological gates in the cell wall of the neurons which allow for a very high flow of ions down their electrochemical gradient when they are "open" but do not allow ions to pass in other conformations. Depending on several factors, primarily membrane potential, an ion channel has a chance to change

its state but there is no guarantee. Each neuron has a large but finite number of these ion channels, thus we cannot completely ignore their stochastic nature. Previous studies have indicated that they are the primary source of intrinsic neural noise [31]. Extrinsic noise, on the other hand, is largely due to neurons receiving synaptic inputs from a huge number of sources, many of which will have nothing to do with the input or feature that neuron is trying to measure. These extra inputs can be regarded as a constant source of external background noise [31].

It is a difficult problem to convert this noise at the single neuron level to noise at the population level. One possible approach is to take an extremely simple model of an underlying neuron such as the integrate and fire model and add Gaussian white noise as an input to these neurons. Proceeding along these lines it is possible to then show that although the spike trains are Poisson distributed, the asynchronous firing of the neurons results in a standard firing rate function as $N \to \infty$ [58]. N is merely large and not infinite and so it is possible that intrinsic noise could occur in populations as a finite size effect. As previously mentioned there does not currently exist a rigorous, complete, multi-scale approach resulting in the derivation of a neural field equation. As a result of this models of noise in neural fields which have been considered thus far have been phenomenological [14]. To this end we seek plausible modifications of existing neural field equations which will help us deal with noise. Previous authors have used a Langevin equation approach with phenomenological noise terms which have been either added Gaussian noise or multiplicative Gaussian noise, though there has been progress made towards a systematic approach which currently suggests multiplicative noise (see Touboul [77]). These studies suggest that an appropriate generalisation of equation (1.13) is a stochastic equation of the form

$$du(x,t) = \left(-u(x,t) + \int_{-\infty}^{\infty} w(x-y) f(u(y,t)) dy + I(x,t)\right) dt + g(u) dW(x,t) \tag{1.81}$$

where the term $dW(x,t)$ is interpreted to mean that $dW_x(t) = dW(x,t)$ for any fixed x is a Brownian motion and $g(u) \sim 1$ for additive noise, $g(u) \sim u$ for multiplicative noise. Though this seems arbitrary, in the case of a more general function for the noise, one could still perform a Taylor expansion and get an approximation in terms of additive/multiplicative noise. Furthermore, we will take the noise term to be of Stratonovich type as is common [39] for physical systems where extrinsic noise is being modelled. It is necessary to be extremely careful when dealing with this new object $dW(x,t)$. One possible approach is the pure mathematics one (see Touboul [77]) where we would very carefully define the object $dW(x,t)$. Another approach which will be suitable for our purposes is a physical one - consider the neurons within the small but finite region $(0,h)$, they will be driven

by a spectrum of Brownian motions and since these neurons are spatially very close we would expect these Brownian motions to agree as $h \to 0$. This means that the naive assumption that dW_x and dW_y are independent is inappropriate and in fact they must be correlated by some function which is 1 for $x = y$ and tends to zero as $|x - y| \to \infty$. Thus the noise is not only specified by the function $g(x)$ but also a correlation length scale. This correlation length is another physical parameter of the system which can be interpreted as the size of a neural population or a lattice spacing in the case of simulations. In order to make this concept clear, let us introduce a correlation function C and correlation length λ onto our line of Brownian motions:

$$\langle dW(x,t)\rangle = 0, \quad \langle dW(x,t)dW(x',t')\rangle = 2C([x-x']/\lambda)\delta(t-t')dtdt' \tag{1.82}$$

where $C(\frac{x}{\lambda}) \to \delta(x)$ as $\lambda \to 0$. For example, if we take C to be the function

$$C(\frac{x}{\lambda}) = \begin{cases} \frac{1}{2\lambda} & x \in (-\lambda, \lambda) \\ 0 & otherwise \end{cases} \tag{1.83}$$

then $\langle dW(x,t)dW(y,t')\rangle = \frac{1}{\lambda}\delta(t-t')dtdt'$ for $|x-y| < \lambda$ and zero otherwise. Suppose now that we wanted to simulate a system driven by this kind of "noisy line", then we do not need to simulate correlated Brownian motions at all, since from the previous equation it is sufficient to place our grid points λ apart and simulate independent Brownian motions with variance $\langle dW(t)dW(t')\rangle = \frac{1}{\lambda}\delta(t-t')dtdt'$. In this example, the correlation length λ can be identified with the spatial grid size in simulations and this is a trick we will employ several times throughout this work.

1.4.1 Stochastic Reaction-Diffusion

Though stochastic waves in neural fields had not been studied prior to this work there has been a large amount of research for systems which bear many similarities to neural field equations. Sancho *et. al.* [4] were able to analyze travelling waves in reaction-diffusion equations of the form

$$du(x,t) = \left(-u(x,t) + \nabla^2 u(x,t)\right)dt + g(u)dW(x,t) \tag{1.84}$$

where the noise is of Stratonovich type. Their approach was to regard the stochastic wavefront as being made up of two distinct motions. First, the drift-diffusion of an average front shape on long time scales, that is, that the wave has an overall shape which is constant over many realisations and

during a single realisation of noise has a definable position which obeys a drift-diffusion process. Second, the fluctuation of this wavefront shape about its average shape on short time scales. We will show that this general approach can be extended to neural field systems as well.

1.5 Computer simulations of Neural Field equations

Though finding exact solutions to neural field equations and understanding their classes of behaviour will sometimes prove difficult, for the equations contained in this work simulating them is relatively straightforward. The author's simulations are based around a simple discretisation in both space and time. Suppose that we wish to simulate the stochastic neural field equation

$$du(x,t) = \left(-u(x,t) + \int_{-\infty}^{\infty} w(x-y)f(u(y,t))dy + I(x,t)\right)dt + g(u)dW(x,t) \tag{1.85}$$

where $dW(x,t)$ is Stratonovich noise and has the same correlation structure as in section 1.4. Let L be the length of the spatial region we simulate over and T be the final time we integrate to. Then, define $\Delta x = \frac{L}{N_x}$ to be the spatial grid spacing, where $N_x + 1$ is the number of grid points. In particular, we aim to resolve the function $u(x,t)$ at the points $u(n\Delta x, t)$ for $n \in (0, 1, ..., N_x)$. The key approximation is the following:

$$\begin{aligned}\int_{-\infty}^{\infty} w(x-y)f(u(y,t))dy &= f(u(0,t))\int_{-\infty}^{0} w(x-y)dy + \sum_{n=0}^{N_x} w(x-n\Delta x)f(u(n\Delta x,t))\Delta x \\ &\quad + f(u(L,t))\int_{L}^{\infty} w(x-y)dy,\end{aligned}$$

where the boundary conditions are implicit here in the first and third terms. We are essentially assuming that the function u has zero derivative with respect to space outside the region $(0, L)$, which is consistent with what we would expect for the travelling fronts that we analyze in this work. Using the results of section 1.3.4 it is then possible to re-write the noise in Ito form

$$g(u)dW(x,t) \to g(u)dW(x,t) + \frac{1}{2}\frac{\partial g}{\partial u}g(u)dt. \tag{1.86}$$

Furthermore, from section 1.4 we know that we can re-write $dW(x,t)$ discretely as $dW(n\Delta x, t) = \frac{1}{\Delta x}dW_n(t)$ where the dW_n are independent Brownian motions. Putting all this together gives us a

system of stochastic differential equations:

$$\begin{aligned} du(n\Delta x,t) &= \left(-u(n\Delta x,t)+f(u(0,t))\int_{-\infty}^{0} w(x-y)dy+\sum_{n} w(x-n\Delta x)f(u(n\Delta x,t))\Delta x\right)dt \\ &\quad+\left(f(u(L,t))\int_{L}^{\infty} w(x-y)dy+\frac{1}{2}\frac{\partial g}{\partial u}g(u(n\Delta x,t))\right)dt+\frac{1}{\Delta x}g(u(n\Delta x,t))dW_n(t) \end{aligned}$$

and although this looks unwieldy, it is now in a form which can be readily simulated via any method for dealing with systems of coupled stochastic ODEs, such as the Euler-Maruyama method. In the case where $g = 0$ it is no longer a stochastic system but simply a system of ODEs which can be easily simulated via many standard solvers. In this work, for the discrete systems Mathematica 8.0's NDSolve function was used and for the stochastic systems, a standard Euler-Maruyama method in C++/Python.

1.6 Overview of the thesis

From the state of the field when this work was undertaken, it was clear that travelling waves in binocular rivalry presented a very good problem to be studied via a neural field approach. Though previous studies, computational in nature, had been able to simulate binocular rivalry waves there was not any analytical basis for studying the waves in general, even in a deterministic regime. Rivalrous wave propagation had also not yet been considered in a neural field framework, though several models which exhibited other features of binocular rivalry, such as the oscillations, had been studied. Furthermore, though noise is clearly an extremely important feature of these systems judging by experimental results, very little had been done to study the effects of noise in a systematic way. In this thesis significant contributions to both deterministic and stochastic binocular rivalry, and stochastic neural fields in general will be presented. In chapter 2 binocular rivalry waves will be handled using deterministic neural field equations. However handling noise will prove difficult and chapter 3 will present a general method for handling noise in one dimensional stochastic neural fields. Chapter 4 will then extend the analysis of chapters 2 and 3 to develop a theory of stochastic binocular rivalry waves. An important consequence of this will be a testable hypothesis of stochastic neural field theory. Finally chapter 5 will look at other ways to approach stochastic neural field theory, specifically noisy versions of the Wilson-Cowan firing rate model and a master equation approach. These results are presented here as a continuous narrative though they have already been published over the course of three papers authored by myself and my supervisor, Paul Bressloff [17, 16, 80].

Chapter 2

Deterministic Binocular Rivalry Waves.

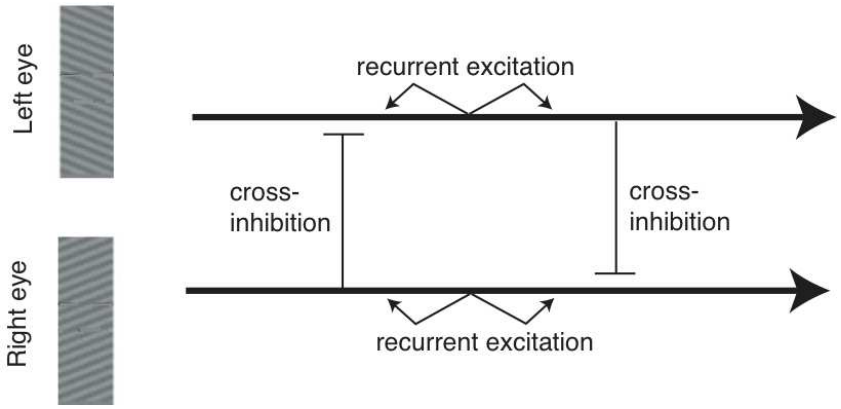

Figure 2.1: Schematic diagram of network architecture consisting of two one–dimensional neural fields. Suppose that the left eye is shown a 135 degree grating and the right eye is shown a 45 degree grating. Then one of the neural fields represents the activity of neurons tuned to 135 degree orientations in the left eye, whilst the other neural field represents the activity of neurons tuned to 45 degree orientations in the right eye. Recurrent connections within each one dimensional network are assumed to be excitatory, whereas connections between the two networks are inhibitory (cross-inhibition). The excitatory and inhibitory weight distributions are taken to be Gaussian. Slow adaptation is incorporated into the model by taking the network connections to exhibit synaptic depression.

In this chapter we will present a model of binocular rivalry waves in the primary visual cortex using deterministic neural field equations. For each eye a one dimensional network of neurons that respond maximally to a particular feature of the underlying stimulus such as orientation will be considered. As suggested in sections 1.1.1 and 1.1.3 both by the underlying biology, and the fact

that similar models have been used to model binocular rivalry in the past, recurrent connections will be taken to be excitatory and cross-connections to be inhibitory. Slow adaptation will also be taken into account via a synaptic depression variable. Using a neural field approach we will then analytically derive both the wave form and wave speed as a function of various neurophysical parameters. In addition to providing a framework for studying binocular rivalry waves we will show how our neural field approach is able to provide additional insights into the underlying biological mechanisms allowing for the generation of waves. In particular it will be shown that a "symmetry breaking" mechanism is required for waves to propagate for which we will show synaptic depression is a possible substrate.

2.1 The Model

Let $u(x,t)$ and $v(x,t)$ denote the activity of the left and right eye networks at position $x \in \mathbb{R}$ at time t. The associated neural field equations are taken to be of the form

$$\begin{aligned} \tau \frac{\partial u(x,t)}{\partial t} &= -u(x,t) + I_u(x,t) \\ &+ \int_{-\infty}^{\infty} w_e(x-x') q_u(x',t) f(u(x',t))) dx' \\ &- \int_{-\infty}^{\infty} w_i(x-x') q_v(x',t) f(v(x',t))) dx' \end{aligned} \tag{2.1a}$$

$$\tau_s \frac{\partial q_u(x,t)}{\partial t} = 1 - q_u(x,t) - \beta q_u(x,t) f(u(x,t)), \tag{2.1b}$$

and

$$\begin{aligned} \tau \frac{\partial v(x,t)}{\partial t} &= -v(x,t) + I_v(x,t) \\ &+ \int_{-\infty}^{\infty} w_e(x-x') q_v(x',t) f(v(x',t))) dx' \\ &- \int_{-\infty}^{\infty} w_i(x-x') q_u(x',t) f(u(x',t))) dx', \end{aligned} \tag{2.2a}$$

$$\tau_s \frac{\partial q_v(x,t)}{\partial t} = 1 - q_v(x,t) - \beta q_v(x,t) f(v(x,t)). \tag{2.2b}$$

Where as before f represents the mean firing rate of a local population and is taken to be the sigmoid function, which for the sake of analysis will be approximated as the Heaviside with threshold κ.

The distribution w_e of excitatory connections between neurons of the same eye preference and the distribution of cross-inhibitory connections between neurons of the opposite eye preference are both taken to be Gaussian, explicitly given by:

$$w_e(r) = \frac{a_e}{\sqrt{2\pi\sigma_e^2}} e^{-\frac{r^2}{2\sigma_e^2}}, \quad w_i(r) = \frac{a_i}{\sqrt{2\pi\sigma_i^2}} e^{-\frac{r^2}{2\sigma_i^2}}. \tag{2.3}$$

It is assumed that excitatory connections are longer range than inhibitory connections, $\sigma_e > \sigma_i$ and length scales are fixed by setting $\sigma_e = 2$ and $\sigma_i = 1$ as baseline parameters. We expect excitatory connections to span a cortical hypercolumn so that σ_e will be of the order 200 μm. The parameters a_e and a_i are in units of electrical current and represent the strength of the connection, for concreteness the baseline parameters in our simulations are $a_e = 0.4$ and $a_i = 1$, which represents inhibitory connections being electrically stronger than excitatory ones. We also fix the temporal scale of the network by setting the membrane time constant $\tau = 1$; the membrane time constant is typically around 10 ms. Depressing synapses are incorporated into the model in the form of the presynaptic scaling factors q_u, q_v evolving according to equations (2.1b) and (2.2b). Specifically, we will study the effect of slow short term synaptic depression (experimentally shown to recover over 5-10s [79, 20]). Slow short term synaptic depression has been implicated as a mechanism for contrast adaptation in V1, due to its comparable recovery timescale of 5-10s [79]. Thus, there is evidence for participation of this slower depression in processes of V1 in addition to faster short term synaptic depression, which recovers on timescales of roughly 200-800 ms [1, 79]. Finally, we take I_u, I_v to represent the effective strength of the left and right eye stimuli, respectively. Recall that we are only modeling neurons whose orientation preference coincides with the corresponding stimulus orientation so that we can take the unperturbed network to have constant homogeneous inputs. (The induction of traveling waves requires locally perturbing one of the inputs).

2.2 Travelling Waves

2.2.1 Non-depressing synapses ($\beta = 0$)

In our simplified model, we interpret the binocular rivalry wave seen in the experiments of Kang *et. al.* [44, 45] as a traveling wave front solution of the neural field equations (2.1) and (2.2), in which a high activity state invades the suppressed left eye network, say, whilst retreating from the dominant right eye network. Let us begin by ignoring the effects of synaptic depression, that is, set $\beta = 0$ and $q_u = q_v \equiv 1$. We also assume that both inputs have the same strength or contrast so

that $I_u = I_v = I$. We then obtain the reduced system of equations (for $\tau = 1$ and f given by the Heaviside (1.6))

$$\begin{aligned}\frac{\partial u}{\partial t} + u = &\int_{-\infty}^{\infty} w_e(x-x')H(u(x',t)-\kappa)dx' \\ &- \int_{-\infty}^{\infty} w_i(x-x')H(v(x',t)-\kappa)dx' + I,\end{aligned} \tag{2.4}$$

and

$$\begin{aligned}\frac{\partial v}{\partial t} + v = &\int_{-\infty}^{\infty} w_e(x-x')H(v(x',t)-\kappa)dx' \\ &- \int_{-\infty}^{\infty} w_i(x-x')H(u(x',t)-\kappa)dx' + I.\end{aligned} \tag{2.5}$$

Given that the differential operator $D = \frac{\partial}{\partial t} + 1$ has a Green's function given by $G(t,s) = \eta(t-s)$ with

$$\eta(t) = \begin{cases} 0 & t < 0 \\ e^{-t} & t > 0, \end{cases} \tag{2.6}$$

we can re-write the above equations in purely integral form:

$$\begin{aligned}u(x,t) &= I + \int_0^{\infty} \eta(s)G_e[u](x,t-s)ds \\ &\quad - \int_0^{\infty} \eta(s)G_i[v](x,t-s)ds\end{aligned} \tag{2.7}$$

$$\begin{aligned}v(x,t) &= I + \int_0^{\infty} \eta(s)G_e[v](x,t-s)ds \\ &\quad - \int_0^{\infty} \eta(s)G_i[u](x,t-s)ds\end{aligned} \tag{2.8}$$

where

$$G_p[u](x,t) = \int_{-\infty}^{\infty} w_p(y)H(u(x-y,t)-\kappa)dy \tag{2.9}$$

for $p = e, i$.

Homogeneous fixed point solutions (U^*, V^*) of equations (2.7) and (2.8) satisfy the pair of equa-

tions

$$U^* = \overline{w}_e H(U^* - \kappa) - \overline{w}_i H(V^* - \kappa) + I$$
$$V^* = \overline{w}_e H(V^* - \kappa) - \overline{w}_i H(U^* - \kappa) + I,$$

where

$$\overline{w}_e = \int_{-\infty}^{\infty} w_e(x)dx, \quad \overline{w}_i = \int_{-\infty}^{\infty} w_i(x)dx. \tag{2.10}$$

There are a maximum of four possible fixed point solutions, all of which are linearly stable [47]. First, there is the off state $U^* = V^* = I$, which occurs when $I < \kappa$, that is, the input is not strong enough to directly activate either population. Second there is the on-state or fusion state $U^* = V^* = \overline{w}_e - \overline{w}_i + I$, which occurs when $I > \kappa + \overline{w}_i - \overline{w}_e$. This case is more likely when recurrent excitation is strong or cross-inhibition is weak [47]. Finally, there are two winner–take–all (WTA) states in which one population dominates the other: the left eye dominant state $(U^*, V^*) = \mathbf{X}_L \equiv (\overline{w}_e + I, I - \overline{w}_i)$ and the right eye dominant state $(U^*, V^*) = \mathbf{X}_R \equiv (I - \overline{w}_i, \overline{w}_e + I)$. These states exist when $I > \kappa - \overline{w}_e$ and $I < \kappa + \overline{w}_i$. We will assume that the equations operate in a regime where the homogeneous WTA fixed points exist.

Let us now consider a traveling wave front solution of the form

$$u(x,t) = U(x - ct), \quad v(x,t) = V(x - ct) \tag{2.11}$$

where c is the wave speed and $\xi = x - ct$ is a traveling wave coordinate. We assume that

$$(U(\xi), V(\xi)) \to \mathbf{X}_L \text{ as } \xi \to -\infty,$$
$$(U(\xi), V(\xi)) \to \mathbf{X}_R \text{ as } \xi \to \infty$$

with $U(\xi)$ a monotonically decreasing function of ξ and $V(\xi)$ a monotonically increasing function of ξ. It follows that if $c > 0$ then the wavefront represents a solution in which activity invades a suppressed left eye network and retreats from a dominant right eye network. Substituting the traveling front solution into equations (2.7) and (2.8) gives

$$\begin{aligned} U(\xi) &= I + \int_0^{\infty} \eta(s)\widehat{G}_e[U](\xi + cs)ds \\ &\quad - \int_0^{\infty} \eta(s)\widehat{G}_i[V](\xi + cs)ds \end{aligned}$$

$$V(\xi) = I + \int_0^\infty \eta(s)\widehat{G}_e[V](\xi + cs)ds - \int_0^\infty \eta(s)\widehat{G}_i[U](\xi + cs)ds.$$

where

$$\widehat{G}_p[U](\xi) = \int_{-\infty}^\infty w_p(y)H(U(\xi - y) - \kappa)dy, p = e, i. \tag{2.12}$$

Given the asymptotic behaviour of the solution and the requirements of monotonicity, we see that $U(\xi)$ and $V(\xi)$ each cross threshold at a single location, which may be different for the two eyes. Exploiting translation invariance we take $U(0) = \kappa$ and $V(\xi_0) = \kappa$. These threshold crossing conditions imply that the above equations simplify further according to

$$U(\xi) = \int_0^\infty \eta(s)\left[\int_{\xi+cs}^\infty w_e(y)dy - \int_{-\infty}^{\xi-\xi_0+cs} w_i(y)dy\right]ds + I \tag{2.13}$$

$$V(\xi) = \int_0^\infty \eta(s)\left[\int_{-\infty}^{\xi-\xi_0+cs} w_e(y)dy - \int_{\xi+cs}^\infty w_i(y)dy\right]ds + I. \tag{2.14}$$

It is convenient to introduce the function

$$\Psi_{\xi_0}(z) = \int_z^\infty w_e(y)dy - \int_{-\infty}^{z-\xi_0} w_i(y)dy. \tag{2.15}$$

Exploiting the fact that the Gaussian weight distributions $w_e(y)$ and $w_i(y)$ are even functions of y, it can be seen that

$$\Psi_{\xi_0}(\xi_0 - z) = \int_{-\infty}^{z-\xi_0} w_e(y)dy - \int_z^\infty w_i(y)dy, \tag{2.16}$$

so that equations (2.13) and (2.14) can be rewritten in the more compact form

$$U(\xi) = \int_0^\infty \eta(s)\Psi_{\xi_0}(\xi + cs)ds + I \tag{2.17}$$

$$V(\xi) = \int_0^\infty \eta(s)\Psi_{\xi_0}(\xi_0 - \xi - cs) + I. \tag{2.18}$$

Finally, imposing the threshold conditions $U(0) = V(\xi_0) = \kappa$ gives

$$\kappa = \int_0^\infty \eta(s)\Psi_{\xi_0}(cs)ds + I, \tag{2.19}$$

$$\kappa = \int_0^\infty \eta(s)\Psi_{\xi_0}(-cs)ds + I. \tag{2.20}$$

It is now straightforward to show that a traveling front solution cannot exist for the neural field model without adaptation given by equations (2.4) and (2.5). For subtracting equation (2.20) from (2.19) implies that

$$\int_0^\infty \eta(s)\left[\Psi_{\xi_0}(cs) - \Psi_{\xi_0}(-cs)\right]ds = 0, \tag{2.21}$$

which does not have a solution for any c, ξ_0 such that $c \neq 0$. The latter follows from equation (2.15), which shows that for $c \neq 0$,

$$\begin{aligned} &c\left[\Psi_{\xi_0}(cs) - \Psi_{\xi_0}(-cs)\right] \\ &= -c\int_{-cs}^{cs} w_e(y)dy - c\int_{-cs-\xi_0}^{cs-\xi_0} w_i(y)dy < 0 \end{aligned}$$

whereas $\eta(s) > 0$ for all $s \in [0, \infty)$. The non-existence of traveling fronts is consistent with the observation that in the absence of any cross-inhibition ($w_i \equiv 0$), the system reduces to two independent one–dimensional neural fields with excitatory connections. In order to construct a front solution that simultaneously invades one network whilst retreating from the other we would require a one–dimensional excitatory neural field to be able to support a pair of counter-propagating front solutions with speeds $\pm c$, which is not consistent with Amari neural fields (wave speeds are unique, see equation (1.36)). Therefore, some mechanism must be introduced that breaks the exchange symmetry of the two one–dimensional networks. This cannot be achieved simply by taking $I_u \neq I_v$, since binocular rivalry waves are still observed when the left and right eye stimuli have the same contrast. An alternative approach is to introduce slow synaptic depression.

2.2.2 Slow synaptic depression ($\beta > 0$, $\tau_s \gg 1$)

Let us now consider the full neural field model with depressing excitatory connections given by equations (2.1) and (2.2) with $f(u) = H(u - \kappa)$. As in the case $\beta = 0$, there are four possible homogeneous fixed points corresponding to an off-state, a fusion state and two WTA states, and all are stable. In fact for $\beta \neq 0$ the homogeneous system is the same as that considered in the

introduction. To recap, denoting a homogeneous fixed point by (U^*, V^*, Q_u^*, Q_v^*), we have

$$\begin{aligned}
U^* &= Q_u^* \overline{w}_e H(U^* - \kappa) - Q_v^* \overline{w}_i H(V^* - \kappa) + I \\
Q_u^* &= \frac{1}{1 + \beta H(U^* - \kappa)} \\
V^* &= Q_v^* \overline{w}_e H(V^* - \kappa) - Q_u^* \overline{w}_i H(U^* - \kappa) + I \\
Q_v^* &= \frac{1}{1 + \beta H(V^* - \kappa)}
\end{aligned}$$

with $\overline{w}_e, \overline{w}_i$ given by equation (2.10). Hence, the fusion state is now

$$\begin{aligned}
(U^*, V^*) &= \left(\frac{\overline{w}_e - \overline{w}_i}{1 + \beta} + I, \frac{\overline{w}_e - \overline{w}_i}{1 + \beta} + I \right), \\
(Q_u^*, Q_v^*) &= \left(\frac{1}{1 + \beta}, \frac{1}{1 + \beta} \right),
\end{aligned} \tag{2.22}$$

and occurs when $I > \kappa - (\bar{w}_e - \bar{w}_i)/(1 + \beta)$. This case is more likely for very strong depression (β large), since cross inhibition will be weak, or when the local connections are strong and excitation-dominated. The left eye dominant WTA state now takes the form

$$\begin{aligned}
(U^*, V^*) &= \left(\frac{\overline{w}_e}{1 + \beta} + I, I - \frac{\overline{w}_i}{1 + \beta} \right), \\
(Q_u^*, Q_v^*) &= \left(\frac{1}{1 + \beta}, 1 \right)
\end{aligned} \tag{2.23}$$

whereas the right eye dominant WTA state becomes

$$\begin{aligned}
(U^*, V^*) &= \left(I - \overline{w}_i, \frac{\overline{w}_e}{1 + \beta} + I \right), \\
(Q_u^*, Q_v^*) &= \left(1, \frac{1}{1 + \beta} \right).
\end{aligned} \tag{2.24}$$

The WTA states exist provided that

$$I > \kappa - \frac{\overline{w}_e}{1 + \beta}, \quad I < \kappa + \frac{\overline{w}_i}{1 + \beta}. \tag{2.25}$$

This will occur in the presence of weak depression (β small) and strong cross-inhibition such that depression cannot exhaust the dominant hold one population has on the other. As shown in section 1.1.3, the system supports rivalrous oscillations which cannot arise via a standard Hopf bifurcation. To recap, instead the system supports bistable regimes in which a rivalry state coexists with a fusion

state as illustrated in Fig. 2.2. (Such behaviour persists in the case of smooth sigmoid firing rate functions, at least for sufficiently high gain ([47])).

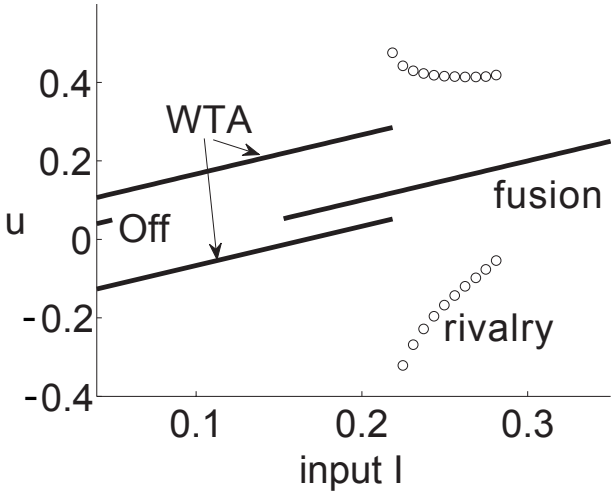

Figure 2.2: Bifurcation diagram showing homogeneous solutions for the left population activity u as a function of the input amplitude I. Solid lines represent stable states, whereas circles represent the maximum and minimum of rivalrous oscillations. It can be seen that there are regions of off/WTA bistability, WTA/fusion bistability, and fusion/rivalry bistability. Parameters are $\tau_s = 500$, $\kappa = 0.05$, $\beta = 5$, $\overline{w}_e = 0.4$ and $\overline{w}_i = -1$. Reproduced from [47].

Suppose that the full system given by equations (2.1) and (2.2) is initially in a stable right eye dominated WTA state, and is then perturbed away from this state by introducing a propagating front that generates a switch from right to left eye dominance. We further assume that over a finite spatial domain of interest the time taken for the wave front to propagate is much smaller than the relaxation time τ_s of synaptic depression. Thus, to a first approximation we can ignore the dynamics of the depression variables and assume that they are constant, that is, $(q_u(x,t), q_v(x,t)) = (Q_u, Q_v)$ with $Q_u = 1$ and $Q_v = (1+\beta)^{-1}$. A similar adiabatic approximation can also be made if the network is in a binocular rivalry state, provided that (a) the duration of wave propagation is short compared to the natural switching period and (b) the induction of the wave does not occur close to the point at which spontaneous switching occurs. In this case Q_u and Q_v will not be given by the WTA solution, but we can assume that $Q_u \neq Q_v$. Under the adiabatic approximation, we obtain a slightly modified version of equations (2.4) and (2.5) given by

$$\begin{aligned} u(x,t) &= I + Q_u \int_0^\infty \eta(s) G_e[u](x,t-s)ds \\ &\quad -Q_v \int_0^\infty \eta(s) G_i[v](x,t-s)ds \end{aligned} \tag{2.26}$$

$$v(x,t) = I + Q_v \int_0^\infty \eta(s) G_e[v](x,t-s)ds \\ -Q_u \int_0^\infty \eta(s) G_i[u](x,t-s)ds. \tag{2.27}$$

with $G_{e,i}$ given by equation (2.9). The analysis of the existence of a traveling wave front solution proceeds along identical lines to section 2.2.1, except that now the asymptotic states take the form

$$\mathbf{X}_L = (q_u \overline{w}_e + I, I - q_v \overline{w}_i),\ \mathbf{X}_R = (I - q_u \overline{w}_i, q_v \overline{w}_e + I). \tag{2.28}$$

We thus obtain the following modified threshold conditions:

$$\kappa = \int_0^\infty \eta(s) \Psi_{\xi_0}(cs)ds + I, \tag{2.29}$$

$$\kappa = \int_0^\infty \eta(s) \Phi_{\xi_0}(-cs)ds + I, \tag{2.30}$$

with Ψ and Φ defined by

$$\Psi_{\xi_0}(z) = Q_u \int_z^\infty w_e(y)dy - Q_v \int_{-\infty}^{z-\xi_0} w_i(y)dy, \tag{2.31}$$

$$\Phi_{\xi_0}(z) = Q_v \int_z^\infty w_e(y)dy - Q_u \int_{-\infty}^{z-\xi_0} w_i(y)dy. \tag{2.32}$$

It can be seen that synaptic depression breaks the symmetry of the consistency equations, and this will allow us to find solutions for c, ξ_0 and thus establish the existence of traveling front solutions.

2.2.3 Calculation of wave speed

In order to establish the existence of a wave speed c and a threshold crossing point ξ_0, define the functions

$$F_1(c,\xi_0) = \int_0^\infty \eta(s) \Psi_{\xi_0}(cs)ds \tag{2.33}$$

and

$$F_2(c,\xi_0) = \int_0^\infty \eta(s) \Phi_{\xi_0}(-cs)ds. \tag{2.34}$$

Evaluating the integrals using equations (2.3), (2.31), (2.32) and $\eta(s) = e^{-s}$ gives (for $c > 0$)

$$\begin{aligned} F_1(c,\xi_0) &= \frac{a_e Q_u}{2}\left(1 - e^{\frac{\sigma_e^2}{2\tau^2 c^2}}\,\mathrm{Erfc}\left[\frac{\sigma_e}{\sqrt{2}\tau c}\right]\right) \\ &\quad -\frac{a_i Q_v}{2}\left(\mathrm{Erfc}\left[\frac{\xi_0}{\sqrt{2}\sigma_i}\right]\right. \\ &\quad \left. -e^{\frac{\sigma_i^2 - 2\tau c\xi_0}{2\tau^2 c^2}}\,\mathrm{Erfc}\left[\frac{\sigma_i^2 - \tau c\xi_0}{\sqrt{2}\sigma_i \tau c}\right]\right) \end{aligned} \tag{2.35}$$

$$\begin{aligned} F_2(c,\xi_0) &= \frac{a_e Q_v}{2}\left(1 + e^{\frac{\sigma_e^2}{2\tau^2 c^2}}\,\mathrm{Erfc}\left[\frac{\sigma_e}{\sqrt{2}\tau c}\right]\right) \\ &\quad -\frac{a_i Q_u}{2}\left(\mathrm{Erfc}\left[\frac{\xi_0}{\sqrt{2}\sigma_i}\right]\right. \\ &\quad \left. -e^{\frac{\sigma_i^2 + 2\xi_0\tau c}{2\tau^2 c^2}}\,\mathrm{Erfc}\left[\frac{\sigma_i^2 + \xi_0\tau c}{\sqrt{2}\sigma_i \tau c}\right]\right) \end{aligned} \tag{2.36}$$

where

$$\mathrm{Erfc}(x) = \frac{2}{\sqrt{\pi}}\int_x^\infty e^{-t^2}dt \tag{2.37}$$

is the complementary error function. Subtracting equation (2.30) from (2.29), we then have the implicit equation

$$G(c,\xi_0) \equiv F_1(c,\xi_0) - F_2(c,\xi_0) = 0. \tag{2.38}$$

It is straightforward to show that for fixed ξ_0,

$$\lim_{c\to\infty} G(c,\xi_0) > 0, \quad \lim_{c\to-\infty} G(c,\xi_0) < 0. \tag{2.39}$$

Hence, the intermediate value theorem guarantees at least one solution $c = c(\xi_0)$, which is differentiable by the implicit function theorem. If $Q_u = Q_v$, then $F_1(0,\xi_0) = F_2(0,\xi_0)$ and the only point where G vanishes is at $c = 0$. On the other hand, if $Q_v \neq Q_u$ then $G(0,\xi_0) \neq 0$ for all finite ξ_0 so that $c(\xi_0) \neq 0$. Given a solution $c = c(\xi_0)$ of equation (2.38), the existence of a traveling wavefront solution reduces to the single threshold condition

$$\kappa = F_1(c(\xi_0),\xi_0) + I. \tag{2.40}$$

We find that there exists a unique traveling front solution for a range of values of κ.

In Figs. 2.3 and 2.4, we plot wave speed as a function of various model parameters. We choose

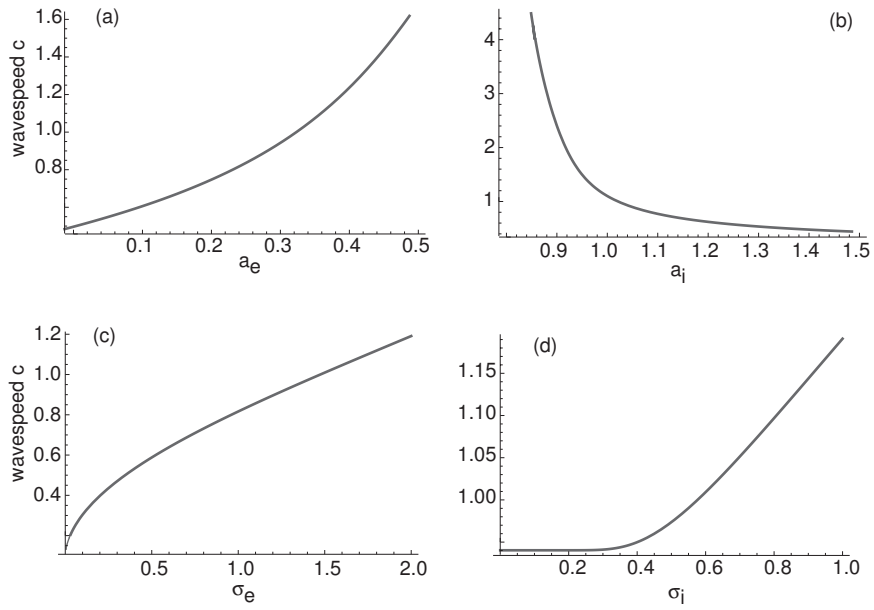

Figure 2.3: Plot of wave speed c as a function of various weight parameters: (a,b) the amplitudes a_e, a_i and (c,d) the length constants σ_e, σ_i. The default parameters are taken to be $a_i = 1, a_e = 0.4, \sigma_i = 1, \sigma_e = 2, \beta = 5, \kappa = 0.05, I = 0.24, Q_u = 0.42, Q_v = 0.25$ and the corresponding wave speed is $c = 1.2$. For this set of parameters, the network operates in a regime that supports both traveling waves and homogeneous oscillatory solutions, that is, spontaneous switching occurs in the absence of traveling waves.

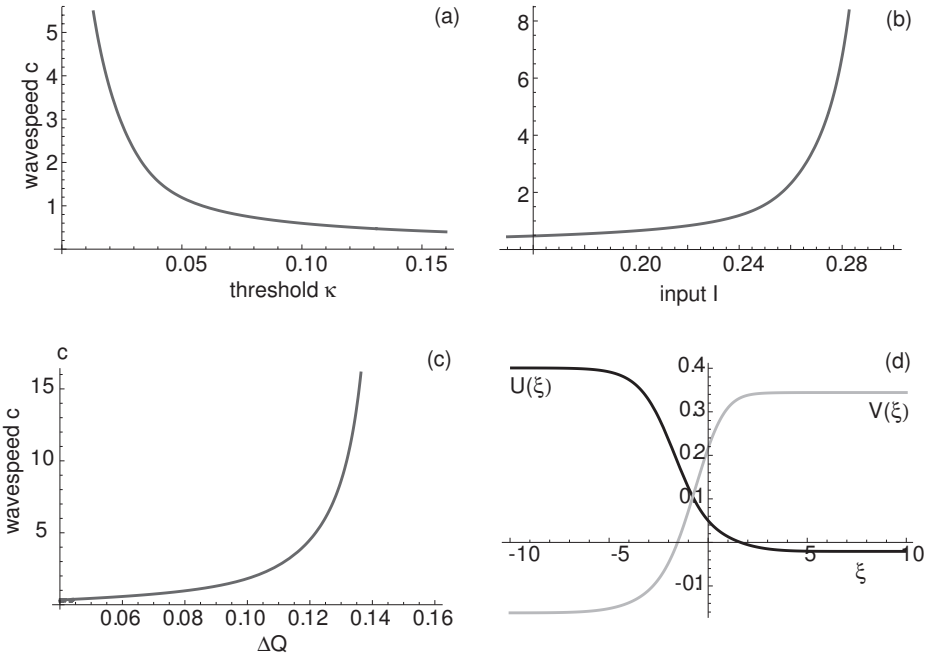

Figure 2.4: (a-c) Plot of wave speed c as a function of (a) the threshold κ, (b) the external input strength I and (c) ΔQ where $Q_u = Q_0 + \Delta Q, Q_v = Q_0 - \Delta Q$ with $Q_0 = 0.335$. (d) Plot of right–moving traveling front solution in which in which a high activity state invades the suppressed left eye network whilst retreating from the dominant right eye network. Parameters are at the baseline values of Fig. 2.3 unless specified otherwise.

baseline parameter values such that spontaneous oscillations and traveling fronts co-exist, as found experimentally [44, 45]. The model wave speed is of the order $c = 1$ in dimensionless units, that is, $c = \sigma_e/2\tau$ where σ_e is the range of excitation and τ is the membrane time constant. In the psychophysical experiments of Kang *et. al.* [44, 45], it was found that binocular rivalry waves took approximately 0.8 seconds to traverse 2 degrees of the visual field. The magnification factor in humans throughout the foveal region is approximately $0.4cm/deg$, which corresponds to $0.8cm$ of cortex. Hence the wave speed we would expect to see in cortex based on the psychophysical experiments is approximately $10mm/sec$. This is consistent with our analytical results, if we take σ_e to be of the order 200μm and τ to be of the order 10 milliseconds. Fig. 2.3 shows that increasing the strength of excitation (cross–inhibition) increases (decreases) the speed of the wave, whereas Fig. 2.3(a) shows that the speed of the wave decreases as the threshold κ increases. However, these parameters cannot be manipulated in psychophysical experiments. On the other hand, it is possible to vary the contrast of the sinusoidal grating stimuli. For example, Kang *et. al.* [44, 45] showed that increasing the stimulus contrast increases wave speed. This is consistent with Fig. 2.4(b), which plots wave speed as a function of input amplitude I. Another variable that could be manipulated is the time at which a rivalry wave is induced relative to the phase of the limit cycle representing spontaneous rivalry oscillations. In our model, under the adiabatic approximation, this would correspond to changing the values of Q_u and Q_v. In Fig. 2.4(c) we plot wave speed as a function of $\Delta Q = (Q_u - Q_v)/2$ with $Q_u + Q_v$ fixed. It can be seen that c increases with ΔQ, which is analogous to inducing a wave closer to the point at which spontaneous switching would occur (see also section 2.3). Note that in the experimental protocol of Kang *et. al.* [44, 45], see Fig. 1.5, the wave speed is determined after averaging with respect to the switching events induced by a sequence of periodic trigger stimuli rather than a single triggering event. In terms of our model, this would correspond to averaging the wave speed with respect to a range of values of Q_u and Q_v, since spontaneous binocular rivalry oscillations are actually noisy. Hence, the dependence of wave speed on the timing of the inducing stimuli relative to the phase of spontaneous oscillations is effectively reduced. However, Kang *et. al.* [44, 45] did find that there is an optimal trigger period for inducing reliable switching that depends on the natural period of spontaneous oscillations. It is likely that this phase–locking phenomenon reflects some residual dependence of wave propagation on the relative timing of the trigger stimuli. Finally, a typical example of a wavefront profile is shown in Fig. 2.4(d). Note that the symmetry breaking mechanism necessary to support wave propagation is reflected by the fact that $\lim_{\xi\to-\infty} U(\xi) > \lim_{\xi\to\infty} V(\xi)$. That is, the initial activity in the dominant right eye is depressed compared to the final activity in the dominant left eye (under the adiabatic

approximation).

2.2.4 Wave stability

In order to determine wave stability, we follow the procedure outlined in section 1.2.4 and linearize equations (2.26) and (2.27) around the traveling wave solution $(U(\xi), V(\xi))$ with Q_u, Q_v fixed. Writing $u(x,t) = U(\xi) + r(\xi)e^{\lambda t}$ and $v(x,t) = V(\xi) + p(\xi)e^{\lambda t}$ with $\mathrm{Re}[\lambda] > -1$, we obtain the linear system

$$\begin{aligned} r(\xi) &= Q_u \int_0^\infty \eta(s) \int_{-\infty}^\infty w_e(y) r(\xi + cs - y) e^{-\lambda s} \\ &\quad \times \delta(U(\xi + cs - y) - \kappa) dy ds \\ &\quad - Q_v \int_0^\infty \eta(s) \int_{-\infty}^\infty w_i(y) p(\xi + cs - y) e^{-\lambda s} \\ &\quad \times \delta(V(\xi + cs - y) - \kappa) dy ds \end{aligned}$$

$$\begin{aligned} p(\xi) &= Q_v \int_0^\infty \eta(s) \int_{-\infty}^\infty w_e(y) p(\xi + cs - y) e^{-\lambda s} \\ &\quad \times \delta(V(\xi + cs - y) - \kappa) dy ds \\ &\quad - Q_u \int_0^\infty \eta(s) \int_{-\infty}^\infty w_i(y) r(\xi + cs - y) e^{-\lambda s} \\ &\quad \times \delta(U(\xi + cs - y) - \kappa) dy ds, \end{aligned}$$

where $\delta(U - \kappa)$ denotes the Dirac delta function. Using the threshold conditions $U(0) = \kappa$, $V(\xi_0) = \kappa$ and a property of Dirac delta functions, we have

$$\delta(U(\xi)) = \frac{\delta(\xi)}{|U'(0)|}, \quad \delta(V(\xi)) = \frac{\delta(\xi - \xi_0)}{|V'(\xi_0)|}. \tag{2.41}$$

Hence,

$$\begin{aligned} r(\xi) &= Q_u \int_0^\infty \eta(s) w_e(\xi + cs) \frac{r(0)}{|U'(0)|} e^{-\lambda s} ds \\ &\quad - Q_v \int_0^\infty \eta(s) w_i(\xi + cs - \xi_0) \frac{p(\xi_0)}{|V'(\xi_0)|} e^{-\lambda s} ds \end{aligned} \tag{2.42}$$

$$
\begin{aligned}
p(\xi) &= Q_v \int_0^\infty \eta(s) w_e(\xi + cs - \xi_0) \frac{p(\xi_0)}{|V'(\xi_0)|} e^{-\lambda s} ds \\
&\quad -Q_u \int_0^\infty \eta(s) w_i(\xi + cs) \frac{r(0)}{|U'(0)|} e^{-\lambda s} ds.
\end{aligned}
\tag{2.43}
$$

Introducing an appropriate norm (e.g. L^2 norm) on the space of functions $(r(\xi), p(\xi))$, the linear equations (2.42) and (2.43) generate a well defined spectral problem. In particular, the discrete spectrum of eigenvalues λ is obtained by finding solutions $r(\xi)$ and $p(\xi)$ that decay sufficiently fast as $|\xi| \to \infty$ – the rate of decay is determined by the weight functions w_e, w_i. These eigensolutions can be found by setting $\xi = 0$ in equation (2.42) and $\xi = \xi_0$ in equation (2.43), and solving the resulting self–consistency equations for $r(0)$ and $p(\xi_0)$:

$$
\begin{pmatrix} r(0) \\ p(\xi_0) \end{pmatrix} = \begin{pmatrix} \frac{Q_u \widehat{W}_e(\lambda,0)}{|U'(0)|} & -\frac{Q_v \widehat{W}_i(\lambda,-\xi_0)}{|V'(\xi_0)|} \\ -\frac{Q_u \widehat{W}_i(\lambda,\xi_0)}{|U'(0)|} & \frac{Q_v \widehat{W}_e(\lambda,0)}{|V'(\xi_0)|} \end{pmatrix} \begin{pmatrix} r(0) \\ p(\xi_0) \end{pmatrix} \tag{2.44}
$$

where

$$
\widehat{W}_p(\lambda, \xi) = \int_0^\infty \eta(s) w_p(cs + \xi) e^{-\lambda s} ds \tag{2.45}
$$

for $p = e, i$. The self–consistency equation has a non-trivial solution provided that λ is a zero of the function

$$
E(\lambda) = \det \begin{pmatrix} \frac{Q_u \widehat{W}_e(\lambda,0)}{|U'(0)|} - 1 & -\frac{Q_v \widehat{W}_i(\lambda,-\xi_0)}{|V'(\xi_0)|} \\ -\frac{Q_u \widehat{W}_i(\lambda,\xi_0)}{|U'(0)|} & \frac{Q_v \widehat{W}_e(\lambda,0)}{|V'(\xi_0)|} - 1 \end{pmatrix}. \tag{2.46}
$$

We identify $E(\lambda)$ as the Evans function of the traveling wave solution [83, 25, 65]. That is, the complex number λ is an eigenvalue of the linear system if and only if $E(\lambda) = 0$ [25]. Moreover, the algebraic multiplicity of each eigenvalue is equal to the order of the corresponding zero of the Evans function. In this case $E(\lambda)$ is analytic in λ and thus normal numeric root finding may be used to find λ. The wave will be linearly stable if all non-zero eigenvalues λ have negative real part and $\lambda = 0$ is a simple eigenvalue. The existence of a zero eigenvalue reflects translation invariance of the dynamical system given by equations (2.26) and (2.27). (Note that there is also a continuous part of the spectrum, but this always lies in the left–half complex λ–plane for this system and thus does not contribute to any wave instabilities [25, 65]). Numerically plotting the zero sets $\mathrm{Re}[E[\lambda]]$ and $\mathrm{Im}[E[\lambda]]$ for the baseline parameter values shows that (2.46) has a single root at the origin, so there

exists only a single eigenvalue (at $\lambda = 0$), indicating that the traveling front is linearly stable. This result persists for many choices of parameters for which a traveling front exists.

2.3 Numerical simulations

In our analysis of binocular rivalry waves (section 2.2), we neglected the dynamics of the depression variables by making an adiabatic approximation. In this section we numerically solve the full system of equations (2.1) and (2.2) and show that traveling fronts persist when the dynamics of the depression variables is included.

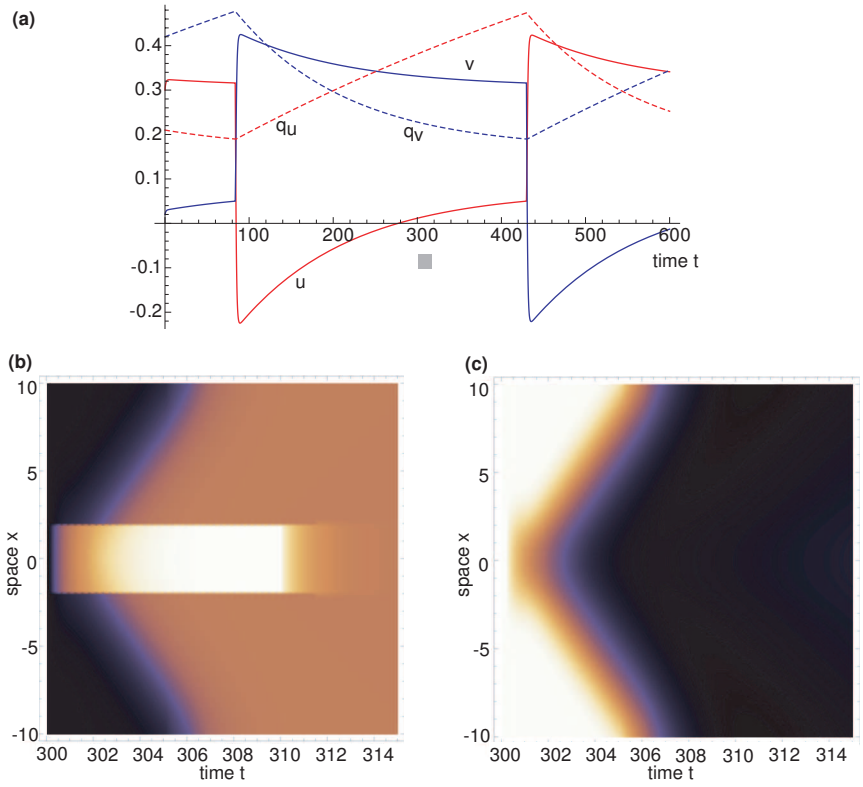

Figure 2.5: Induction of a solitary binocular rivalry wave. Parameter values are $\tau_s = 800, a_i = 1, a_e = 0.4, \sigma_i = 1, \sigma_e = 2, \beta = 5, \kappa = 0.05, I = 0.24$. (a) Homogeneous oscillatory solution in which there is spontaneous periodic switching between left and right eye dominance. Plot against time of the left eye neural activity u (solid red), the right eye neural activity v (solid blue) together with the corresponding depression variables q_u (dashed red) and q_v (dashed blue). (b,c) Space–time plots of $u(x,t)$ and $v(x,t)$ following onset of the trigger stimulus to the left eye at time $t_0 = 300$, which involves a temporary increase in the input strength I_u from 0.24 to 0.74 within the domain $-2 \leq x \leq 2$. (The duration of the trigger stimulus is also indicated by the grey bar in part (a)). Lighter (darker) colors indicate higher (lower) activity values. The mean wave speed of the front (calculated numerically as the average speed of the level set $u(x(t),t) = 0.3$)) is $c \sim 2$. This is in good agreement with our analytical results based on taking fixed depression variables $Q_u = q_u(t_0), Q_v = q_v(t_0)$.

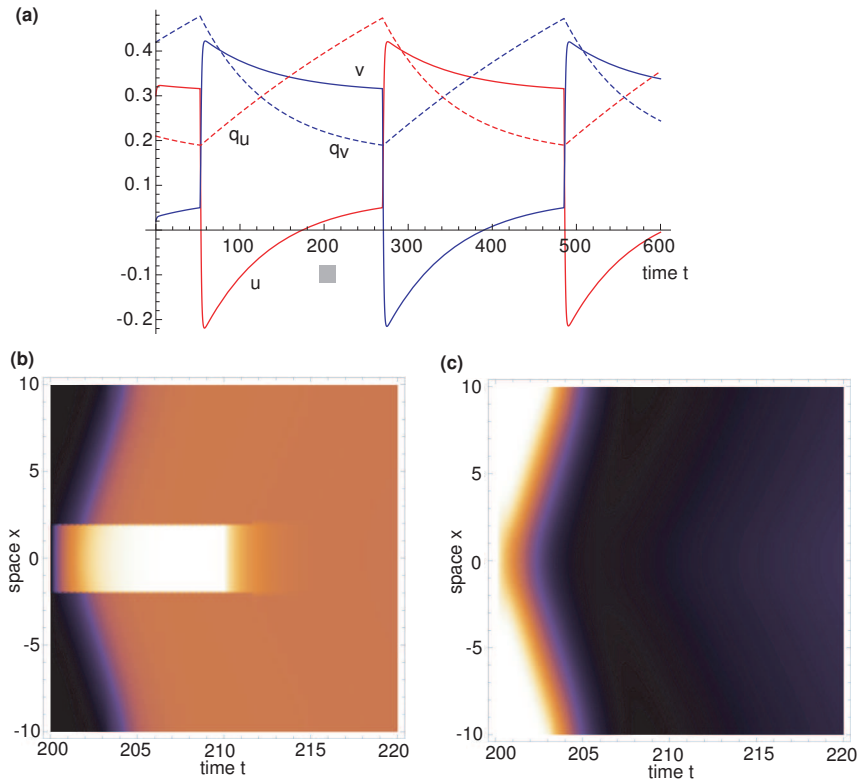

Figure 2.6: Same as Fig. 2.5 except that $\tau_s = 500$. Onset of trigger stimulus is at $t_0 = 200$. Both the frequency of spontaneous oscillations and the speed of the wave are higher with $c \sim 3$

We begin by considering a single trigger stimulus in the form of a temporary, spatially localized increase in the input strength to the suppressed eye network, which for concreteness we take to be the left eye. Thus,

$$\begin{aligned} I_u(x,t) &= \Theta(t-t_0)\Theta(\Delta t + t_0 - t)\Theta(\Delta x - |x|)\Delta I \\ &\quad + I, \\ I_v(x,t) &= I \end{aligned}$$

where Θ is the Heaviside function. The trigger stimulus is switched on at $t = t_0$ and switched off at time $t = t_0 + \Delta t$, and consists of an increase in input strength ΔI in a region of width $2\Delta x$ centered about $x = 0$. In order for traveling waves to be induced in our model, the size Δx of the excited region has to be of the order of σ_e, otherwise the effects of the perturbation simply die away. This is consistent with the size of perturbation used in the experiments by Kang *et. al.* [44, 45], which was of size 0.2 degrees, corresponding to $0.8mm$ of cortical tissue. Their perturbations were shown for $200ms$, similar to the time interval of $\Delta t = 10$ used in our simulations. Two examples of induced binocular rivalry waves are shown in Fig. 2.5 and Fig. 2.6. In these examples, the wave speed is fast relative to the frequency of spontaneous oscillations so the depression variables change very little over the time during which the wave is traveling. Hence, there is a good match between properties of the numerically simulated wave and our analytical results of section 2.2. In Fig. 2.7 we further illustrate the good agreement between theory and numerics by plotting the location x vs. time t of a fixed point in traveling wave coordinates given by $u(x,t) = 0.3$. As expected, there is a small variation in wave speed due to the dynamics of the depression variables but the mean speed is consistent with theory.

Since the network operates in a regime where spontaneous rivalry oscillations occur in the absence of any trigger stimuli, it follows from our analytical results (section 2.2) that the speed of the induced wave will depend on which phase of the limit cycle the trigger stimulus is initiated. That is, let the time of stimulus onset be $t_0 = nT + \theta T/(2\pi)$, where T is the period of spontaneous oscillations, n is an integer and $0 \leq \theta < 2\pi$. Denoting the oscillatory solution of the depression variables on the limit cycle by $\{q_u^*(\phi), q_v^*(\phi) | 0 \leq \phi < 2\pi\}$, we set $Q_u = q_u^*(\theta), Q_v = q_v^*(\theta)$ where Q_u, Q_v are the fixed values appearing in equations (2.26) and (2.27) under the adiabatic approximation. It follows that the wave speed calculated from equation (2.40) is phase–dependent: $c = c(Q_u, Q_v) = c(\theta)$. An example plot of wave speed vs phase θ is shown in Fig. 2.8. We see that a rivalry wave only exists if the trigger stimulus occurs in the latter $\sim \frac{2}{3}$ of the half–cycle, with faster waves induced closer to the

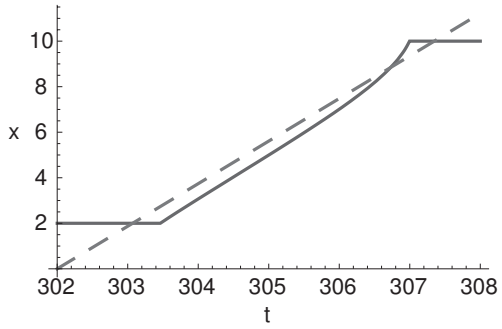

Figure 2.7: Plot of the spatial location x vs. time t of the point at which $u(x,t) = 0.3$ (solid curve). Same parameter values as Fig. 2.5 with onset of trigger stimulus at $t_0 = 300$. There is a latency period before the wave front reaches the initial location of the point $u = 0.3$. The wave front moves with approximately constant speed that is consistent with the theoretical value as indicated by the dashed line of constant slope.

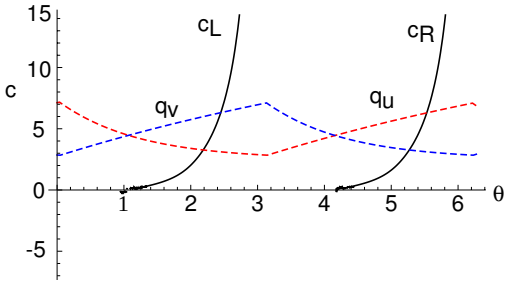

Figure 2.8: Wavespeed vs phase (solid curve) along one cycle of spontaneous oscillations. Here c_L (c_R) denotes the speed of a wave induced in the suppressed left (right) eye network. Also shown are the temporal profiles of the depression variables (dashed curves). Same parameter values as Fig. 2.6.

point of spontaneous switching. Now suppose that we keep the phase of the trigger stimulus fixed and determine how both the natural frequency $1/T$ and wave speed c vary with stimulus contrast I. The results are presented in Fig. 2.9. The wave speed is determined from equation (2.40), whereas the period T is calculated using the analytical results of [47]. It can be seen that faster natural alternation rates lead to faster wave speeds. (Wavespeed and frequency also covary with changes in the depression rate constant β, for example). Interestingly, an analogous result was obtained by Kang *et. al.* [44, 45], who found experimentally that traveling waves were faster for subjects whose natural rate of binocular rivalry oscillations was higher. However, as noted in section 2.2, the wave speed was averaged over several cycles of trigger stimuli in the psychophysical experiments. Given the stochastic nature of spontaneous oscillations, we expect such averaging to reduce the dependence on the phase θ.

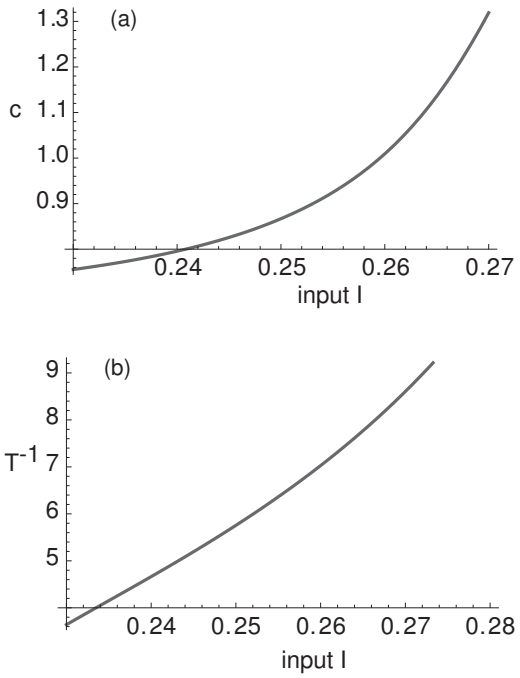

Figure 2.9: Wavespeed and frequency of spontaneous oscillations covary. Plot of (a) wavespeed c and alternation rate $\frac{1}{T}$ as a function of stimulus contrast I. The depression parameters Q_u, Q_v are determined by taking the phase θ of stimulus onset to be $\theta = 3\pi/2$. All other parameters are given by the baseline values of Fig. 2.3.

In order to relate our model more closely with the experimental protocol of Kang *et al.* [44, 45], we have also carried out simulations of the full model (2.1) and (2.2) in the presence of additive noise and periodic trigger stimuli. For the sake of illustration, we introduce spatially uncorrelated

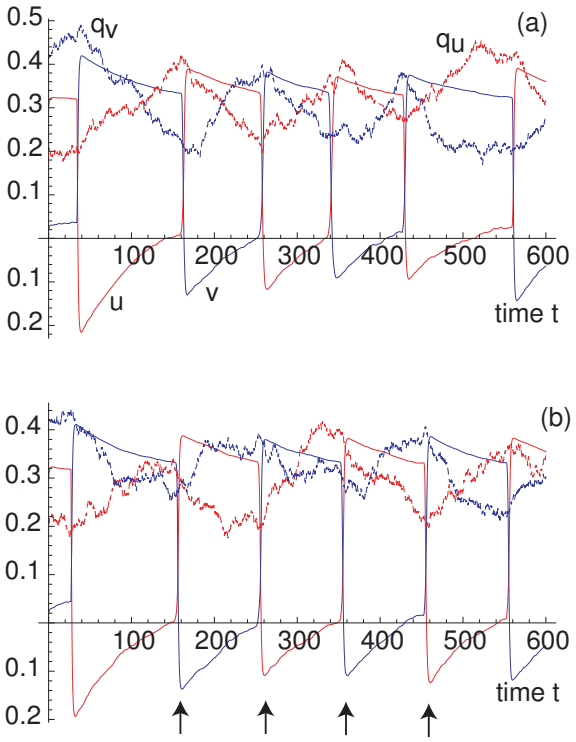

Figure 2.10: Comparison of spontaneous and periodically forced binocular rivalry oscillations in the presence of noise. The time evolution of the activity and depression variables are shown at a fixed spatial location ($x = 7$). Noise strength $\sigma = 1$ and all other parameter values are as in Fig. 2.6. Left (right) eye variables are shown in red (blue) with noise in the depression variables. (a) Homogeneous oscillatory solution, which shows some irregularity due to noise in the depression variables (b) Periodically triggered alternations in dominance. Onset of each trigger stimulus is indicated by an arrow. Initial trigger occurs at $t_0 = 150$ and time between triggers is $T_0 = 100$.

additive white noise terms to the the dynamical equations for the depression variables according to

$$\begin{aligned}\tau_s \frac{\partial q_{u,x}(t)}{\partial t} &= 1 - q_{u,x}(t) - \beta q_{u,x}(t) f(u(x,t)) \\ &\quad + \sigma \xi_{u,x}(t) \qquad (2.47)\\ \tau_s \frac{\partial q_{v,x}(t)}{\partial t} &= 1 - q_{v,x}(t) - \beta q_{v,x}(t) f(v(x,t)) \\ &\quad + \sigma \xi_{v,x}(t) \qquad (2.48)\end{aligned}$$

with

$$\langle \xi_{u,x}(t) \rangle = \langle \xi_{v,x}(t) \rangle = 0 \qquad (2.49)$$

and

$$\begin{aligned}\langle \xi_{u,x}(t) \xi_{u,x'}(t') \rangle &= \delta(x - x') \delta(t - t'), \\ \langle \xi_{v,x}(x) \xi_{v,x'}(t') \rangle &= \delta(x - x') \delta(t - t') \\ \langle \xi_{u,x}(t) \xi_{v,x'}(t') \rangle &= 0.\end{aligned}$$

Note that unlike the situation where there is noise in activity variables (such as the examples in section 1.4), we do not need to introduce any correlation structure here. Furthermore, the inputs I_u and I_v in equations (2.1a) and (2.2a) take the form

$$\begin{aligned}I_u(x,t) &= I + \sum_{m=0,2,4,\ldots} \Theta(t - t_0 - mT_0) \\ &\quad \times \Theta(\Delta t + t_0 + mT_0 - t) \Theta(\Delta x - |x|) \Delta I, \\ I_v(x,t) &= I + \sum_{m=1,3,5,\ldots} \Theta(t - t_0 - mT_0) \\ &\quad \times \Theta(\Delta t + t_0 + mT_0 - t) \Theta(\Delta x - |x|) \Delta I.\end{aligned}$$

That is, starting at time $t = t_0$, the left and right eye networks receive a T_0–periodic alternating sequence of trigger stimuli, each of which consists of an enhancement of input strength in the domain $|x| < \Delta x$ that has duration Δt.

Results from numerical simulations of the full model given by equations (2.1a), (2.2a), (2.47) and (2.48) are shown in Figs. 2.10 and 2.11. It can be seen that provided the noise strength σ is not too large then there is reliable switching between left and right eye dominance that phase locks to the periodic trigger stimuli. However, as σ increases to a value of around $\sigma \approx 2$, phase

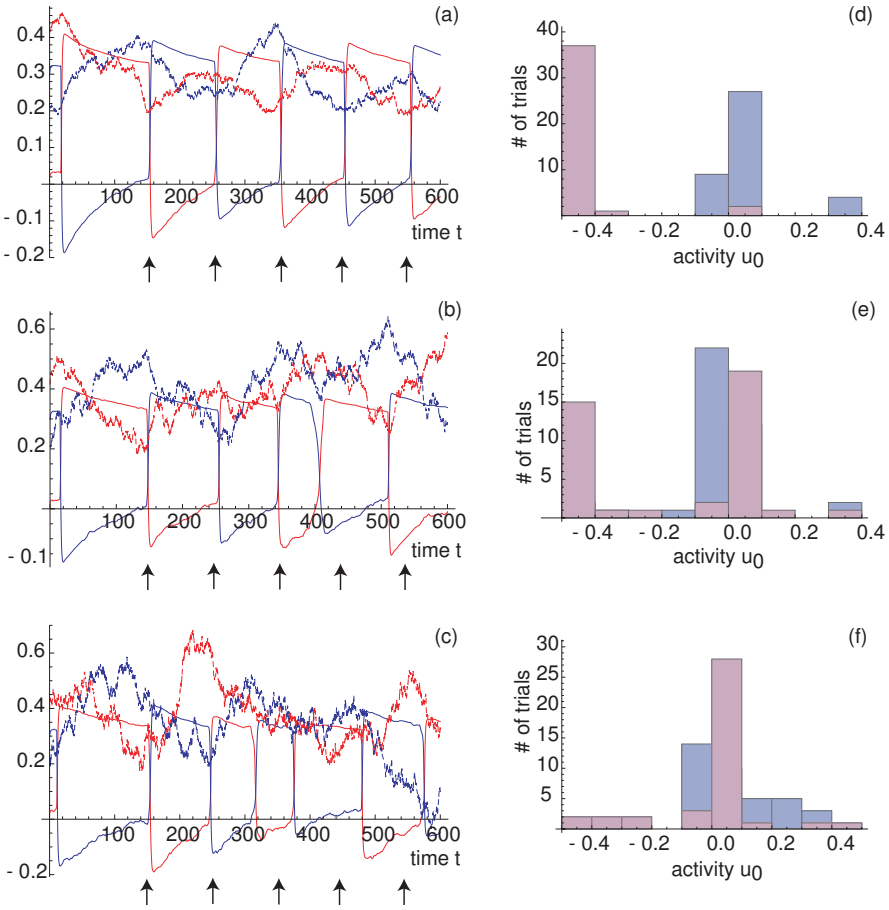

Figure 2.11: Breakdown of mode–locking as noise strength increases. (a-c). The time evolution of the activity and depression variables are shown at a fixed spatial location ($x = 7$) for various noise strengths: (a) $\sigma = 1$, (b) $\sigma = 2$, (c) $\sigma = 3$. All other parameter values are as in Fig. 2.10. Onset of each trigger stimulus is indicated by an arrow. Initial trigger occurs at $t_0 = 150$ and time between triggers is $T_0 = 100$. (d-e) Corresponding histograms showing how the change in activity $\Delta u = u(x, t_1) - u(x, t_2)$ at a fixed location $x = 7$ and two different times $(t_1 = 450, t_2 = 470)$ is distributed over multiple trials. Pink (purple) bars indicate distribution in the presence (absence) of periodic trigger stimuli

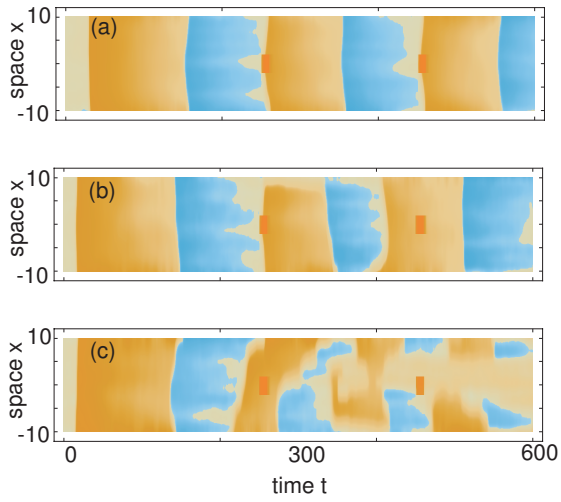

Figure 2.12: Space–time plots of periodically triggered binocular rivalry waves in left eye network for increasing levels of noise: (a) $\sigma = 1$, (b) $\sigma = 2$, (c) $\sigma = 3$. Red rectangles indicate duration and spatial extent of trigger stimuli. All other parameters as in Fig. 2.11.

locking starts to break down. As a further illustration of how mode–locking depends on the level of noise, we also plot in Fig. 2.11 histograms comparing the spontaneous and forced distributions of activity $\Delta u = u(x, t_1) - u(x, t_2)$ at a fixed location x and fixed times time t_1, t_2 over multiple trials (simulation runs). For a noise strength $\sigma = 1$ it can be seen that mode locking causes a very strong tendency to be in the completely opposite state to that without mode locking, whereas for higher noise strengths $\sigma = 2, 3$ the distribution is much wider and in some situations the forcing did not change the state from the unforced case (breakdown of mode-locking). Finally, the disruption of binocular rivalry waves with increasing noise is illustrated by the space–time plots of the left network activity variable $u(x, t)$ in Fig. 2.12.

So far we have taken the firing rate function to be the Heaviside function (1.6) in order to compare our numerics with the analysis of section 2.2. As in many previous studies of neural field equations dating back to Amari [2], the use of Heavisides allowed us to construct explicit traveling wave solutions and to derive an explicit formula for the speed of the wave. However, it is important to check that the same basic mechanism of wave induction and propagation carries over to more realistic sigmoidal rate functions. This is indeed found to be the case, as is illustrated in Fig. 2.13. The speed of the wave is more variable than the Heaviside case but is still comparable in magnitude to theoretical predictions.

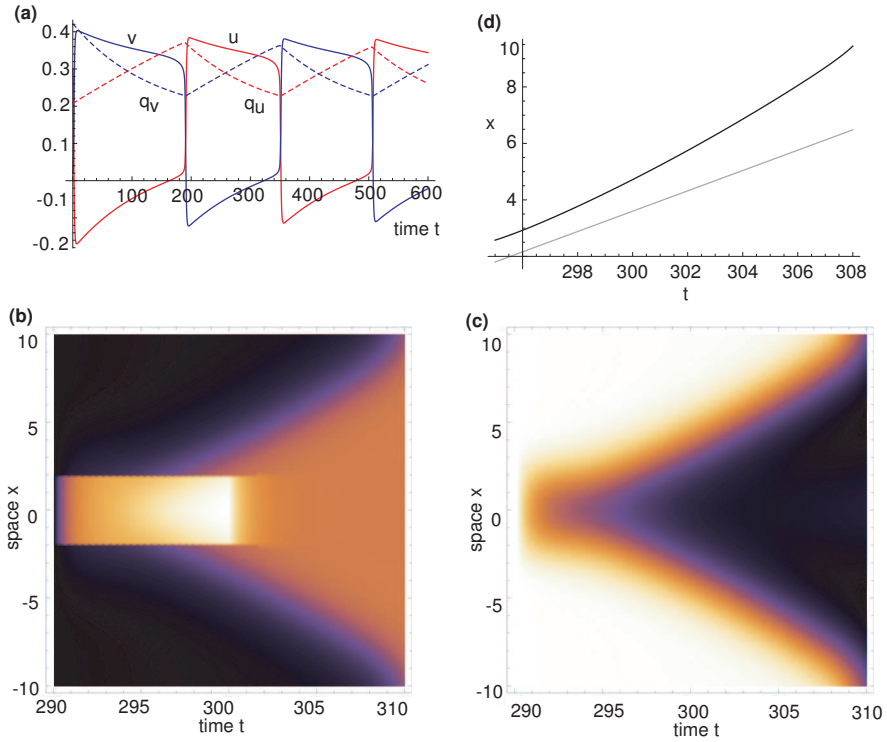

Figure 2.13: Induction of a solitary binocular rivalry wave in the case of a smooth sigmoidal firing rate function. Gain of sigmoid is $\eta = 80$. Other parameter values are as in Fig. 2.5 . (a) Homogeneous oscillatory solution in which there is spontaneous periodic switching between left and right eye dominance. Plot against time of the left eye neural activity u (solid red), the right eye neural activity v (solid blue) together with the corresponding depression variables q_u (dashed red) and q_v (dashed blue). (b,c) Space–time plots of $u(x,t)$ and $v(x,t)$ following onset of the trigger stimulus to the left eye at time $t_0 = 290$, which involves a temporary increase in the input strength I_u from 0.24 to 0.74 within the domain $-2 \leq x \leq 2$. Lighter (darker) colors indicate higher (lower) activity values. (d) Plot of the spatial location x vs. time t of the point at which $u(x,t) = 0.2$ (black curve). The speed calculated for the Heaviside case is given by the slope of the straight line (grey curve).

2.4 Discussion

In this section we analyzed a neural field model of binocular rivalry waves in primary visual cortex. Formulating the problem in terms of continuum neural field equations allowed us to study the short time behaviour associated with the propagation of eye dominance from an analytical perspective. In particular, we established that in order for traveling waves to exist, a symmetry breaking mechanism needs to be present. That is, the equations for the left and right eye networks have to be different on the time scales during which traveling waves propagate. We identified one possible mechanism for providing the necessary symmetry breaking, namely, synaptic depression. However any form of slow adaptation would work including spike frequency adaptation. We then showed analytically that for plausible values of biological parameters such as the range of synaptic interactions and the membrane time constant, we could recover wave speeds similar to those seen in experiments ([81, 44, 45]). Moreover, our model exhibited the expected dependence of wave speed on parameters that can be experimentally varied, such as stimulus contrast. It also replicated the experimental finding that wave speed depends in a monotonic way on the natural frequency of spontaneous rivalry oscillations. Finally, numerical simulations of the full system were in good agreement with our analytical short time scale results in the case of a Heaviside firing rate function. We also found that binocular rivalry waves persisted in the case of smooth sigmoid firing rate functions and in the presence of additive white noise in the depression variable dynamics. However, this treatment of noise relied on pure computer simulation. In order to gain a more complete understanding of noise it will first be necessary to develop a theory which will allow us to handle travelling waves in noisy neural fields. This is the subject of chapter 3.

Chapter 3

One Dimensional Stochastic Neural Fields

As previously mentioned in Section 1.4.1 stochastic front propagation has been an active research topic in the case of reaction-diffusion PDE systems. In this section we develop a general theory of fluctuating fronts in neural fields with extrinsic multiplicative noise by adapting these methods to our equations. The key idea will be to assume a separation of time scales in which there is a diffusive–like displacement (wandering) of the front from its uniformly translating position at long time scales, and fluctuations in the front profile around its instantaneous position at short time scales. In section 3.1 and section 3.2, we consider fronts propagating into a metastable state by taking the nonlinear firing rate function to be a sigmoid or Heaviside function. One major result of our analysis is a comparison between freely propagating fronts (see section 3.1) and fronts locked to an externally moving stimulus (see section 3.2). We show that the latter are much more robust to noise, since the center of mass of the front wanders according to an Ornstein–Uhlenbeck process rather than a Wiener process, so that the variance in front position saturates in the long time limit rather than increasing linearly with time.

3.1 Effects of multiplicative noise on freely propagating fronts

3.1.1 Stochastic neural field with multiplicative noise

We begin by considering a stochastic generalisation of Amari's original model, with phenomenological noise terms, as stated in section 1.4, for field variable $U(x,t)$:

$$dU(x,t) = \left[-U(x,t) + \int_{-\infty}^{\infty} w(x-y)F(U(y,t))dy\right]dt + \varepsilon^{1/2}g(U(x,t))dW(x,t) \tag{3.1}$$

As before, the object $dW(x,t)$ represents a line of Brownian motions such that

$$\langle dW(x,t)\rangle = 0, \quad \langle dW(x,t)dW(x',t')\rangle = 2C([x-x']/\lambda)\delta(t-t')dtdt'. \tag{3.2}$$

Here λ is explicitly the spatial correlation length of the noise such that $C(x/\lambda) \to \delta(x)$ in the limit $\lambda \to 0$, and ϵ determines the strength of the noise, which is assumed to be weak. For concreteness, we take C to have the same explicit form as that given in section 1.4. The multiplicative noise term is taken to be of Stratonovich form [39].

The effects of multiplicative noise on front propagation can be analyzed using methods previously developed for reaction–diffusion equations [55, 66, 26, 4, 64]; we will follow the particular formulation of Armero *et. al.* [4]. The starting point of such methods is the observation that multiplicative noise in the Stratonovich sense leads to a systematic shift in the mean speed of the front (assuming a front of speed c exists when $\varepsilon = 0$). This is a consequence of the fact that $\langle g(U)dW\rangle \neq 0$ even though $\langle dW\rangle = 0$. The former average can be calculated using Novikov's theorem [56]:

$$\varepsilon^{1/2}\langle g(U)dW\rangle = \varepsilon C(0)\langle g'(U)g(U)\rangle dt. \tag{3.3}$$

An alternative way to derive the above result is to Fourier transform equation (3.1) and evaluate averages using the corresponding Fokker–Planck equation in Fourier space (see appendix and [64]). Note that in the limit $\lambda \to 0$, $C(0) \to 1/\Delta x$ where Δx is a lattice cut–off, which can be identified with the step size of the spatial discretization scheme used in numerical simulations. Following [4], it is convenient to rewrite equation (3.1) so that the fluctuating term has zero mean:

$$dU(x,t) = \left[h(U(x,t)) + \int_{-\infty}^{\infty} w(x-y)F(U(y,t))dy\right]dt + \varepsilon^{1/2}dR(U,x,t), \tag{3.4}$$

where

$$h(U) = -U + \varepsilon C(0) g'(U) g(U) \tag{3.5}$$

and

$$dR(U,x,t) = g(U)dW(x,t) - \varepsilon^{1/2} C(0) g'(U) g(U) dt. \tag{3.6}$$

The stochastic process R has zero mean (so does not contribute to the effective drift, that is, the average wave speed) and variance

$$\langle dR(U,x,t) dR(U,x',t) \rangle = \langle g(U(x,t)) dW(x,t) g(U(x',t) dW(x',t) \rangle + \mathcal{O}(\varepsilon^{1/2}). \tag{3.7}$$

The next step in the analysis is to assume that the fluctuating term in equation (3.4) generates two distinct phenomena that occur on different time–scales: a diffusive–like displacement of the front from its uniformly translating position at long time scales, and fluctuations in the front profile around its instantaneous position at short time scales [55, 66, 26, 4, 64]. In particular, following [4], we express the solution U of equation (3.4) as a combination of a fixed wave profile U_0 that is displaced by an amount $\Delta(t)$ from its uniformly translating mean position $\xi = x - c_\varepsilon t$, and a time–dependent fluctuation Φ in the front shape about the instantaneous position of the front:

$$U(x,t) = U_0(\xi - \Delta(t)) + \varepsilon^{1/2} \Phi(\xi - \Delta(t), t). \tag{3.8}$$

Here c_ε denotes the mean speed of the front. We will assume that $\Delta(t)$ is only very weakly coupled to the stochastic neural field equation (3.4) so that to a first approximation, the stochastic variable $\Delta(t)$ undergoes Brownian motion with a diffusion coefficient $D(\varepsilon) = \mathcal{O}(\varepsilon)$ (see below), which represents the effects of slow fluctuations, whereas Φ represents the effects of fast fluctuations. Note that the expansion (3.8) is not equivalent to a standard small–noise expansion, since the wave profile U_0 implicitly depends on ε. Indeed, substituting equation (3.8) into equation (3.4) and taking averages generates to leading order the following deterministic equation for U_0:

$$-c_\varepsilon \frac{dU_0}{d\xi} - h(U_0(\xi)) = \int_{-\infty}^{\infty} w(\xi - \xi') F(U_0(\xi')) d\xi'. \tag{3.9}$$

Both the mean speed c_ε and U_0 depend non–trivially on the noise strength ε due to the ε–dependence of the function h, see equation (3.5). Thus, $c_\varepsilon \neq c$ for $\varepsilon > 0$ and $c_0 = c$, where c is the speed of the front in the absence of multiplicative noise. The next step is to substitute equation (3.8) into

equation (3.4) and Taylor expand both U and f to first order in $\mathcal{O}(\varepsilon^{\frac{1}{2}})$:

$$\begin{aligned}
-c_\varepsilon U_0'(\xi-\Delta(t))dt - U_0'(\xi-\Delta(t))d\Delta(t) + \varepsilon^{\frac{1}{2}}\left[d\Phi(\xi-\Delta(t),t) - c_\varepsilon\Phi'(\xi-\Delta(t),t)dt\right] \\
-\varepsilon^{\frac{1}{2}}\Phi'(\xi-\Delta(t),t)d\Delta(t) \\
= h(U_0(\xi-\Delta(t)))dt + h'(U_0(\xi-\Delta(t)))\varepsilon^{\frac{1}{2}}\Phi(\xi-\Delta(t),t)dt \\
+\int_{-\infty}^{\infty} w(\xi-\xi')\left(F(U_0(\xi'-\Delta(t))) + F'(U_0(\xi'-\Delta(t)))\varepsilon^{\frac{1}{2}}\Phi(\xi'-\Delta(t),t)\right)d\xi' dt \\
+\varepsilon^{\frac{1}{2}}dR(U_0(\xi-\Delta(t)),\xi,t) + \mathcal{O}(\varepsilon) \qquad (3.10)
\end{aligned}$$

Imposing equation (3.9), after shifting $\xi \to \xi - \Delta(t)$, we find that $\Delta(t) = \mathcal{O}(\varepsilon^{1/2})$ and

$$d\Phi(\xi,t) = \widehat{L}\circ\Phi(\xi,t)dt + \varepsilon^{-1/2}U_0'(\xi)d\Delta(t) + dR(U_0,\xi,t) \qquad (3.11)$$

where $\widehat{L}$ is the non–self–adjoint linear operator

$$\widehat{L}A(\xi) = c_\varepsilon\frac{dA(\xi)}{d\xi} + h'(U_0(\xi))A(\xi) + \int_{-\infty}^{\infty} w(\xi-\xi')F'(U_0(\xi'))A(\xi')d\xi' \qquad (3.12)$$

for any function $A(\xi) \in L_2(\mathbb{R})$.

It can be shown that for a sigmoid firing rate function and exponential weight distribution, the operator $\widehat{L}$ has a 1D null space spanned by $U_0'(\xi)$ [30]. (The fact that $U_0'(\xi)$ belongs to the null space follows immediately from differentiating equation (3.9) with respect to ξ). We then have the solvability condition for the existence of a nontrivial solution of equation (3.11), namely, that the inhomogeneous part is orthogonal to all elements of the null space of the adjoint operator $\widehat{L}^*$. The latter is defined with respect to the inner product

$$\int_{-\infty}^{\infty} B(\xi)\widehat{L}A(\xi)d\xi = \int_{-\infty}^{\infty}\left[\widehat{L}^*B(\xi)\right]A(\xi)d\xi \qquad (3.13)$$

where $A(\xi)$ and $B(\xi)$ are arbitrary integrable functions. Hence,

$$\widehat{L}^*B(\xi) = -c_\varepsilon\frac{dB(\xi)}{d\xi} + h'(U_0(\xi))B(\xi) + F'(U_0(\xi))\int_{-\infty}^{\infty} w(\xi-\xi')B(\xi')d\xi'. \qquad (3.14)$$

It can be proven that $\widehat{L}^*$ also has a one dimensional null-space [30], that is, it is spanned by some function $\mathcal{V}(\xi)$. Thus taking the inner product (3.13) of both sides of equation (3.11) with respect to

$\mathcal{V}(\xi)$ leads to the solvability condition

$$\int_{-\infty}^{\infty} \mathcal{V}(\xi) \left[U_0'(\xi) d\Delta(t) + \varepsilon^{1/2} dR(U_0, \xi, t) \right] d\xi = 0. \tag{3.15}$$

Thus $\Delta(t)$ satisfies the stochastic differential equation (SDE)

$$d\Delta(t) = -\varepsilon^{1/2} \frac{\int_{-\infty}^{\infty} \mathcal{V}(\xi) dR(U_0, \xi, t) d\xi}{\int_{-\infty}^{\infty} \mathcal{V}(\xi) U_0'(\xi) d\xi}. \tag{3.16}$$

Using the lowest order approximation $dR(U_0, \xi, t) = g(U_0(\xi)) dW(\xi, t)$, we deduce that (for $\Delta(0) = 0$)

$$\langle \Delta(t) \rangle = 0, \quad \langle \Delta(t)^2 \rangle = 2D(\varepsilon) t \tag{3.17}$$

where $D(\varepsilon)$ is the the effective diffusivity

$$\begin{aligned} D(\varepsilon) &= \varepsilon \frac{\int_{-\infty}^{\infty} \int_{-\infty}^{\infty} \mathcal{V}(\xi) \mathcal{V}(\xi') g(U_0(\xi)) g(U_0(\xi')) \langle dW(\xi, t) dW(\xi', t) \rangle d\xi d\xi'}{\left[\int_{-\infty}^{\infty} \mathcal{V}(\xi) U_0'(\xi) d\xi \right]^2} \\ &= \varepsilon \frac{\int_{-\infty}^{\infty} \mathcal{V}(\xi)^2 g^2(U_0(\xi)) d\xi}{\left[\int_{-\infty}^{\infty} \mathcal{V}(\xi) U_0'(\xi) d\xi \right]^2}. \end{aligned} \tag{3.18}$$

3.1.2 Explicit results for Heaviside rate function

We now illustrate the above analysis by considering a particular example where the mean speed c_ε and diffusion coefficient $D(\varepsilon)$ can be calculated explicitly. That is, we take $g(U) = g_0 U$ for the multiplicative noise term and set $F(U) = H(U - \kappa)$. (The constant g_0 has units of $\sqrt{\text{length/time}}$). The deterministic equation (3.9) for the mean profile U_0 then reduces to

$$-c_\varepsilon \frac{dU_0}{d\xi} + U_0(\xi)[1 - \varepsilon g_0^2 C(0)] = \int_{-\infty}^{\infty} w(\xi - \xi') H(U_0(\xi') - \kappa) d\xi'. \tag{3.19}$$

This is identical in structure to equation (1.27) for the deterministic neural field modulo the rescaling of the decay term. The analysis of the wave speeds proceeds as in section 1.2.3 and we find that for $c_\varepsilon > 0$,

$$c_\varepsilon = \gamma(\varepsilon) c_+(\gamma(\varepsilon)\kappa) = \frac{\sigma}{2\kappa}[1 - 2\kappa\gamma(\varepsilon)], \tag{3.20}$$

whereas, for $c_\varepsilon < 0$,

$$c_\varepsilon = \gamma(\varepsilon)c_+(\gamma(\varepsilon)\kappa) = \frac{\sigma\gamma(\varepsilon)}{2}\frac{1-2\kappa\gamma(\varepsilon)}{1-\kappa\gamma(\varepsilon)}, \tag{3.21}$$

with

$$\gamma(\varepsilon) = (1 - \epsilon g_0^2 C(0)), \tag{3.22}$$

and $c_\pm(\kappa)$ defined in equation (1.36). Assuming that $0 \leq \gamma(\varepsilon) \leq 1$, we see that multiplicative noise shifts the mean velocity of front propagation in the positive ξ direction.

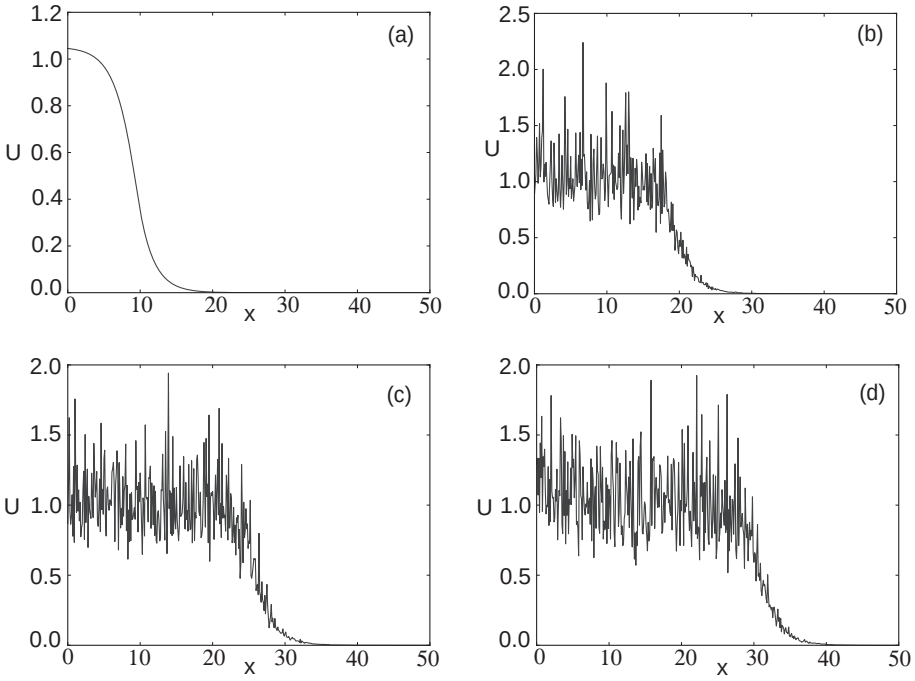

Figure 3.1: Numerical simulation showing the propagation of a front solution of the stochastic neural field equation (3.1) for Heaviside weight function $F(U) = H(U - \kappa)$ with $\kappa = 0.35$, exponential weight function (1.18) with $\sigma = 2$, and multiplicative noise $g(U) = U$. Noise strength $\epsilon = 0.005$ and $C(0) = 10$. The wave profile is shown at successive times (a) $t = 0$ (b) $t = 12$ (c) $t = 18$ and (d) $t = 24$, with the initial profile at $t = 0$ given by equation (3.25). In numerical simulations we take the discrete space and time steps $\Delta x = 0.1, \Delta t = 0.01$.

In order to calculate the diffusion coefficient, it is first necessary to determine the null vector $\mathcal{V}(\xi)$ of the adjoint linear operator $\widehat{L}^*$ defined by equation (3.14). Setting $F(U) = H(U - \kappa)$ and $g(U) = g_0 U$, the null vector $\mathcal{V}$ satisfies the equation

$$c_\varepsilon \mathcal{V}'(\xi) + [1 - \varepsilon g_0^2 C(0)]\mathcal{V}(\xi) = -\frac{\delta(\xi)}{U_0'(0)}\int_{-\infty}^{\infty} w(\xi')\mathcal{V}(\xi')d\xi'. \tag{3.23}$$

This can be solved explicitly to give [11]

$$\mathcal{V}(\xi) = -H(\xi)\exp\left(-\Gamma(\varepsilon)\xi\right), \quad \Gamma(\epsilon) = \frac{\gamma(\varepsilon)}{c_\varepsilon}. \tag{3.24}$$

We have used the fact that the solution to equation (3.19) is of the form

$$U_0(\xi) = -\frac{1}{c_\varepsilon}\int_0^\infty e^{-\Gamma(\varepsilon)y} W(y+\xi)dy, \tag{3.25}$$

with $W(\xi)$ defined in equation (1.21) and, hence,

$$U_0'(\xi) = -\frac{1}{c_\varepsilon}\int_0^\infty e^{-\Gamma(\varepsilon)y} w(y+\xi)dy. \tag{3.26}$$

In the case of an exponential weight distribution, $U_0(\xi)$ can be evaluated explicitly to give

$$U_0(\xi) = \begin{cases} \dfrac{1}{2c_\varepsilon}\dfrac{\sigma e^{-\xi/\sigma}}{1+\sigma\Gamma(\varepsilon)} & \xi \geq 0 \\ \dfrac{1}{2c_\varepsilon}\left[\dfrac{2e^{\xi\Gamma(\varepsilon)}}{\Gamma(\varepsilon)\left(-1+\sigma^2\Gamma(\varepsilon)^2\right)} + \dfrac{2}{\Gamma(\varepsilon)} + \dfrac{\sigma e^{\xi/\sigma}}{1-\sigma\Gamma(\varepsilon)}\right] & \xi < 0. \end{cases} \tag{3.27}$$

Using equation (3.24), equation (3.18) reduces to the form

$$D(\varepsilon) = \varepsilon\frac{\displaystyle\int_0^\infty e^{-2\Gamma(\varepsilon)\xi}U_0(\xi)^2 d\xi}{\left[\displaystyle\int_0^\infty e^{-\Gamma(\varepsilon)\xi}U_0'(\xi)d\xi\right]^2}. \tag{3.28}$$

which can be evaluated explicitly using equation (3.27) to obtain

$$D(\varepsilon) = \frac{1}{2}\varepsilon\sigma g_0^2(1+\sigma\Gamma(\varepsilon)) \tag{3.29}$$

In Fig. 3.1 we show the temporal evolution of a single stochastic wave front, which is obtained by numerically solving the Langevin equation (3.1) for $F(U) = H(U-\kappa)$, $g(U) = U$ and an exponential weight distribution w. Until this point we have assumed that the stochastic wave front has a well defined position, but it is not clear how we should define it. One possible approach which has been used by other authors [53] is to assume the wave has a certain shape (e.g. the deterministic solution) and then compute where this shape would have to be to minimise the L^2 norm of the difference between the observed stochastic wave and the deterministic shape. However,

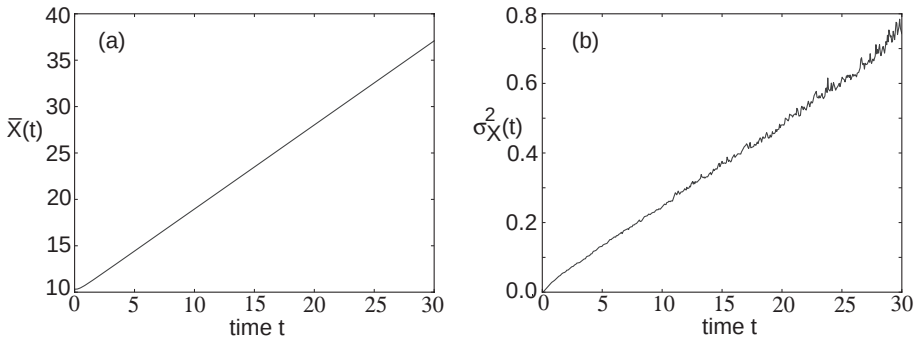

Figure 3.2: Plot of (a) mean $\overline{X}(t)$ and (b) variance $\sigma_X^2(t)$ of front position as a function of time, averaged over $N = 4096$ trials. Same parameter values as Fig. 3.1

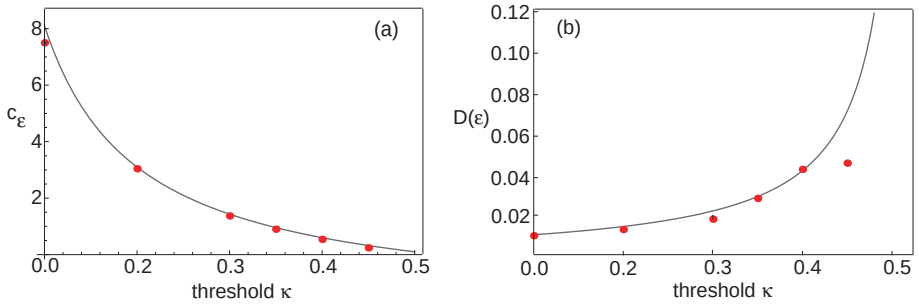

Figure 3.3: Plot of (a) wave speed c_ε and (b) diffusion coefficient $D(\varepsilon)$ as a function of threshold κ. Numerical results (solid dots) are obtained by averaging over $N = 4096$ trials starting from the initial condition given by equation (3.25). Corresponding theoretical predictions (solid curves) for c_ε and $D(\varepsilon)$ are based on equations (3.20)and (3.28), respectively. Other parameters as in Fig. 3.1.

we will define the wave position in a more heuristic way. In order to define the mean location of the front as a function of time, we carry out a large number of level set position measurements. That is, we determine the positions $X_a(t)$ such that $U(X_a(t),t) = a$, for various level set values $a \in (0.5\kappa, 1.3\kappa)$ and then define the mean location to be $\overline{X}(t) = \mathbb{E}[X_a(t)]$, where the expectation is first taken with respect to the sampled values a and then averaged over N trials. The corresponding variance is given by $\sigma_X^2(t) = \mathbb{E}[(X_a(t) - \bar{X}(t))^2]$. In Fig. 3.2 we plot $\overline{X}(t)$ and $\sigma_X^2(t)$ as a function of t. It can be seen that both vary linearly with t, consistent with the assumption that there is a diffusive–like displacement of the front from its uniformly translating position at long time scales. The slopes of these curves then determine the effective wave speed and diffusion coefficient according to $\overline{X}(t) \sim c_\varepsilon t$ and $\sigma_X^2(t) \sim 2D(\varepsilon)t$. In Fig. 3.3 we plot the numerically estimated speed and diffusion coefficient for various values of the threshold κ and compare these to the corresponding theoretical curves obtained using the above analysis. It can be seen that there is excellent agreement with our theoretical predictions provided that κ is not too large. As $\kappa \to 0.5$, the wave speed decreases towards zero so that the assumption of relatively slow diffusion breaks down. It is possible that including higher order terms in our intial expansion (equation (3.10)) could improve our predictions in this limit.

3.2 Effects of multiplicative noise on stimulus-locked fronts

3.2.1 Stimulus–locked fronts

So far we have assumed that the underlying deterministic neural field equation is homogeneous in space so that there exists a family of traveling front solutions related by a uniform shift. Now suppose that there exists an external front–like input that propagates at a uniform speed v, so that the deterministic equation (1.13) becomes

$$\frac{\partial u(x,t)}{\partial t} = -u(x,t) + \int_{-\infty}^{\infty} w(x-x')F(u(x',t))dx' + I(x-vt), \tag{3.30}$$

where the input is taken to be a positive, bounded, monotonically decreasing function of amplitude $I_0 = I(-\infty) - I(\infty)$. Previously it has been shown that the resulting inhomogeneous neural field equation can support a traveling front that locks to the stimulus, provided that the amplitude of the stimulus is sufficiently large [36]. Consider, in particular, the case of a Heaviside firing rate function $F(u) = H(u-\kappa)$. (See [29] for a recent extension to the case of a smooth sigmoid function F). We seek a traveling wave solution $u(x,t) = \mathcal{U}(\xi)$ where $\xi = x - vt$ and $\mathcal{U}(\xi_0) = \kappa$ at a single

threshold crossing point $\xi_0 \in \mathbb{R}$. The front is assumed to travel at the same speed as the input (stimulus–locked front). If $I_0 = 0$ then we recover the homogeneous equation (1.27) and ξ_0 becomes a free parameter, whereas the wave propagates at the natural speed $c(\kappa)$ given by equation (1.36). Substituting the front solution into equation (3.30), we have

$$-v\frac{d\mathcal{U}(\xi)}{d\xi} = -\mathcal{U}(\xi) + \int_{-\infty}^{\xi_0} w(\xi - \xi')d\xi' + I(\xi). \tag{3.31}$$

This can be solved for $v > 0$ by integrating over the interval $[\xi, \infty)$ to give

$$\mathcal{U}(\xi) = \frac{1}{v}\int_{\xi}^{\infty} e^{(\xi-\xi')/v}[W(\xi' - \xi_0) + I(\xi')]d\xi', \tag{3.32}$$

with $W(\xi)$ defined as $W(\xi) = \int_{\xi}^{\infty} w(x)dx$. Similarly, for $v < 0$ we integrate over $(-\infty, \xi]$ to find

$$\mathcal{U}(\xi) = -\frac{1}{v}\int_{-\infty}^{\xi} e^{(\xi-\xi')/v}[W(\xi' - \xi_0) + I(\xi')]d\xi'. \tag{3.33}$$

The threshold crossing condition $\mathcal{U}(\xi_0) = \kappa$ then determines the position ξ_0 of the front relative to the input as a function of speed v, input amplitude I_0 and threshold κ.

As a specific example, suppose that $I(\zeta) = I_0 H(-\zeta)$ and $w(x)$ is the exponential weight distribution (1.18). The threshold condition reduces to

$$\kappa = \begin{cases} \dfrac{\sigma}{2(\sigma+v)} + \begin{cases} 0, & \xi_0 \geq 0, \\ I_0(1 - e^{\xi_0/v}), & \xi_0 < 0, \end{cases} & v > 0; \\ \dfrac{\sigma + 2|v|}{2(\sigma+|v|)} + \begin{cases} I_0 e^{\xi_0/v}, & \xi_0 > 0, \\ I_0, & \xi_0 \leq 0, \end{cases} & v < 0. \end{cases} \tag{3.34}$$

Note that in the absence of any input ($I_0 = 0$), we recover equation (1.36) with $v \to c(\kappa)$, the natural wave speed. Equation (3.34) for $I_0 > 0$ can then be used to determine the regions of the (v, I_0)-parameter subspace for which stimulus-locked waves exist. Let us first consider the case $v > 0$. If $\xi_0 \geq 0$ then $\kappa = \sigma/[2(\sigma + v)]$, which implies that stimulus locking only occurs when the input speed equals the natural wave speed, that is, $v = c_+(\kappa)$ for $0 < \kappa < \frac{1}{2}$ and $\xi_0 > 0$. There are infinitely many such waves, which are parametrized by $\xi_0 \in [0, \infty)$. This degeneracy is a consequence

of using the Heaviside input and would not occur, if a continuous, strictly monotonic input were used; however, the analysis is considerably more involved [29]. On the other hand, if $\xi_0 < 0$ then $\kappa = \sigma/[2(\sigma + v)] + I_0(1 - e^{\xi_0/v})$, which can be inverted to solve for ξ_0 as a function of v:

$$\xi_0(v) = v \ln \left[1 - \frac{1}{I_0} \left(\kappa - \frac{\sigma}{2(\sigma + v)} \right) \right]. \tag{3.35}$$

Since $\xi_0 < 0$ and $v > 0$, it follows that solutions only exist if

$$2(\kappa - I_0) \; < \; \frac{\sigma}{\sigma + v} \; \leq \; 2\kappa. \tag{3.36}$$

The right inequality of (3.36) implies that, if $\kappa < \frac{1}{2}$, then $v > c_+(\kappa)$ where $c_+(\kappa)$ is the wavespeed of freely propagating fronts, see equation (1.36). Similarly, the left inequality implies that, if $I_0 < \kappa$, then $0 < v < c_+(\kappa - I_0)$. Hence, for $0 < \kappa \leq \frac{1}{2}$ we obtain the existence regions in the (v, I_0)-plane shown in Fig. 3.4(a). The left boundary is given by $v = c_+(\kappa)$ and the right boundary by $v = c_+(\kappa - I_0)$. The two boundaries form a tongue that emerges from the natural speed $c_+(\kappa)$ at $I_0 = 0$.

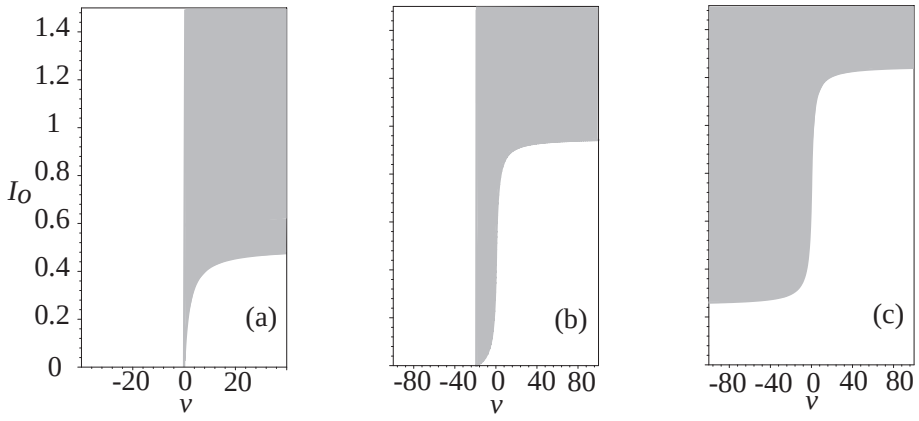

Figure 3.4: Existence regions for stimulus-locked traveling fronts in the (I_0, v)–plane (gray) for various thresholds κ: (a) $\kappa = 0.5$, (b) $\kappa = 0.95$, (c) $\kappa = 1.25$.

Now consider the case $v < 0$. For $\xi_0 < 0$ we have the threshold condition $\kappa = (\sigma + 2|v|)/(2(\sigma + |v|)) + I_0$, which implies that $v = c_-(\kappa - I_0) < 0$. Again we have an infinite family of waves corresponding to a single speed. Since $|v| \geq 0$, such solutions only exist for $\kappa - 1 < I_0 < \kappa - 1/2$. On the other hand, for $\xi_0 \geq 0$ we have the threshold condition $\kappa = (\sigma + 2|v|)/(2(\sigma + |v|)) + I_0 e^{\xi_0/v}$,

which can be inverted to give

$$\xi_0(v) = v \ln \left[\frac{1}{I_0} \left(\kappa - \frac{\sigma + 2|v|}{2(\sigma + |v|)} \right) \right]. \tag{3.37}$$

Since $v < 0$ and $\xi_0 \geq 0$, it follows that waves only exist for v satisfying

$$\kappa - I_0 \leq \frac{\sigma + 2|v|}{2(\sigma + |v|)} < \kappa. \tag{3.38}$$

The right inequality of (3.38) implies that, if $\frac{1}{2} < \kappa < 1$, then $c_-(\kappa) < v < 0$. Thus, for $1/2 < \kappa < 1$ we obtain the existence region shown in Fig. 3.4(b); the left boundary is given by $v = c_-(\kappa)$ and the right boundary by $v = c_-(\kappa - I_0)$ for $v < 0$ and $v = c_+(\kappa - I_0)$ for $v > 0$. Again there is a tongue with tip at the natural speed. For $\kappa > 1$ the left boundary disappears, and one only finds stimulus-locked waves when $I_0 > \kappa - 1$, i.e., there no longer exists natural waves. The left inequality of (3.38) implies that if $1/2 < \kappa - I_0 < 1$ then $v < c_-(\kappa - I_0) < 0$, whereas, if $\kappa - I_0 > 1$ then no solution exists, see Fig. 3.4(c).

3.2.2 Locking in the presence of multiplicative noise

We now extend the analysis of section 3.1 in order to determine the effects of multiplicative noise on stimulus–locked fronts, and show that diffusive–like behaviour found for freely propagating fronts no longer holds. Incorporating the external input into the Langevin equation (3.1) gives

$$\begin{aligned} dU(x,t) &= \left[-U(x,t) + \int_{-\infty}^{\infty} w(x-y) F(U(y,t)) dy + I(x - vt) \right] dt \\ &\quad + \varepsilon^{1/2} g(U(x,t)) dW(x,t). \end{aligned} \tag{3.39}$$

Applying equation (3.3), we then rewrite equation (3.39) so that the fluctuating term has zero mean:

$$dU(x,t) = \left[h(U(x,t)) + \int_{-\infty}^{\infty} w(x-y) F(U(y,t)) dy + I(x - vt) \right] dt + \varepsilon^{1/2} dR(U,x,t), \tag{3.40}$$

where h and R are given by equations (3.5) and (3.6), respectively. Proceeding along similar lines to our analysis of freely propagating fronts, we express the solution U of equation (3.40) as a combination of a fixed wave profile U_0 that is displaced by an amount $\Delta(t)$ from its uniformly translating mean position $\xi = x - vt$, and a time–dependent fluctuation Φ in the front shape about

the instantaneous position of the front:

$$U(x,t) = U_0(\xi - \Delta(t)) + \varepsilon^{1/2}\Phi(\xi - \Delta(t), t). \tag{3.41}$$

We are assuming that the mean profile U_0 is locked to the stimulus (has speed v). However, multiplicative noise still has an effect on U_0 by generating an ε–dependent threshold crossing point ξ_ε such that $U_0(\xi_\varepsilon) = \kappa$.

Substituting equation (3.41) into equation (3.40) and taking averages gives to leading order the following deterministic equation for U_0:

$$-v\frac{dU_0}{d\xi} - h(U_0(\xi)) - I(\xi) = \int_{-\infty}^{\infty} w(\xi - \xi')F(U_0(\xi'))d\xi'. \tag{3.42}$$

Note that U_0 depends non–trivially on the noise strength ε due to the ε–dependence of the function h, see equation (3.5). Proceeding to the next order and imposing equation (3.42), we find that $\Delta(t) = \mathcal{O}(\varepsilon^{1/2})$ and

$$d\Phi(\xi,t) = \widehat{L} \circ \Phi(\xi,t)dt + \varepsilon^{-1/2}U_0'(\xi)d\Delta(t) + dR(U_0,\xi,t) + \varepsilon^{-1/2}I'(\xi)\Delta(t)dt \tag{3.43}$$

where $\widehat{L}$ is the non–self–adjoint linear operator (3.12) with $c_\varepsilon \to v$. The last term on the right–hand side of equation (3.43) arises from the fact that in equation (3.41), U_0 and Φ are expressed as functions of $\xi - \Delta(t)$ so that we have made the approximation $I(\xi) = I(\xi - \Delta(t) + \Delta(t)) \approx I(\xi - \Delta(t)) + I'(\xi - \Delta(t))\Delta(t)$. We then have the solvability condition for the existence of a nontrivial solution of equation (3.43), namely, that the inhomogeneous part is orthogonal to the null vector $\mathcal{V}(\xi)$ of the adjoint operator $\widehat{L}^*$ defined by equation (3.14) with $c_\varepsilon \to v$. Taking the inner product of both sides of equation (3.43) with respect to $\mathcal{V}(\xi)$ thus leads to the solvability condition

$$\int_{-\infty}^{\infty} \mathcal{V}(\xi)\left[U_0'(\xi)d\Delta(t) + I'(\xi)\Delta(t)dt + \varepsilon^{1/2}dR(U_0,\xi,t)\right]d\xi = 0. \tag{3.44}$$

It follows that, to leading order, $\Delta(t)$ satisfies the Ornstein–Uhlenbeck equation

$$d\Delta(t) + A\Delta(t)dt = d\widehat{W}(t), \tag{3.45}$$

where

$$A = \frac{\int_{-\infty}^{\infty} \mathcal{V}(\xi) I'(\xi) d\xi}{\int_{-\infty}^{\infty} \mathcal{V}(\xi) U_0'(\xi) d\xi}. \tag{3.46}$$

and

$$\widehat{W}(t) = -\varepsilon^{1/2} \frac{\int_{-\infty}^{\infty} \mathcal{V}(\xi) g(U_0(\xi)) W(\xi, t) d\xi}{\int_{-\infty}^{\infty} \mathcal{V}(\xi) U_0'(\xi) d\xi}. \tag{3.47}$$

Note that $A > 0$ for $I_0 > 0$, since both $U_0(\xi)$ and $I(\xi)$ are monotonically decreasing functions of ξ. Moreover

$$\langle d\widehat{W}(t) \rangle = 0, \quad \langle d\widehat{W}(t) d\widehat{W}(t) \rangle = 2D(\varepsilon) dt \tag{3.48}$$

with $D(\epsilon)$ given by equation (3.18). Using the results of section 1.3.2, we conclude that

$$\langle \Delta(t) \rangle = \Delta(0) e^{-At}, \quad \langle \Delta(t)^2 \rangle - \langle \Delta(t) \rangle^2 = \frac{D(\varepsilon)}{A} \left[1 - e^{-2At} \right]. \tag{3.49}$$

In particular, the variance approaches a constant $D(\varepsilon)/A$ in the large t limit.

3.2.3 Heaviside rate function

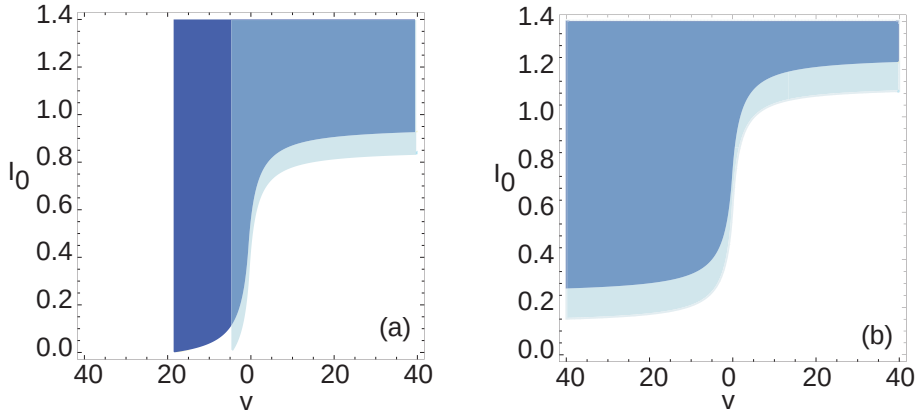

Figure 3.5: Plot of existence regions of a stimulus-locked front without noise ($\gamma = 1$, dark blue) and in the presence of noise ($\gamma = 0.9$, light blue) for a) $\kappa = 0.95$ b) $\kappa = 1.25$. Stimulus taken to be of the form $I(x,t) = I_0 H(-\xi), \xi = x - vt$ with amplitude I_0 and speed v. Other parameter values as in Fig. 3.1.

In order to illustrate the above analysis, we take $g(U) = g_0 U$ for the multiplicative noise term (see section 1.4) and set $F(U) = H(U - \kappa)$. The deterministic equation (3.42) for the mean profile

U_0 then reduces to

$$-v\frac{dU_0}{d\xi}+U_0(\xi)[1-\varepsilon g_0^2C(0)]+I(\xi)=\int_{-\infty}^{\infty}w(\xi-\xi')H(U_0(\xi')-\kappa)d\xi'. \tag{3.50}$$

Proceeding as in section 3.1, we can explicitly calculate the existence regions for stimulus locked fronts when $I(\xi)=I_0H(-\xi)$, that is, for a step function input of speed v and amplitude I_0. Setting $\gamma(\varepsilon)=1-\varepsilon g_0^2C(0)$ with $0<\gamma(\varepsilon)\leq 1$, and introducing the threshold crossing point ξ_ε for which $U_0(\xi_\varepsilon)=\kappa$, we derive a similar set of threshold conditions as equation (3.34) under the rescalings $\kappa\to\eta\gamma(\varepsilon)$ and $v\to v/\gamma(\varepsilon)$:

$$\gamma(\varepsilon)\kappa = \begin{cases} \dfrac{\sigma}{2(\sigma+v/\gamma(\varepsilon))} + \begin{cases} 0, & \xi_0\geq 0, \\ I_0(1-e^{\gamma(\varepsilon)\xi_0/v}), & \xi_0<0, \end{cases} & v>0; \\ \dfrac{\sigma+2|v|/\gamma(\varepsilon)}{2(\sigma+|v|/\gamma(\varepsilon))} + \begin{cases} I_0e^{\gamma(\varepsilon)\xi_0/v}, & \xi_0>0, \\ I_0, & \xi_0\leq 0, \end{cases} & v<0. \end{cases} \tag{3.51}$$

It follows that the boundaries of the existence tongues are now determined by the modified functions $\gamma(\varepsilon)c_\pm(\gamma(\varepsilon)\kappa-I_0)$. The resulting ε–dependent shift in the existence tongues is illustrated in Fig. 3.5.

In Fig. 3.6 we show the temporal evolution of a single stimulus–locked front, which is obtained by numerically solving the Langevin equation (3.39) for $F(U)=H(U-\kappa)$, $g(U)=U$ and an exponential weight distribution w. Numerically speaking, it is convenient to avoid discontinuities in the input by taking $I(x,t)=I_0\mathrm{Erfc}[x-vt]$ rather than a Heaviside. Next we determine the mean $\overline{X}(t)$ and variance $\sigma_X^2(t)$ of the position of the front by averaging over level sets along identical lines to section 3.1. The results are shown in Fig. 3.7. It can be seen that, as predicted by the analysis, $\overline{X}(t)$ varies linearly with t with a slope equal to the stimulus speed $v=1.5$. Moreover, the variance $\sigma_X^2(t)$ approaches a constant value as $t\to\infty$, which is comparable to the theoretical value $D(\varepsilon)/A$ evaluated for the given input. Thus, we find that stimulus-locked fronts are much more robust to noise than freely propagating fronts, since the variance of the mean position saturates as $t\to\infty$. Consequently, stimulus locking persists in the presence of noise over most of the parameter range for which stimulus locking is predicted to occur. This is further illustrated in Fig. 3.8, where we plot the mean speed of the wave as a function of the threshold κ.

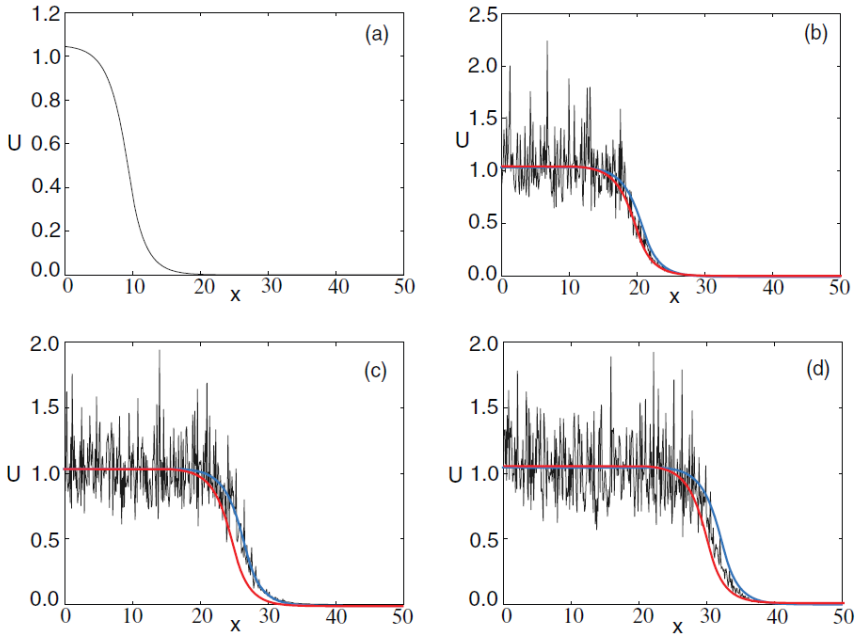

Figure 3.6: Numerical simulation showing the propagation of a stimulus–locked wavefront solution (black curves) of the stochastic neural field equation (3.39) for Heaviside weight function $F(U) = H(U - \kappa)$ with $\kappa = 0.35$, exponential weight function (1.18) with $\sigma = 2$, and multiplicative noise $g(U) = U$. The external input (light blue curves) is taken to be of the form $I(x,t) = I_0 \mathrm{Erfc}[x - vt]$ with amplitude $I_0 = 0.4$ and speed $v = 1.5$. Noise strength $\epsilon = 0.005$ and $C(0) = 10$. The mean profile U_0 is also shown (red curves). The wave profile is shown at successive times (a) $t = 0$ (b) $t = 6$ (c) $t = 12$ and (d) $t = 24$, with the initial profile at $t = 0$ given by the solution U_0 of equation (3.42). In numerical simulations we take the discrete space and time steps $\Delta x = 0.1, \Delta t = 0.01$.

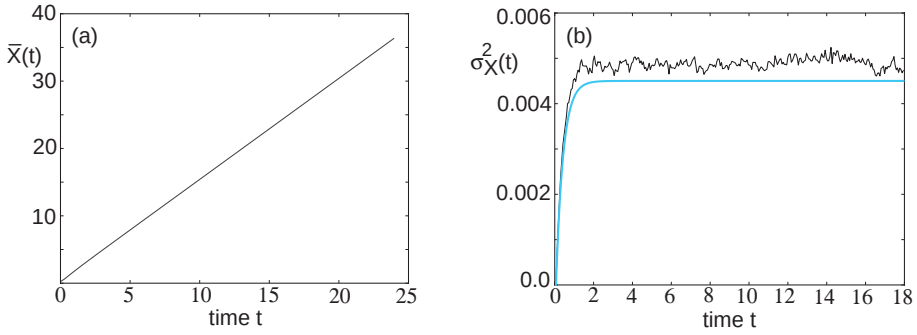

Figure 3.7: Plot of (a) mean $\overline{X}(t)$ and (b) variance $\sigma_X^2(t)$ of the position of a stimulus–locked front as a function of time, averaged over $N = 4096$ trials. Smooth blue curve in (b)indicates theoretical prediction of variance. Stimulus taken to be of the form $I(x,t) = I(x - ct) = I_0 \mathrm{Erfc}[x - vt]$ with amplitude $I\_0 = 0.4$ and speed $v = 1.5$. Other parameter values as in Fig. 3.1 and initial condition satisfying equation (3.25).

3.3 Discussion

In this section we have explored the effects of multiplicative noise on front propagation in a stochastic generalisation of Amari's original neural field equation. We have shown that the effects of noise on the

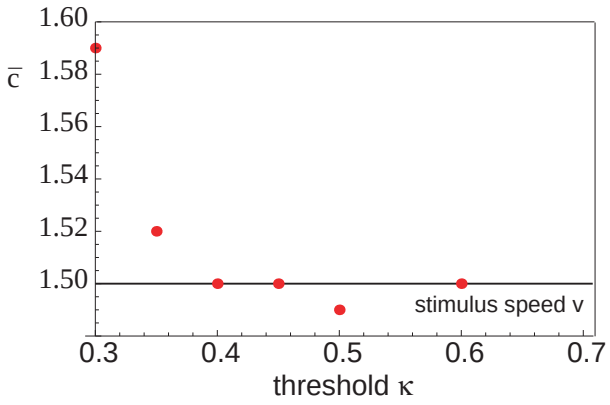

Figure 3.8: Plot of mean wave speed $\bar{c}$ as a function of threshold κ. Other parameters as in Fig. 3.7. Horizontal curve indicates speed v of stimulus. Stimulus–locked waves do not exist for $\kappa < 0.30$ which explains why the datapoint at $\kappa = 0.30$ is an outlier.

wandering of the mean front position depends on properties of the underlying deterministic front. In the case of a freely propagating front linking a stable and metastable state, we find that the position of the wave obeys a drift-diffusion stochastic differential equation. On the other hand, if the front is locked to a moving stimulus, then the front position is described by an Ornstein-Uhlenbeck process, so the variance of the wave position saturates to a constant value. A consequence of this is that the noise has a limited impact on the system indicating that important functions such as detecting a moving object are somewhat protected from the effects of noise. Thus this could be seen as an example where the important functions of a biological system are robust to the effects of noise - so-called "biological robustness". Though the method we have developed is a physical and intuitive approach to the problem, we have also shown via computer simulation, that the predictions of the theory are correct. In the next chapter we will extend our analysis of stochastic front propagation to the case of binocular rivalry.

Appendix (Novikov's Theorem)

Here we present a derivation of equation (3.3), see also [64]. Consider the Langevin equation

$$dU(x,t) = \left[-U(x,t) + \int_{-\infty}^{\infty} w(x-y) F(U(y,t)) dy \right] dt + \varepsilon^{1/2} g(U(x,t)) dW(x,t) \tag{3.52}$$

with (in the limit $\lambda \to 0$)

$$\langle dW(x,t) \rangle = 0, \quad \langle dW(x,t) dW(x',t) \rangle = \delta(x-x') dt. \tag{3.53}$$

It is convenient to restrict x to a bounded domain, $-L/2 \leq x \leq L/2$, and to impose periodic boundary conditions. We can then introduce the discrete Fourier series

$$U(x,t) = \frac{1}{L}\sum_n e^{ik_n x} U_n(t), \quad W(x,t) = \frac{1}{L}\sum_n e^{ik_n x} W_n(t) \tag{3.54}$$

with $k_n = 2\pi n/L$ and $W_n(t)$ an independent Wiener process such that

$$\langle dW_n(t)\rangle = 0, \quad \langle dW_n(t) dW_m(t)\rangle = 2L\delta_{m+n,0} dt. \tag{3.55}$$

Fourier transforming equation (3.52) gives

$$dU_n(t) = [-U_n(t) + w_n F_n(t)]dt + \frac{\varepsilon^{1/2}}{L}\sum_m g_{n-m}(t) dW_m(t), \tag{3.56}$$

where w_n is the nth Fourier coefficient of the weight distribution $w(x)$, and F_n, g_n are the Fourier coefficients of the time dependent functions $F \circ U(t)$ and $g \circ U(t)$ respectively. The associated Stratonovich Fokker–Planck equation takes the form [38]

$$\frac{\partial P}{\partial t} = -\sum_l \frac{\partial}{\partial u_l}[(-u_l + w_l F_l)P] + \frac{\varepsilon}{L}\sum_{l,m,q} \frac{\partial}{\partial u_l} g_{l-q} \frac{\partial}{\partial u_m} g_{m+q} P. \tag{3.57}$$

Multiplying both sides of this equation by u_n and integrating with respect to u_m, integer m, leads to the following evolution equation for the mean:

$$\frac{d\langle U_n\rangle}{dt} = -\langle U_n\rangle + w_n\langle F_n\rangle + \frac{\varepsilon}{L}\sum_{m,q}\left\langle \frac{\partial g_{n-q}}{\partial U_m} g_{m+q}\right\rangle. \tag{3.58}$$

Finally, taking the inverse transform of equation (3.58) gives

$$\begin{aligned}\frac{d\langle U(x,t)\rangle}{dt} &= -\langle U(x,t)\rangle + \int w(x-y)\langle F(U(y,t))\rangle dy \\ &\quad + \frac{\varepsilon}{\Delta x}\left\langle g(U(x,t)) g'(U(x,t))\right\rangle,\end{aligned} \tag{3.59}$$

where we have used the result $\partial g_n/\partial U_m = [g'(U)]_{n-m}$. Note that it is necessary to introduce a cut–off in the frequencies, which is equivalent to introducing a fundamental lattice spacing of Δx. Alternatively, the multiplicative noise can be taken to have a small but finite correlation length in space so that $C(0) = 1/\Delta x$. Comparison of equation (3.58) with the mean of equation (3.52) yields the desired result.

Chapter 4

Stochastic Binocular Rivalry

The previous chapter was concerned with one dimensional neural field equations. In order to extend this analysis to the case of binocular rivalry it will be necessary to instead consider four neural field variables. Not only do we require one neural field variable for each eye, but as shown in chapter 2 an additional adaptation variable for each eye is necessary to allow the symmetry breaking required for wave propagation to occur. This presents an additional problem of where and how should we add noise to our modelling equations. Suitable candidates would appear to be either the activity variables or the adaptation variables. In this chapter we will first consider noise in the activity variables by extending the analysis of chapter 3 to a stochastic version of eqs. 2.26 and 2.27. In particular we will show that the first passage time for waves approaching a fixed barrier is given by an inverse Gaussian distribution. Noise in the depression variables will be explored using computer simulation and we will show that in this case for a variety of parameters the distribution of first passage times is also inverse Gaussian. This is a key prediction which presents an opportunity for further experimental verification of the theories presented in this thesis, in particular our treatment of stochastic binocular rivalry waves.

4.1 Effects of multiplicative noise in the fast activity variables

It is now possible to follow on from the analysis of binocular rivalry waves using deterministic neural field equations developed in chapter 2. In particular we take eqs 2.1a and 2.2a under the adiabatic approximation which is necessary for wave propagation. Furthermore, motivated by the examples of stochastic neural field equations considered in chapter 3 and section 1.4 we consider the following Langevin equation (or stochastic PDE) for the stochastic activity variables $U(x,t)$ and $V(x,t)$, which

as before represent the activities of the left and right eye neurons:

$$\begin{aligned} dU &= \left[-U + Q_u \int w_e(x-y) f(U(y,t))dy - Q_v \int w_i(x-y) f(V(y,t))dy + I_u\right] dt \\ &\quad +\epsilon^{\frac{1}{2}} g(U) dW_u \end{aligned} \tag{4.1}$$

$$\begin{aligned} dV &= \left[-V + q_v \int w_e(x-y) f(V(y,t))dy - Q_u \int w_i(x-y) f(U(y,t))dy + I_v\right] dt \\ &\quad +\epsilon^{\frac{1}{2}} g(V) dW_v. \end{aligned} \tag{4.2}$$

with Q_u, Q_v fixed. We assume that W_u, W_v represent independent Wiener processes such that

$$\langle dW_{\{u,v\}}(x,t)\rangle = 0, \qquad \langle dW_i(x,t) dW_j(x',t')\rangle = 2\delta_{i,j} C([x-x']/\lambda)\delta(t-t')dtdt', \tag{4.3}$$

where $i,j = u,v$ and $\langle\cdot\rangle$ denotes averaging with respect to the Wiener processes. As before, λ is the spatial correlation length of the noise such that $C(x/\lambda) \to \delta(x)$ in the limit $\lambda \to 0$, and ϵ determines the strength of the noise, which is assumed to be weak. Following standard formulations of Langevin equations [39], the multiplicative noise term is taken to be of Stratonovich form in the case of extrinsic noise.

Having formulated the problem in this way it is now possible to apply the method of chapter 3. Once again we have the observation that multiplicative noise in the Stratonovich sense leads to a systematic shift in the speed of the front (assuming a front of speed c exists when $\epsilon = 0$). This is a consequence of the fact that $\langle g(U)dW_u\rangle \neq 0$ and $\langle g(V)dW_v\rangle \neq 0$ even though $\langle dW_{\{u,v\}}\rangle = 0$. These averages can be calculated using Novikov's theorem [56]:

$$\langle g(U)dW_u\rangle = \epsilon^{1/2} C(0)\langle g'(U)g(U)\rangle dt, \quad \langle g(V)dW_v\rangle = \epsilon^{1/2} C(0)\langle g'(V)g(V)\rangle dt \tag{4.4}$$

Note that in the limit $\lambda \to 0$, $C(0) \to 1/\Delta x$ where Δx is a lattice cut–off, which can be identified with the step size of the spatial discretization scheme used in numerical simulations. Following chapter 3, it is convenient to rewrite equations (4.1) and (4.2) so that the fluctuating term has zero mean:

$$\begin{aligned} dU &= \left[h(U) + Q_u \int w_e(x-y) f(U(y,t))dy - Q_v \int w_i(x-y) f(V(y,t))dy + I_u\right] dt \\ &\quad +\epsilon^{\frac{1}{2}} dR_u(U,x,t) \end{aligned} \tag{4.5}$$

$$dV = \left[h(V) + Q_v \int w_e(x-y) f(V(y,t))dy - Q_u \int w_i(x-y) f(U(y,t))dy + I_v\right] dt + \epsilon^{\frac{1}{2}} dR_v(V,x,t), \tag{4.6}$$

where

$$h(U) = -U + \epsilon C(0) g'(U) g(U), \tag{4.7}$$

and

$$dR_u(U,x,t) = g(U) \circ dW_u - \epsilon^{\frac{1}{2}} C(0) g(U) g'(U) dt \tag{4.8}$$

$$dR_v(V,x,t) = g(V) \circ dW_v - \epsilon^{\frac{1}{2}} C(0) g(V) g'(V) dt \tag{4.9}$$

The stochastic processes R_u, R_v have zero mean (so do not contribute to the effective drift, that is, the average wave speed) and covariance

$$\begin{aligned}
\langle dR_u(U,x,t) dR_u(U,x',t)\rangle &= \langle g(U(x,t)) dW_u(x,t) g(U(x',t) dW_u(x',t)\rangle + \mathcal{O}(\epsilon^{1/2}), \\
\langle dR_v(V,x,t) dR_v(V,x',t)\rangle &= \langle g(V(x,t)) dW_v(x,t) g(V(x',t) dW_v(x',t)\rangle + \mathcal{O}(\epsilon^{1/2}) \\
\langle dR_u(U,x,t) dR_v(V,x',t)\rangle &= \langle g(U(x,t)) dW_u(x,t) g(V(x',t) dW_v(x',t)\rangle + \mathcal{O}(\epsilon^{1/2}).
\end{aligned}$$

The next step in the analysis is to assume that the fluctuating terms in equations (4.5) and (4.6) generate two distinct phenomena that occur on different time–scales: a diffusive–like displacement of the binocular rivalry wave from its uniformly translating position at long time scales, and fluctuations in the wave profile around its instantaneous position at short time scales [55, 26, 4, 64]. It is important to point out that, in contrast to traveling front solutions of scalar neural field equations (as in chapter 3), we are now considering composite wave solutions consisting of an invading front in the left eye network, say, comoving with a retreating front in the right eye network. Thus in addition to the center–of–mass of the composite wave, which moves with speed c in the absence of noise, there is an additional degree of freedom corresponding to the "width" of the composite wave. (In the case of a Heaviside rate function, the width is determined by the threshold crossing point ξ_0, see section 2.2.2. For simplicity, we assume that the width of the composite wave is only weakly affected by the noise; this is consistent with what is found numerically. We now express the solution (U,V) of equations (4.5) and (4.6) as a combination of a fixed wave profile (U_0, V_0) that is displaced by an amount $\Delta(t)$ from its uniformly translating position $\xi = x - c_\epsilon t$ and a time–dependent fluctuation

(U_1, V_1) in the wave shape about its instantaneous position:

$$U(x,t) = U_0(\xi - \Delta(t)) + \epsilon^{1/2} U_1(\xi - \Delta(t), t), \tag{4.10}$$

$$V(x,t) = V_0(\xi - \Delta(t)) + \epsilon^{1/2} V_1(\xi - \Delta(t), t). \tag{4.11}$$

The wave profile (U_0, V_0) and associated wave speed c_ϵ are obtained by solving the modified deterministic equation

$$\begin{aligned} -c\frac{dU_0}{d\epsilon} - h(U_0) &= Q_u \int_{-\infty}^{\infty} w_e(\xi - \xi') f(U_0(\xi'))d\xi' - Q_v \int_{-\infty}^{\infty} w_i(\xi - \xi') f(V_0(\xi'))d\xi' \\ &\quad + I_u \end{aligned} \tag{4.12}$$

$$\begin{aligned} -c\frac{dV_0}{d\epsilon} - h(V_0) &= Q_v \int_{-\infty}^{\infty} w_e(\xi - \xi') f(V_0(\xi'))d\xi' - Q_u \int_{-\infty}^{\infty} w_i(\xi - \xi') f(U_0(\xi'))d\xi' \\ &\quad + I_v \end{aligned} \tag{4.13}$$

Both c_ϵ and U_0 depend non–trivially on the noise strength ϵ due to the ϵ–dependence of the function h, see equation (4.7). Thus, $c_\epsilon \neq c$ for $\epsilon > 0$ and $c_0 = c$, where c is the speed of the front in the absence of multiplicative noise. It also follows that the expansions (4.10) and (4.11) are not equivalent to a standard small–noise expansion in ϵ. Equations (4.12) and (4.13) are chosen so that to leading order, the stochastic variable $\Delta(t)$ undergoes unbiased Brownian motion with a diffusion coefficient $D(\epsilon) = \mathcal{O}(\epsilon)$ (see below). Thus $\Delta(t)$ represents the effects of slow fluctuations, whereas (U_1, V_1) represents the effects of fast fluctuations.

The next step is to substitute the decompositions (4.10) and (4.11) into equations (4.5) and (4.6) and expand to first order in $\mathcal{O}(\varepsilon^{1/2})$:

$$\begin{aligned} &-[c_\varepsilon + d\Delta(t)]U_0'(\xi_\Delta)dt + \epsilon^{1/2}\left[dU_1(\xi_\Delta, t) - [c_\epsilon + d\Delta(t)]U_1'(\xi_\Delta, t)dt\right] \\ &\quad = h(U_0(\xi_\Delta))dt + \epsilon^{1/2} h'(U_0(\xi_\Delta))U_1(\xi_\Delta, t)dt \\ &\qquad + Q_u \int_{-\infty}^{\infty} w_e(\xi - \xi')\left(f(U_0(\xi'_\Delta)) + \epsilon^{1/2} f'(U_0(\xi'_\Delta))U_1(\xi'_\Delta, t)\right)d\xi' dt \\ &\qquad - Q_v \int_{-\infty}^{\infty} w_i(\xi - \xi')\left(f(V_0(\xi'_\Delta)) + \epsilon^{1/2} f'(V_0(\xi'_\Delta))V_1(\xi'_\Delta, t)\right)d\xi' dt \\ &\qquad + \epsilon^{1/2} dR(U_0(\xi_\Delta), \xi, t) + \mathcal{O}(\epsilon). \end{aligned}$$

where we have set $\xi_\Delta = \xi - \Delta(t)$ and $\xi'_\Delta = \xi' - \Delta(t)$. A similar equation holds for dV. We now use the steady state equations (4.12) and (4.13) for U_0, V_0, after shifting $\xi \to \xi - \Delta(t)$, to eliminate

terms and then divide through by $\sqrt{\epsilon}$. This gives the inhomogeneous equations to $\mathcal{O}(\epsilon^{1/2})$

$$dU_1(\xi_\Delta,t) - L_u(U_1(\xi_\Delta,t),V_1(\xi_\Delta,t)) = \epsilon^{-\frac{1}{2}}U_0'(\xi_\Delta)d\Delta(t) + dR_u(U_0(\xi_\Delta),\xi,t) \tag{4.14}$$

$$dV_1(\xi_\Delta,t) - L_v(U_1(\xi_\Delta,t),V_1(\xi_\Delta,t)) = \epsilon^{-\frac{1}{2}}V_0'(\xi_\Delta)d\Delta(t) + dR_v(V_0(\xi_\Delta),\xi,t) \tag{4.15}$$

with L_u, L_v non-self-adjoint linear operators

$$\begin{aligned} L_u(A_1,A_2) &= c\frac{dA_1}{d\xi} + h'(U_0)A_1 + Q_u\int w_e(\xi-\xi')f'(U_0(\xi'))A_1(\xi')d\xi' \\ &\quad -Q_v\int w_i(\xi-\xi')f'(V_0(\xi'))A_2(\xi')d\xi' \end{aligned}$$

$$\begin{aligned} L_v(A_1,A_2) &= c\frac{dA_2}{d\xi} + h'(V_0)A_2 + Q_v\int w_e(\xi-\xi')f'(V_0(\xi'))A_2(\xi')d\xi' \\ &\quad -Q_u\int w_i(\xi-\xi')f'(U_0(\xi'))A_1(\xi')d\xi' \end{aligned}$$

for any functions $A_1(\xi), A_2(\xi) \in L_2(\mathbb{R})$. Finally, for all terms in equations (4.14) and (4.15) to be of the same order we require that $\Delta(t) = \mathcal{O}(\varepsilon^{1/2})$. It then follows that $U_0(\xi-\Delta(t)) = U_0(\xi) + \mathcal{O}(\varepsilon^{1/2})$ etc., and equations (4.14) and (4.15) reduce to

$$dU_1(\xi,t) - L_u(U_1(\xi,t),V_1(\xi,t)) = \epsilon^{-\frac{1}{2}}U_0'(\xi)d\Delta(t) + dR_u(U_0(\xi),\xi,t) \tag{4.16}$$

$$dV_1(\xi,t) - L_v(U_1(\xi,t),V_1(\xi_\Delta,t)) = \epsilon^{-\frac{1}{2}}V_0'(\xi)d\Delta(t) + dR_v(V_0(\xi),\xi,t) \tag{4.17}$$

Let $\mathbf{L}$ denote the vector-valued operator with components L_u, L_v. That, is

$$\mathbf{L}\begin{pmatrix} A_1 \\ A_2 \end{pmatrix} = \begin{pmatrix} L_u(A_1,A_2) \\ L_v(A_1,A_2). \end{pmatrix} \tag{4.18}$$

It can be shown that for a sigmoid firing rate function and Gaussian weight distributions, the operator $\mathbf{L}$ has a 1D null space spanned by $(U_0'(\xi),V_0'(\xi))^T$ [30]. (The fact that $(U_0'(\xi),V_0'(\xi))^T$ belongs to the null space follows immediately from differentiating equations (4.13) with respect to ξ). We then have the solvability condition for the existence of a nontrivial solution of equations (4.16) and (4.17), namely, that the inhomogeneous part is orthogonal to all elements of the null space of the adjoint

operator $\mathbf{L}^*$. The latter is defined with respect to the inner product

$$\int_{-\infty}^{\infty} \mathbf{B}(\xi) \cdot \mathbf{L}\mathbf{A}(\xi) d\xi = \int_{-\infty}^{\infty} \mathbf{L}^*\mathbf{B}(\xi) \cdot \mathbf{A}(\xi) d\xi \tag{4.19}$$

where $\mathbf{A}(\xi)$ and $\mathbf{B}(\xi)$ are two-vectors with integrable components. We find that

$$\mathbf{L}^* \begin{pmatrix} B_1 \\ B_2 \end{pmatrix} = \begin{pmatrix} L_u^*(B_1, B_2) \\ L_v^*(B_1, B_2), \end{pmatrix} \tag{4.20}$$

where

$$\begin{aligned} L_u^*(B_1, B_2) \quad &= -c_\epsilon \tfrac{dB_1}{d\xi} + h'(U_0)B_1 + f'(U_0)Q_u \textstyle\int w_e(\xi - \xi')B_1(\xi')d\xi' \\ &\quad -f'(V_0)q_v \textstyle\int w_i(\xi - \xi')B_2(\xi')d\xi' \end{aligned} \tag{4.21}$$

and

$$\begin{aligned} L_v^*(B_1, B_2) \quad &= -c_\epsilon \tfrac{dB_2}{d\xi} + h'(V_0)B_2 + f'(V_0)Q_v \textstyle\int w_e(\xi - \xi')B_2(\xi')d\xi' \\ &\quad -f'(U_0)Q_u \textstyle\int w_i(\xi - \xi')B_1(\xi')d\xi' \end{aligned} \tag{4.22}$$

The adjoint operator $\mathbf{L}^*$ also has a one dimensional null-space, that is, it is spanned by some vector-valued function $\mathcal{V}(\xi)$. Thus taking the inner product of both sides of equations (4.16) and (4.17) with respect to $\mathcal{V}(\xi)$ leads to the solvability condition

$$\begin{aligned} 0 \quad &= \textstyle\int_{-\infty}^{\infty} \mathcal{V}_1(\xi) \left[U_0'(\xi)d\Delta(t) + \epsilon^{1/2} dR_u(U_0, \xi, t)\right] d\xi \\ &\quad + \textstyle\int_{-\infty}^{\infty} \mathcal{V}_2(\xi) \left[V_0'(\xi)d\Delta(t) + \epsilon^{1/2} dR_v(V_0, \xi, t)\right] d\xi. \end{aligned} \tag{4.23}$$

Thus $\Delta(t)$ satisfies the stochastic differential equation (SDE)

$$d\Delta(t) = -\epsilon^{1/2} \frac{\displaystyle\int_{-\infty}^{\infty} \left(\mathcal{V}_1(\xi) dR_u(U_0, \xi, t) + \mathcal{V}_2(\xi) dR_v(V_0, \xi, t)\right) d\xi}{\displaystyle\int_{-\infty}^{\infty} \left(\mathcal{V}_1(\xi) U_0'(\xi) + \mathcal{V}_2(\xi) V_0'(\xi)\right) d\xi}. \tag{4.24}$$

Using the lowest order approximations $dR_u(U_0, \xi, t) = g(U_0(\xi))dW_u(\xi, t)$ and $dR_v(V_0, \xi, t) = g(V_0(\xi))dW_v(\xi, t)$,

we deduce that (for $\Delta(0) = 0$)

$$\langle \Delta(t) \rangle = 0, \quad \langle \Delta(t)^2 \rangle = 2D(\varepsilon)t \tag{4.25}$$

where $D(\epsilon)$ is the effective diffusivity

$$D(\epsilon) = \epsilon \frac{\displaystyle\int_{-\infty}^{\infty} \left(\mathcal{V}_1(\xi)^2 g(U_0(\xi))^2 + \mathcal{V}_2(\xi)^2 g(V_0(\xi))^2 \right) d\xi}{\left[\displaystyle\int_{-\infty}^{\infty} \left(\mathcal{V}_1(\xi) U_0'(\xi) + \mathcal{V}_2(\xi) V_0'(\xi) \right) d\xi \right]^2}. \tag{4.26}$$

Note that since $\Delta(t) = \mathcal{O}(\epsilon^{1/2})$, equation (4.10) implies that $U(x,t) = U_0(x - c_\epsilon t) + \mathcal{O}(\epsilon^{1/2})$. Hence, averaging with respect to the noise shows that $\langle U(x,t) \rangle = U_0(x - c_\epsilon t) + \mathcal{O}(\epsilon^{1/2})$. A similar result holds for V. Thus, in the case of weak noise, averaging over many realizations of the stochastic wave generates a mean wave whose speed is approximately equal to c_ϵ. This is indeed found to be the case numerically, see below.

4.2 Explicit results for a Heaviside rate function

In order to illustrate the above analysis, we consider a particular example where the mean speed c_ϵ and diffusion coefficient $D(\epsilon)$ can be calculated explicitly. That is, set $g(U) = g_0 U$ for the multiplicative noise term and take $f(U) = H(u - \kappa)$. (The constant g_0 has units of $\sqrt{\text{length/time}}$). The deterministic equations (4.12) and (4.13) for (U_0, V_0) reduce to

$$-c\frac{dU_0}{d\xi} + \gamma(\epsilon) U_0 = Q_u \int_{-\infty}^{0} w_e(\xi - \xi') d\xi' - Q_v \int_{\xi_0}^{\infty} w_i(\xi - \xi') d\xi' + I \tag{4.27}$$

$$-c\frac{dV_0}{d\xi} + \gamma(\epsilon) V_0 = Q_v \int_{\xi_0}^{\infty} w_e(\xi - \xi') d\xi' - Q_u \int_{-\infty}^{0} w_i(\xi - \xi') d\xi' + I, \tag{4.28}$$

where

$$\gamma(\epsilon) = 1 - \epsilon C(0) g_0^2. \tag{4.29}$$

These equations can be solved along identical lines to equations 2.26 and 2.27, and lead to the modified threshold conditions

$$\kappa = \frac{1}{\gamma(\epsilon)} \int_0^{\infty} e^{-s} \Psi_{\xi_0}(cs/\gamma(\epsilon)) ds + I, \quad \kappa = \frac{1}{\gamma(\epsilon)} \int_0^{\infty} e^{-s} \Phi_{\xi_0}(-cs/\gamma(\epsilon)) ds + I. \tag{4.30}$$

It immediately follows that both the speed c and displacement X depend on the noise strength ϵ. The corresponding wave profiles are, see equations 2.17 and 2.18,

$$U(\xi) = \frac{1}{c}\int_0^\infty e^{-z\gamma/c}\Psi_{\xi_0}(z+\xi)dz + I \tag{4.31}$$

and

$$V(\xi) = \frac{1}{c}\int_0^\infty e^{-z\gamma/c}\Phi_{\xi_0}(-z-\xi+X)dz + I. \tag{4.32}$$

In order to calculate the diffusion coefficient, it is first necessary to determine the null vector $\mathcal{V}(\epsilon)$ of the adjoint linear operator $\mathbf{L}^*$. Substituting $f(U) = H(U-\kappa)$ and $g(U) = g_0 U$ in equations (4.21) and (4.22) shows that the components of $\mathcal{V}$ satisfy the simultaneous equations

$$c\frac{d\mathcal{V}_1}{d\xi} + \gamma(\epsilon)\mathcal{V}_1 = \frac{\delta(\xi)}{|U_0'(0)|}Q_u\int w_e(z)\mathcal{V}_1(z)dz - \frac{\delta(\xi-\xi_0)}{|V_0'(\xi_0)|}Q_v\int w_i(z-\xi_0)\mathcal{V}_2(z)dz \tag{4.33}$$

$$c\frac{d\mathcal{V}_2}{d\xi} + \gamma(\epsilon)\mathcal{V}_2 = -\frac{\delta(\xi)}{|U_0'(0)|}Q_u\int w_i(z)\mathcal{V}_1(z)dz + \frac{\delta(\xi-\xi_0)}{|V_0'(\xi_0)|}Q_v\int w_e(z-\xi_0)\mathcal{V}_2(z)dz. \tag{4.34}$$

Proceeding along similar lines to [11], we make the ansatz that

$$\begin{aligned}\mathcal{V}_1(\xi) &= \mathcal{A}_1 e^{-\gamma\xi/c}H(\xi) - \mathcal{B}_1 e^{-\gamma[\xi-\xi_0]/c}H(\xi-\xi_0),\\ \mathcal{V}_2(\xi) &= -\mathcal{A}_2 e^{-\gamma\xi/c}H(\xi) + \mathcal{B}_2 e^{-\gamma[\xi-\xi_0]/c}H(\xi-\xi_0).\end{aligned} \tag{4.35}$$

Substituting back into the adjoint equations yields algebraic conditions for the constant coefficients $\mathcal{A}_j, \mathcal{B}_j$:

$$\mathcal{A}_1 = \frac{Q_u}{|U_0'(0)|}\left(\mathcal{A}_1\Omega_e[0] - \mathcal{B}_1\Omega_e[\xi_0]\right) \tag{4.36}$$

$$\mathcal{B}_1 = \frac{Q_v}{|V_0'(\xi_0)|}\left(\mathcal{B}_2\Omega_i[0] - \mathcal{A}_2\Omega_i[-\xi_0]\right) \tag{4.37}$$

$$\mathcal{A}_2 = \frac{Q_u}{|U_0'(0)|}\left(\mathcal{A}_1\Omega_i[0] - \mathcal{B}_1\Omega_i[\xi_0]\right) \tag{4.38}$$

$$\mathcal{B}_2 = \frac{Q_v}{|V_0'(\xi_0)|}\left(\mathcal{B}_2\Omega_e[0] - \mathcal{A}_2\Omega_e[-\xi_0]\right), \tag{4.39}$$

where

$$\Omega_j[x] = \int_0^\infty e^{-z\gamma/c} w_j(x+z)dz, \quad j = e, i. \tag{4.40}$$

Differentiating equations (4.31) and (4.32) with respect to ξ and using equations (2.31) and (2.32), shows that

$$U_0'(0) = -Q_u\Omega_e[0] - Q_v\Omega_i[-X] < 0, \tag{4.41}$$

and

$$V_0'(\xi_0) = Q_v\Omega_e[0] + Q_u\Omega_i[\xi_0] > 0. \tag{4.42}$$

We have also used the fact that the weight distributions $w_e(x), w_i(x)$ are even functions of x. Substituting these derivatives into equations (4.36) and (4.39) gives

$$\mathcal{B}_2 = -\frac{Q_v\Omega_e[-\xi_0]}{Q_u\Omega_i[\xi_0]}\mathcal{A}_2, \quad \mathcal{B}_1 = -\frac{Q_v\Omega_i[-\xi_0]}{Q_u\Omega_e[\xi_0]}\mathcal{A}_1. \tag{4.43}$$

4.3 Numerical results

In order to proceed analytically, it was convenient to make an adiabatic approximation where we assumed that the depression variables q_u and q_v do not change with time. We also made the further approximation that the fronts move as a composite wave and never drift with respect to each other. In this section we verify that our analytical assumptions are reasonable by considering numerical simulations of the full system given by equations (4.1), (4.2) (2.1b) and (2.2b) with $Q_{u,v} \to q_{u,v}$, though we retain the Heaviside firing rate function to allow us to compare directly the simulations and the analysis. Simulations were performed on a constant lattice spaced grid of length Δx with constant time step Δt such that the size of the composite waves is far smaller than the simulation region. Fig. 4.1 shows that our predicted mean front shape develops into a stochastic traveling wave moving at the speed resulting from our analysis. It can be seen that there is very good agreement between the mean profile and stochastic wavefront position. Moreover, given that the wave speed is approximately constant helps to verify our assumption that q_u and q_v do not change significantly enough to affect the wave motion.

In Fig. 4.2 we plot the mean and variance of wave position as a function of time, starting from initial conditions which are solutions to Eqs. (4.12) and (4.13). In order to numerically calculate the mean location of the front as a function of time, we carry out a large number of level set position measurements of the front associated with the left eye, say. That is, we determine the

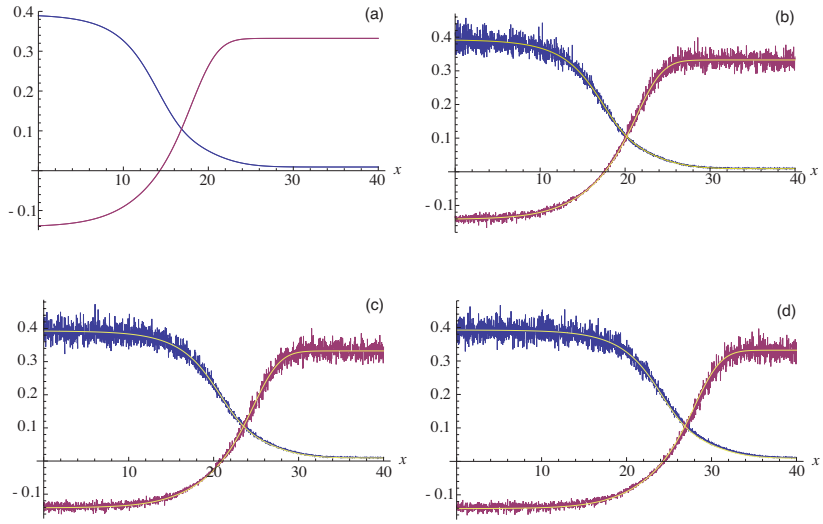

Figure 4.1: Effects of multiplicative noise in the activity variables. Simulation of the activity variables $u(x,t)$ (blue) and $v(x,t)$ (purple) for (a) t=0, (b) t=1, (c) t=2, (d) t=3. The continuous lines are the functions $U_0(x-ct)$ and $V_0(x-ct)$ which were found by solving equation (4.13). The functions U_0 and V_0 were also used for the initial condition. Parameter values were $a_i = 1, a_e = 0.4, \sigma_i = 1, \sigma_e = 2, \beta = 5, \kappa = 0.05, I = 0.24, \epsilon = 0.006$ with spatial and temporal grid sizes both being 0.01.

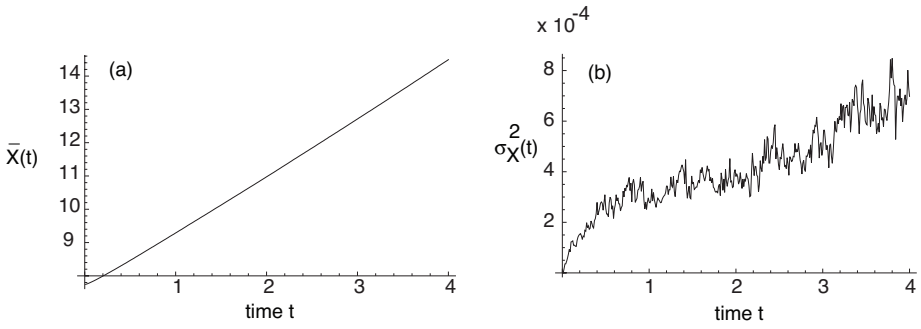

Figure 4.2: (a) Mean and (b) variance of the wave position for an ensemble of 128 stochastic simulations. Parameters were the same as Fig. 4.1

positions $X_a(t)$ such that $U(X_a(t),t) = a$, for various level set values $a \in (0.5\kappa, 1.3\kappa)$ and then define the mean location to be $\overline{X}(t) = \mathbb{E}[X_a(t)]$, where the expectation is first taken with respect to the sampled values a and then averaged over N trials. The corresponding variance is given by $\sigma_X^2(t) = \mathbb{E}[(X_a(t) - \bar{X}(t))^2]$. It can be seen that $\overline{X}(t)$ varies linearly with t, consistent with the assumption that there is constant speed wave, $\overline{X}(t) \sim c_\varepsilon t$. The variance initially increases rapidly with respect to t, but then follows linear behaviour consistent with a diffusive–like displacement of the wave from its uniformly translating position at long time scales, $\sigma_X^2(t) \sim 2D(\varepsilon)t$. The initial sharp increase in the variance results from the fact that the left and right fronts do move slightly with respect to each other, resulting in higher order behaviour. However, we find numerically that this component of the variance is small and bounded so that it becomes negligible as time increases.

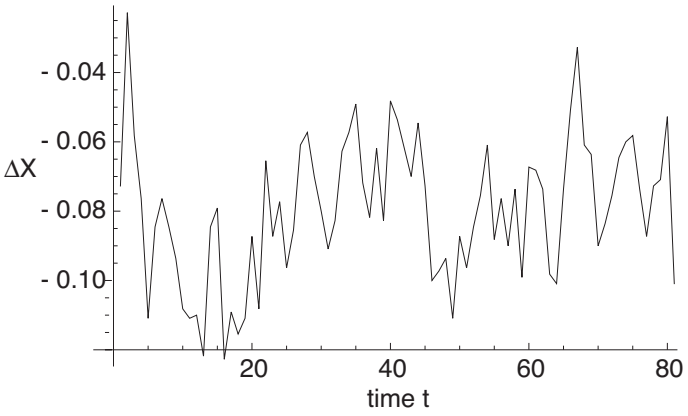

Figure 4.3: Difference ΔX in the position of the left-eye and right-eye fronts as a function of time t for a single realization. Parameters were the same as Fig. 4.1.

In order to show this, we carry out corresponding level set measurements of the right- front position by introducing $Y_a(t)$ such that $V(Y_a(t), t) = a$. We then define the difference in front positions according to $\Delta X_a(t) = X_a(t) - Y_a(t)$ and set $\Delta X(t) = \mathbb{E}[X_a(t) - Y_a(t)]$. Fig. 4.3 shows a time plot of $\Delta X(t)$, which verifies that this difference in motion is small (same order as the grid spacing for this particular simulation) and bounded.

Since our analysis predicts that the wave position will follow a Brownian motion, the time taken for a wave to travel a distance $L > 0$ has a distribution given by the standard first passage time formula for Brownian motion with drift c. That is, let T_L denote the first passage time for the wave to travel a distance L: $cT_L + \Delta(T_L) = L$ given $\Delta(0) = 0$. Then the first passage time density is

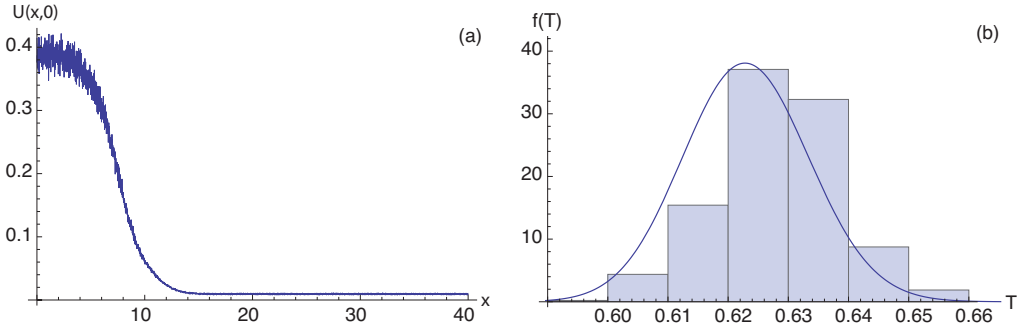

Figure 4.4: (a) Snapshot of a stochastic traveling wave (only left eye activity is shown). (b) First passage time distribution for the wave to travel a distance $L = 1$, starting from the wave profile in (a). Parameter values were $a_i = 1, a_e = 0.4, \sigma_i = 1, \sigma_e = 2, \beta = 5, \kappa = 0.05, I = 0.24, \epsilon = 0.006$ with spatial and temporal grid sizes both being 0.01.The best fit inverse Gaussian $\mathcal{N}^{-1}(\mu, \lambda)$ for the histogram gives the parameters $\mu = 0.62, \lambda = 2200$ which is in very good agreement with the theoretical predictions of $\mu = L/c = 0.6, \lambda = L^2/D = 2100$.

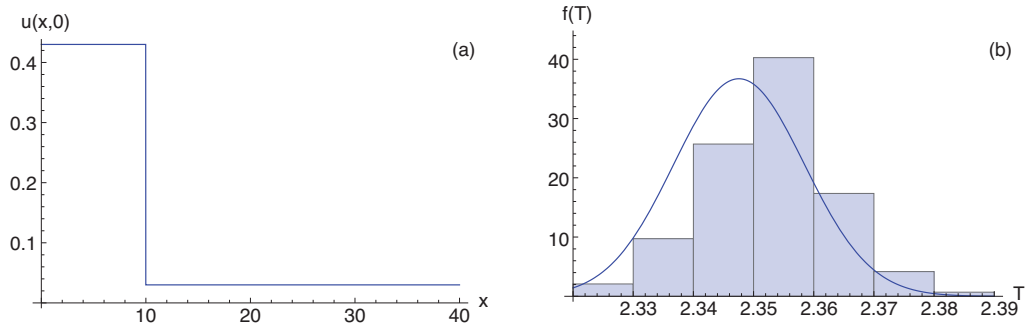

Figure 4.5: Same as Fig. 4.4 except that the initial condition is taken to be a right-eye dominant homogeneous steady-state perturbed by a step-function in left-eye activity. Although the wave now needs time to develop into a stochastic traveling front, the best fit inverse Gaussian still shows strong qualitative agreement.

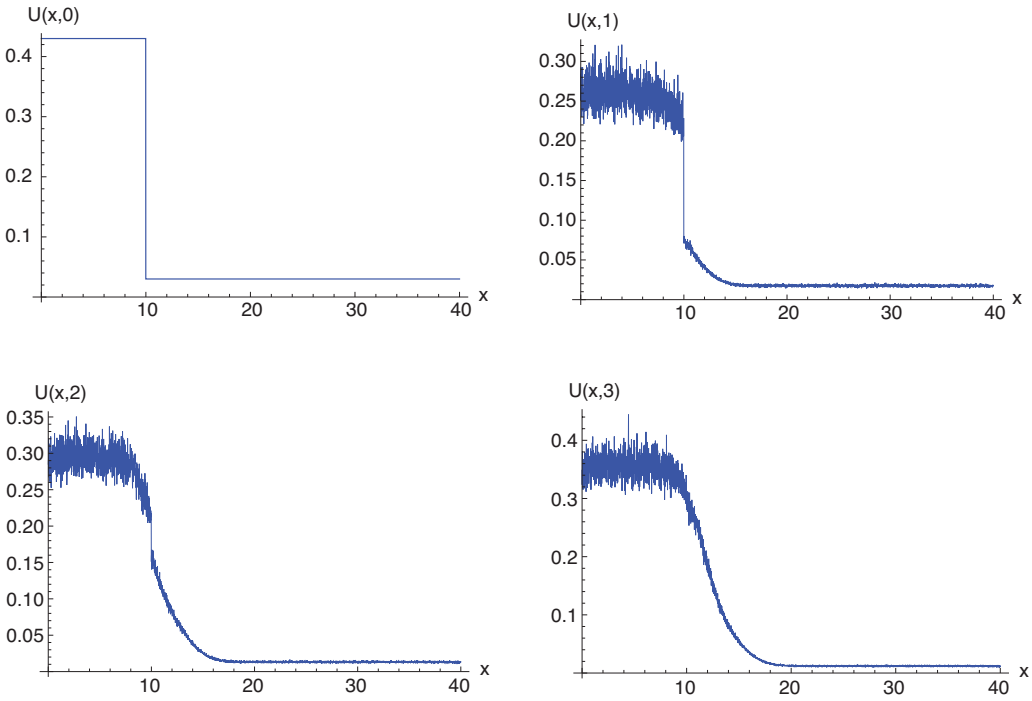

Figure 4.6: Simulation of the activity variable $U(x,t)$ evolving from a step input in the left-eye activity for the times $t = 0, 1, 2, 3$ with the same parameters as in Fig. 4.4.

given by an inverse Gaussian or Wald distribution [39]:

$$f(T_L) = \mathcal{F}(T_L; \frac{L}{c}, \frac{L^2}{D}), \tag{4.44}$$

where

$$\mathcal{F}(T; \mu, \lambda) = \left[\frac{\lambda}{2\pi T^3}\right]^{1/2} \exp\left(-\frac{\lambda(T-\mu)^2}{2\mu^2 T}\right). \tag{4.45}$$

Fig. 4.4 shows the first passage time distribution generated over a large number of simulations for an

initial condition given by a fully developed stochastic traveling wave. We find good agreement with our analysis, namely, that the distribution can be fitted by the predicted inverse Gaussian. If we choose to consider more experimentally realistic initial conditions, which represent a sudden change of contrast in a small region of the depressed stimulus, we find that the wave takes a substantial time to develop, which results in a slightly modified first passage distribution, although it is still well-fitted by an inverse Gaussian, as can be seen in Fig. 4.5. The corresponding development of the wave is illustrated in Fig. 4.6.

So far we have assumed that all the noise is in the activity variables. We now study numerically how noise affects first passage time distributions when placed in the depression variables. We assume once again that a traveling wave crosses cortex significantly faster than the relaxation time of synaptic depression, so that q_u and q_v can be taken to be constant with respect to time. However, they are no longer constant with respect to space nor with respect to trials, that is, $q_u = Q_u(x)$ and $q_v = Q_v(x)$ with Q_u, Q_v random variables of x. So although the wave itself will travel deterministically in a given trial, the functions $Q_u(x)$ and $Q_v(x)$ will be different across trials. In several experimental studies [44, 45] of binocular rivalry waves, a dominance switch was induced about half-way through a normal dominance cycle by locally changing the contrast in the depressed stimulus. The latter can be represented by increasing the input strength I over a small region in our model. This suggests taking q_u and q_v to evolve according to

$$\tau_s dq_u(x,t) = [1 - q_u(x,t)]\, dt + \eta dW_{q_u,x}(t) \tag{4.46}$$

$$\tau_s dq_v(x,t) = [1 - q_v - \beta q_v]\, dt + \eta dW_{q_v,x}(t) \tag{4.47}$$

over the time interval $[t_0, T]$. As before, the Brownian motions $dW_{q_{u/v},x}$ are independent. It is assumed that a switch from left to right eye dominance occurs at $t = t_0$ so that $u(x,t) < \kappa$ and $v(x,t) > \kappa$ for $t \in (t_0, T)$. The time T is then chosen so that the system is about 2/3 of the way through a rivalry oscillation, such that$Q_u(x) = q_u(x,T)$ and $Q_v(x) = q_v(x,T)$. (Similar results were obtained for different cycle lengths and choices of T away from the beginning or end of a cycle). Thus, the quenched random variables $Q_u(x)$ and $Q_v(x)$ are obtained by taking a snapshot of two lines of independent Ornstein-Uhlenbeck processes. Figs. 4.7 and 4.8 show numerically that the first passage time distribution is still well approximated by an inverse Gaussian distribution. Fig. 4.9 illustrates the development and propagation of a wave on top of quenched random depression variables. As can be seen there is still an approximately constant overall shape, though the front's

position will no longer move at a constant speed.

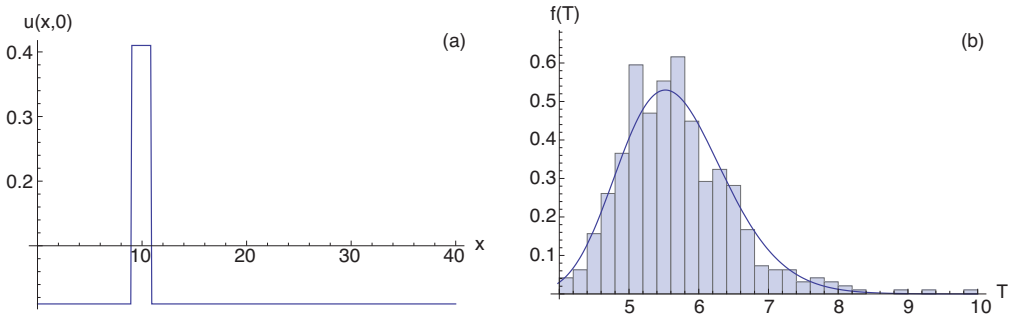

Figure 4.7: Effects of quenched noise in the depression variables. (a) Initial condition given by a right-eye dominant homogeneous steady state perturbed by a narrow square pulse of left-eye activity. (b) First passage time distribution for a wave to travel a distance $L = 6$ starting from the initial condition shown in (a). Parameter values were $a_i = 1, a_e = 0.4, \sigma_i = 1, \sigma_e = 2, \beta = 5, \kappa = 0.05, I = 0.24, \eta = 0.037\langle Q \rangle$, where $\langle Q \rangle$ is the spatial average of the quenched depression variables (to make the results comparable with multiplicative noise). The spatial grid size $\Delta x = 0.1$ and the temporal grid step is $\Delta t = 0.01$. The solid curve in (b) is the best fit inverse Gaussian.

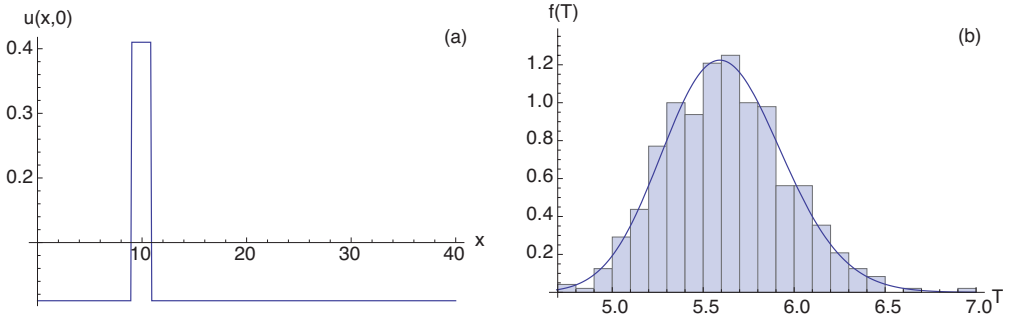

Figure 4.8: Same as in Fig.4.7, except the noise is now smaller with $\eta = 0.025\langle Q \rangle$.

4.4 Discussion

In this section we have extended the deterministic neural field model of binocular rivalry waves presented in chapter 2, and the stochastic neural field analysis of chapter 3 to present a model of stochastic wave propagation in binocular rivalry. As shown in chapter 2, noise in the activity variables is not itself sufficient for the generation of rivalry waves, since it does not create a direction bias. However, as shown in this chapter noise does have a significant impact on binocular rivalry waves in the presence of slow adaptation. In particular, we predict that regardless of whether noise primarily effects the activity or depression variables, the distribution of first passage times is always inverse Gaussian. This is a key prediction which presents an opportunity for further experimental

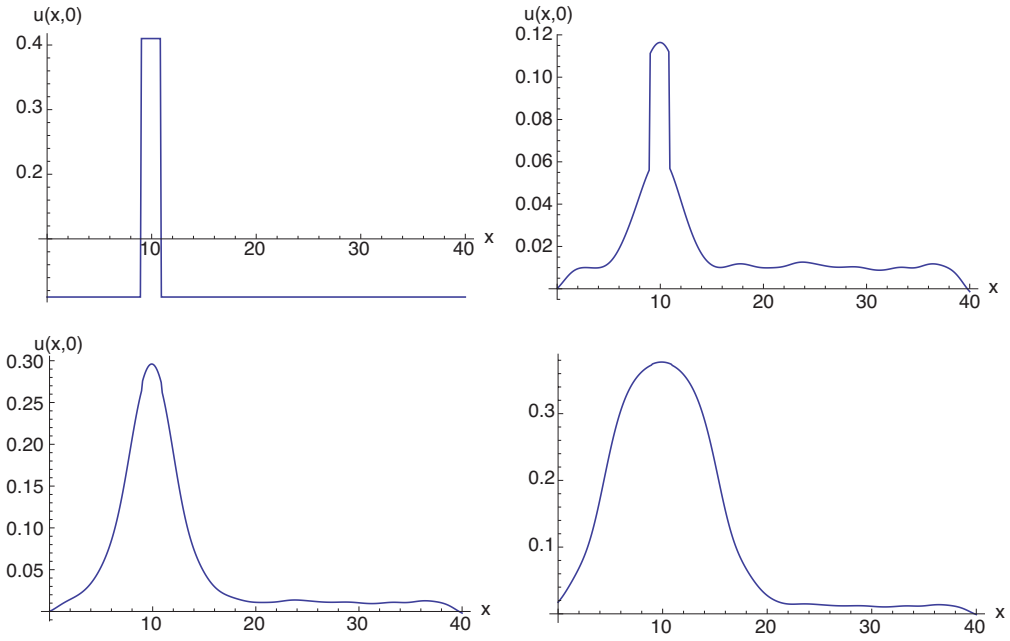

Figure 4.9: Development of an activity variable wave on top of quenched stochastic depression variables $Q_u(x), Q_v(x)$. Parameters are the same as Fig. 4.8

verification of the theories presented in this thesis, in particular our treatment of stochastic binocular rivalry waves.

In future work it would be interesting to extend this neural field theory model to a more realistic network topology. Instead of considering one line of neurons for each eye, one could consider a circle of neurons for each point in the visual field - this would allow orientation information to be taken into account. One could then investigate the experimental observation that the speed of binocular rivalry waves depends on the orientation of the left and right eye grating stimuli [81]. Moreover, experiments on waves crossing gaps in perceptual grating stimuli have found that gap crossing is a stochastic variable and we would hope that it is possible to extend our neural field framework to situations involving non-constant underlying orientations such as this one.

Chapter 5

General Stochastic Neural Field Theory

The analysis of chapter 3 introduced new work on stochastic Amari-type neural fields with the eventual aim of studying stochastic binocular rivalry waves. However, as briefly mentioned in chapter 1, other types of neural field equation are possible and we will show in this chapter that noise affects them in a qualitatively different manner. Up until this point we have been considering fronts propagating between metastable states which are known in the dynamical systems PDE literature as pushed fronts. As a contrast it is also quite possible to have waves which propagate into an unstable state, known as a pulled fronts. So-called pulled fronts can also exist in neural field equations and it will be shown that like their PDE counterparts they display several interesting features in the presence of noise. In particular, Wilson-Cowan type neural fields support a pulled front as opposed to a pushed front. For a stochastic extension of the Wilson-Cowan neural field model this front undergoes subdiffusive wandering as opposed to the diffusive motion found for the pushed fronts in Amari-type fields. To conclude this wider study of stochastic neural fields we will then present a master equation approach to neural field theory and show that it is possible to recover a multiplicative noise term in the field limit.

5.1 Neural fields and pulled fronts

Neural field equations with a sigmoidal or Heaviside nonlinearity tend to support a pair of stable spatially uniform fixed points (corresponding to low and high activity states, respectively) so that

a front solution linking these states propagates into a (meta)stable state rather than an unstable state. However, it is possible to construct a neural field equation in which the low activity state is unstable. Consider, for example, the Wilson-Cowan model

$$\tau \frac{\partial a(x,t)}{\partial t} = -a(x,t) + F\left(\int_{-\infty}^{\infty} w(x-x')a(x',t)dx' \right). \tag{5.1}$$

In contrast to equation (1.13), in which $u(x,t)$ represents a local population current or voltage, the field $a(x,t)$ represents a local population firing rate. (For a detailed discussion of different neural field representations see the reviews [28, 14]). In addition to the convolution integral now being inside the nonlinear rate function F, we have the additional constraint that $a(x,t) \geq 0$ for all (x,t). Note that the restriction to positive values of a is a feature shared with population models in ecology or evolutionary biology, for example, where the corresponding dependent variables represent number densities. Indeed, equation (5.1) has certain similarities with a nonlocal version of the Fisher-Kolmogorov *et. al.* (F-KPP) equation, which takes the form [40, 7]

$$\tau \frac{\partial p(x,t)}{\partial t} = D\frac{\partial^2 p(x,t)}{\partial x^2} + \mu p(x,t)\left(1 - \int_{-\infty}^{\infty} K(x-x')p(x',t)dx'\right). \tag{5.2}$$

One major difference from a mathematical perspective is that equation (5.2) supports traveling fronts even when the range of the interaction kernel K goes to zero, that is, $K(x) \to \delta(x)$, since we recover the standard local F-KPP equation [35]. In particular, as the nonlocal interactions appear nonlinearly in equation (5.2) they do not contribute to the linear spreading velocity in the leading edge of the front. On the other hand, nonlocal interactions play a necessary role in the generation of fronts in the neural field equation (5.1).

5.2 Wave speed and asymptotic convergence

Suppose that $F(a)$ in equation (5.1) is a positive, bounded, monotonically increasing function of a with $F(0) = 0$, $\lim_{a\to 0^+} F'(a) = 1$ and $\lim_{a\to\infty} F(a) = 1$. For concreteness, we take

$$F(a) = \begin{cases} 0, & a \leq 0 \\ a, & 0 < a \leq \kappa \\ \kappa, & a > \kappa \end{cases} \tag{5.3}$$

A homogeneous fixed point solution A^* of equation (5.1) satisfies

$$A^* = F(W_0 A^*), \quad W_0 = \int_{-\infty}^{\infty} w(y)dy. \tag{5.4}$$

In the case of the given piecewise linear firing rate function, we find that if $W_0 > 1$, then there exists an unstable fixed point at $A^* = 0$ and a stable fixed point at $A^* = \kappa$. The construction of a front solution linking the stable and unstable fixed points differs considerably from that considered in chapter 2. Following the PDE theory of fronts propagating into unstable states [78], we expect there to be a continuum of front velocities and associated traveling wave solutions. A conceptual framework for studying such solutions is the linear spreading velocity v^*, which is the asymptotic rate with which an initial localized perturbation spreads into an unstable state based on the linear equations obtained by linearizing the full nonlinear equations about the unstable state. Thus, consider a traveling wave solution $\mathcal{A}(x - ct)$ of equation (5.1) with $\mathcal{A}(\xi) \to \kappa$ as $\xi \to -\infty$ and $\mathcal{A}(\xi) \to 0$ as $\xi \to \infty$. One can determine the range of velocities c for which such a solution exists by assuming that $\mathcal{A}(\xi) \approx e^{-\lambda \xi}$ for sufficiently large ξ. The exponential decay of the front suggests that we linearize equation (5.1), which in traveling wave coordinates (with $\tau = 1$) takes the form

$$-c\frac{d\mathcal{A}(\xi)}{d\xi} = -\mathcal{A}(\xi) + \int_{-\infty}^{\infty} w(\xi - \xi')\mathcal{A}(\xi')d\xi'. \tag{5.5}$$

However, in order to make the substitution $\mathcal{A}(\xi) \approx e^{-\lambda \xi}$ we need to restrict the integration domain of ξ' to the leading edge of the front. Suppose, for example that $w(x)$ is given by the Gaussian distribution

$$w(x) = \frac{W_0}{\sqrt{2\pi\sigma^2}} e^{-x^2/2\sigma^2}. \tag{5.6}$$

Given the fact that the front solution $\mathcal{A}(\xi)$ is bounded, we introduce a cut-off X with $\sigma \ll X \ll \xi$, and approximate equation (5.5) by

$$-c\frac{d\mathcal{A}(\xi)}{d\xi} = -\mathcal{A}(\xi) + \int_{\xi - X}^{\xi + X} w(\xi - \xi')\mathcal{A}(\xi')d\xi'. \tag{5.7}$$

Substituting the exponential solution in (5.5) then yields the dispersion relation $c = c(\lambda)$ with

$$c(\lambda) = \frac{1}{\lambda}\left[\int_{-X}^{X} w(y)e^{-\lambda y}dy - 1\right]. \tag{5.8}$$

Finally, we now take the limit $X \to \infty$ under the assumption that $w(y)$ is an even function to yield

$$c(\lambda) = \frac{1}{\lambda}\left[\widehat{W}(\lambda) + \widehat{W}(-\lambda) - 1\right], \tag{5.9}$$

where $\widehat{W}(\lambda)$ is the Laplace transform of $w(x)$:

$$\widehat{W}(\lambda) = \int_0^\infty w(y)e^{-\lambda y}dy. \tag{5.10}$$

If $W_0 > 1$ (necessary for the zero activity state to be unstable) then $c(\lambda)$ is a positive unimodal function with $c(\lambda) \to \infty$ as $\lambda \to 0$ or $\lambda \to \infty$ and a unique minimum at $\lambda = \lambda^*$, see black curve in Fig. 5.1. Assuming that the full nonlinear system supports a pulled front then a sufficiently localized initial perturbation (one that decays faster than $e^{-\lambda^* x}$) will asymptotically approach the traveling front solution with the minimum wave speed $c^* = c(\lambda^*)$. Note that $c^* \sim \sigma$ and $\lambda^* \sim \sigma^{-1}$.

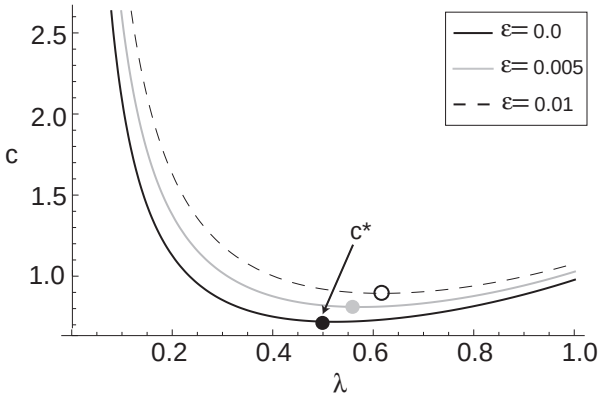

Figure 5.1: Velocity dispersion curve (black) for a Gaussian weight distribution with $\sigma = 1.0$ and $W_0 = 1.2$. Minimum wave speed is $c^* = 0.71$. Also shown are shifted dispersion curves in the presence of multiplicative noise for various noise amplitudes ε and $C(0) = 10$.

One of the most important properties of nonlinear diffusion equations supporting pulled fronts is that the long–time convergence of steep initial conditions towards the pulled front solution is universal in leading and subleading order with respect to an asymptotic expansion in $1/\sqrt{t}$ [27]. This result generalizes to higher order PDEs, difference-differential equations and equations with a memory kernel. For a formal proof of this universal behaviour using matched asymptotics, see Ebert and van Saarloos [27]. Unfortunately, this analysis cannot be applied straightforwardly to the neural field equation (5.1) with F given by equation (5.3), since the nonlinear rate function has a discontinuous first derivative. Nevertheless, it is still possible to give a heuristic argument for the asymptotic convergence to the pulled front, which can also be found in [27]. Linearizing equation

(5.1) about $a = 0$ gives

$$\frac{\partial a(x,t)}{\partial t} = -a(x,t) + \int_{-\infty}^{\infty} w(x-x')a(x',t)dx'. \tag{5.11}$$

An arbitrary initial condition $a(x,0)$ will evolve under equation (5.11) as

$$a(x,t) = \int_{-\infty}^{\infty} G(x-y,t)a(y,0)dy, \tag{5.12}$$

where $G(x,t)$ is the Green's function

$$G(x,t) = \int_{-\infty}^{\infty} e^{ikx - i\omega(k)t}\frac{dk}{2\pi} \tag{5.13}$$

and

$$\omega(k) = i\widehat{W}(ik). \tag{5.14}$$

Given a sufficiently steep initial condition, for which the Fourier transform of $a(x,0)$ is analytic, the asymptotic behaviour of $a(x,t)$ can be obtained from the large–time asymptotics of $G(x,t)$ based on steepest descents. The latter will depend on the frame of reference. In a uniformly moving frame $\xi = x - ct$, we have

$$G(\xi,t) = \int_{-\infty}^{\infty} e^{ik\xi - i[\omega(k)-ck]t}\frac{dk}{2\pi}. \tag{5.15}$$

In the limit $t \to \infty$ and fixed ξ, we can deform the k–contour to go through the saddle point k^* in the complex k plane where $\omega(k) - ck$ varies least, that is,

$$\frac{d[\omega(k)-ck]}{dk} = 0 \implies c = \left.\frac{d\omega(k)}{dk}\right|_{k^*}. \tag{5.16}$$

The integral will then be dominated by the contribution in a neighborhood of the saddle. (If there are several saddle points then the dominant one will be the saddle with the maximal growth rate). Expanding the integral expression for the Green's function about the saddle to second order leads to the Gaussian approximation

$$G(\xi,t) = e^{ik^*\xi - i[\omega(k^*)-ck^*]t}\psi(\xi,t) \tag{5.17}$$

with

$$\psi(\xi,t) \approx \int_{-\infty}^{\infty} e^{i(k-k^*)\xi - \mathcal{D}(k-k^*)^2} = \frac{e^{-\xi^2/(4\mathcal{D}t)}}{\sqrt{4\pi\mathcal{D}t}} \tag{5.18}$$

and

$$\mathcal{D} = \frac{i}{2} \left. \frac{d^2\omega(k)}{dk^2} \right|_{k^*}. \tag{5.19}$$

It is important not to confuse the diffusion coefficient $\mathcal{D}$ associated with the asymptotics of a deterministic pulled front with the diffusion coefficient D associated with the effects of noise on the stochastic wandering of a front.

For general speeds c, the growth or decay rate of the Fourier mode at the saddle, which is given by $\mathrm{Im}[\omega(k^*) - ck^*]$, will be non–zero. The linear spreading velocity is then defined as the one for which there is zero growth rate [27], so that

$$c^* = \frac{\mathrm{Im}\,\omega(k^*)}{\mathrm{Im}\,k^*}, \tag{5.20}$$

which supplements equation (5.16). Let $k_i = \mathrm{Im}\,k^*$, $k_r = \mathrm{Re}\,k^*$, $\omega_i = \mathrm{Im}\,\omega(k^*)$ and $\omega_r = \mathrm{Re}\,\omega(k^*)$. Equating real and imaginary parts in equation (5.16) and using the Cauchy–Riemann relations shows that $c^* = d\omega_i/dk_i$ and $0 = d\omega_i/dk_r$. As with all the examples considered in [27], we find that $k_r = 0$ and $\omega_r = 0$ for a Gaussian weight distribution. Equations (5.14), (5.16) and (5.20) then imply that $c^* = c(\lambda^*)$ as before, with $\lambda^* = k_i$. Moreover, $\mathcal{D}$ is positive and real with

$$\mathcal{D} = \frac{\lambda^*}{2} \left. \frac{d^2c(\lambda)}{d\lambda^2} \right|_{\lambda^*}. \tag{5.21}$$

Positivity of $\mathcal{D}$ follows from the fact that λ^* is a minimum of $c(\lambda)$. We conclude from the asymptotic analysis of the linear problem (5.11) that, given a sufficiently localized initial condition, we have the long–time solution $a(x,t) \sim e^{-\lambda^*\xi}\psi(\xi,t)$ where $\xi = x - c^*t$ and the so–called leading edge variable $\psi(\xi,t)$ satisfies the diffusion equation

$$\frac{\partial\psi}{\partial t} = \mathcal{D}\frac{\partial^2\psi}{\partial\xi^2} + \text{h.o.t.} \tag{5.22}$$

As previously pointed out by Ebert and van Saarloos [27], although the spreading of the leading edge under linearization gives the right qualitative behaviour, it fails to match correctly the traveling front solution of the full nonlinear system. In particular, the asymptotic front profile takes the form $\mathcal{A}(\xi) \sim \xi e^{-\lambda^*\xi}$ for $\xi \gg 1$. The factor of ξ reflects the fact that at the saddle point the two branches of the velocity dispersion curve $c(\lambda)$ meet, indicating a degeneracy. If one considers the asymptotic behaviour of the solution of the full nonlinear neural field equation, we find that in the asymptotic regime $\xi \gg 1, t \gg 1$, we have a linear equation whose Green's function can be analyzed as before

using steepest descents. In particular, we obtain a leading edge variable $\psi(\xi,t)$ that satisfies a diffusion equation. Hence, in order to match the $\xi e^{-\lambda^*\xi}$ asymptotics of the front solution we follow [27] and take the so–called dipole solution of the diffusion equation

$$\psi(x,t) = -\partial_\xi \frac{e^{-\xi^2/(4\mathcal{D}t)}}{\sqrt{4\pi\mathcal{D}t}} = \xi \frac{e^{-\xi^2/(4\mathcal{D}t)}}{\sqrt{2\pi}(2\mathcal{D}t)^{3/2}}. \tag{5.23}$$

Putting all of this together, we expect the leading edge to relax asymptotically as

$$a \sim \xi e^{-\lambda^*\xi} e^{-\xi^2/(4\mathcal{D}t)} t^{-3/2} \tag{5.24}$$

with $\xi = x - v^*t$. Finally, writing

$$e^{-\lambda^*\xi} t^{-3/2} = e^{-\lambda^*[x-v^*t-X(t)]}, \quad X(t) = -\frac{3}{2\lambda^*}\ln t, \tag{5.25}$$

suggests that to leading order the velocity relaxes to the pulled velocity v^* according to (see also [27])

$$v(t) = v^* + \dot{X}(t) = v^* - \frac{3}{2\lambda^* t} + h.o.t. \tag{5.26}$$

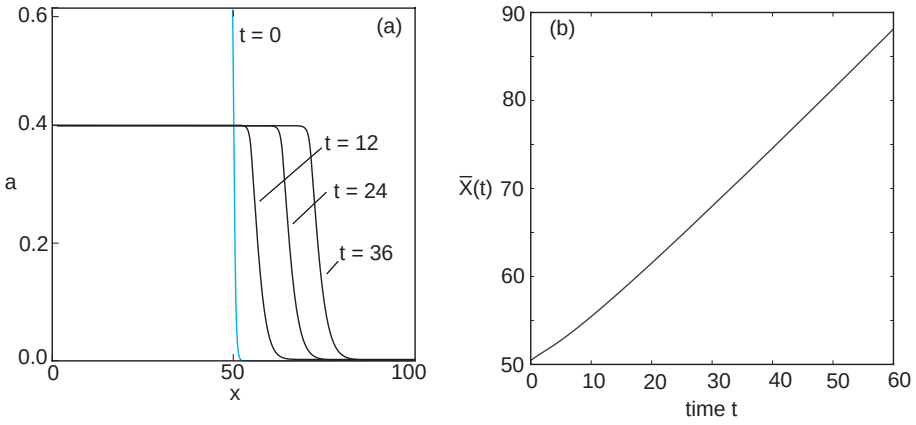

Figure 5.2: Propagation of a pulled front solution of the neural field equation (5.1) with piecewise linear firing rate function (5.3) and a Gaussian weight distribution (5.6). Here $W_0 = 1.2, \sigma = 1.0$ and $\kappa = 0.4$. (a) Snapshots of the front profile evolving from an initial condition consisting of a steep sigmoid function of unit amplitude (light blue curve). (b) Plot of mean displacement $\overline{X}(t)$ as a function of time t.

In the above analysis we have made two major assumptions. First, that the piecewise–linear neural field equation (5.1) and (5.3) supports the propagation of a pulled front rather than a pushed front; in the latter case velocity selection would depend on the full nonlinear system. Second, given

the existence of a pulled front, the asymptotic convergence to the front exhibits universal features also found for the nonlinear diffusion equation even though the nonlinearity is piecewise smooth. These assumptions appear to be confirmed by numerical solutions of equation (5.1). In Fig. 5.2(a) we show snapshots of a traveling front evolving from an initial condition consisting of a steep sigmoid. The corresponding mean displacement is a linear function of time (see Fig. 5.2(b)) with a slope $c \approx 0.68$ consistent with the minimal wave speed $c^* = 0.71$ of Fig. 5.1. Such a wave speed was also found for other values of κ. The universal nature of the asymptotic convergence of the wave speed to its final value independent of the height of the wave (level set) is illustrated in Fig. 5.3

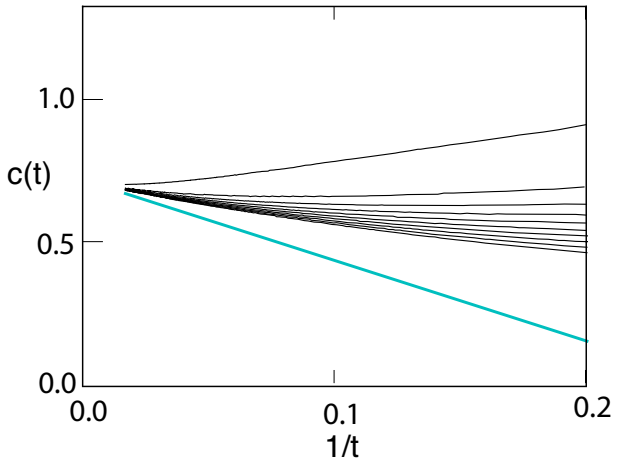

Figure 5.3: Plot of wave speed $v(t)$ as a function of inverse time $1/t$ for various front amplitudes (level sets, black lines). Straight blue line is analytical expression for speed given by equation (5.26). All parameters as in Fig. 5.2.

5.3 Subdiffusive fluctuations in the presence of multiplicative noise

In the case of the F-KPP equation with multiplicative noise, it has previously been shown that the stochastic wandering of a pulled front about its mean position is subdiffusive with $\mathrm{var}\Delta(t) \sim t^{1/2}$, in contrast to the diffusive wandering of a front propagating into a metastable state for which $\mathrm{var}\Delta(t) \sim t$ [63]. Such scaling is a consequence of the asymptotic relaxation of the leading edge of the deterministic pulled front. Since pulled front solutions of the neural field equation (5.1) exhibit similar asymptotic dynamics, see equation (5.24), it suggests that there will also be subdiffusive wandering of these fronts in the presence of multiplicative noise. In order to illustrate this, consider

the Langevin equation

$$dA(x,t) = \left[-A(x,t) + F\left(\int_{-\infty}^{\infty} w(x-y)A(y,t)dy\right)\right]dt + \varepsilon^{1/2} g_0 A(x,t)dW(x,t) \tag{5.27}$$

with $W(x,t)$ a Wiener process satisfying equation (3.2). Note that the noise term has to vanish when $A(x,t) = 0$, since the firing rate A is restricted to be positive. Hence, the noise has to be multiplicative. Formally speaking, we can carry over the analysis of the Langevin equation (3.1). First, the multiplicative noise leads to a modification in the mean speed of the front. That is, writing

$$A(x,t) = A_0(\xi - \Delta(t)) + \varepsilon^{1/2}\Phi(\xi - \Delta(t), t) \tag{5.28}$$

with $\xi = x - ct$, we find that the mean profile A_0 satisfies the deterministic equation

$$-c\frac{dA_0}{d\xi} + A_0(\xi)[1 - \varepsilon g_0^2 C(0)] = F\left(\int_{-\infty}^{\infty} w(\xi - \xi')A_0(\xi')d\xi'\right). \tag{5.29}$$

The mean velocity of the pulled front is now given by the minimum of the dispersion curve $c = c_\varepsilon$ where

$$c_\varepsilon(\lambda) = \frac{1}{\lambda}\left[\widehat{W}(\lambda) + \widehat{W}(-\lambda) - [1 - \varepsilon g_0^2 C(0)]\right]. \tag{5.30}$$

Fluctuations thus shift the dispersion curve to higher velocities as shown in Fig. 5.1. However, it is no longer possible to derive an expression for the diffusion coefficient $D(\varepsilon)$ along the lines of equation (3.18), since both numerator and denominator would diverge for a pulled front. This reflects the asymptotic behaviour of the leading edge of the front. It is also a consequence of the fact that there is no characteristic time scale for the convergence of the front velocity to its asymptotic value, which means that it is not possible to separate the fluctuations into a slow wandering of front position and fast fluctuations of the front shape [27, 59].

Nevertheless, numerical simulations of equation (5.27) with F given by the piecewise linear firing rate (5.3) are consistent with subdiffusive wandering of the front. In Fig. 5.4 we plot the mean $\overline{X}(t)$ and variance $\sigma_X^2(t)$ of the position of a pulled front solution of equation (5.27), which are obtained by averaging over level sets along identical lines to section 3.1.2. It can be seen that $\overline{X}(t)$ varies linearly with t with a slope equal to a speed $c \approx 0.8$, which is consistent with the shifted minimal wave speed, see Fig. 5.1 for $\varepsilon = 0.005$. Moreover, the variance appears to exhibit subdiffusive behaviour over longer time scales. This is further illustrated by plotting a log-log plot of $\sigma_X^2(t)$ against time t, see Fig. 5.5. It can be seen that at intermediate time-scales the slope of the curve is approximately

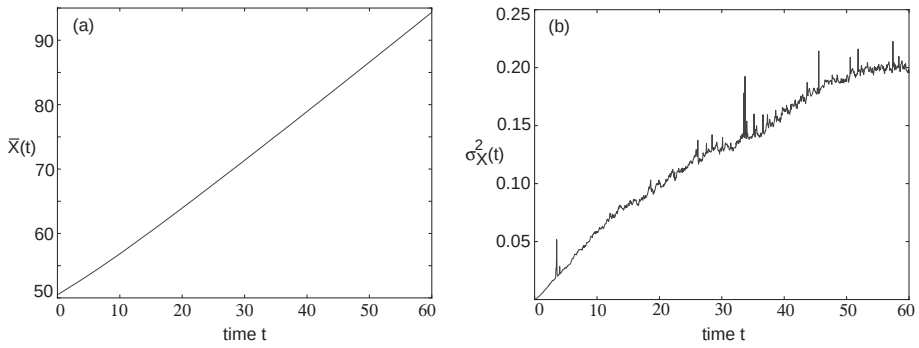

Figure 5.4: Plot of (a) mean $\overline{X}(t)$ and (b) variance $\sigma_X^2(t)$ of the position of a stochastic pulled front as a function of time. Noise amplitude $\varepsilon = 0.005$ and $\kappa = 0.8$. Other parameter values as in Fig. 5.2.

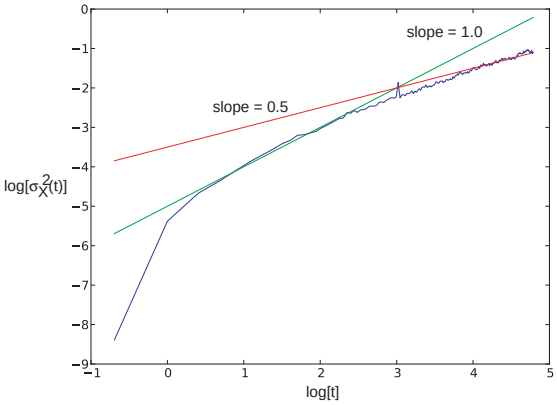

Figure 5.5: Log-log plot of variance $\sigma_X^2(t)$ as a function of time t. Same parameter values as Fig. 5.4.

equal to one, consistent with normal diffusion, but at later times the slope decreases, indicating subdiffusive behaviour.

5.4 Master equation for stochastic neural fields

One of the interesting features of the neural field equation (5.1) is that it forms the starting point for a master equation formulation of stochastic neurodynamics [18, 19, 12, 13]. The latter treats a neural field as a continuum of interacting local populations. The state of each population is represented by the number of currently active neurons, and the state transitions of the associated discrete Markov process are chosen such that deterministic neural field equations of the form (5.1) are recovered in the thermodynamic limit $N \to \infty$, where N is the number of neurons in each local population. In order to develop the basic formalism, it is simpler to start off with a spatially discrete network and take the continuum limit at the end.

Thus, suppose that there exist M homogeneous local neuronal populations labeled $i = 1, \ldots, M$, each of size N. Assume that all neurons of a given population are equivalent in the sense that the effective pairwise synaptic interaction between a neuron of population i and a neuron of population j only depends on i and j. Suppose that there are $N_k(t)$ active neurons in the kth population. The state or configuration of the network is now specified by the vector $\mathbf{N}(t) = (N_1(t), N_2(t), \ldots, N_M(t))$, where each $N_i(t)$ is treated as a stochastic variable that evolves according to a one–step jump Markov process. Let $P(\mathbf{n}, t) = \text{Prob}[\mathbf{N}(t) = \mathbf{n}]$ denote the probability that the network of interacting populations has configuration $\mathbf{n} = (n_1, n_2, \ldots, n_M)$ at time $t, t > 0$, given some initial distribution $P(\mathbf{n}, 0)$. The probability distribution is then taken to evolve according to a master equation of the form [18, 19, 12]

$$\frac{dP(n,t)}{dt} = \sum_{k=1}^{M} \sum_{r=\pm 1} [T_{k,r}(n - r\mathbf{e}_k)P(n - r\mathbf{e}_k, t) - T_{k,r}(n)P(n,t)]. \tag{5.31}$$

Here $\mathbf{e}_k$ denotes the unit vector whose kth component is equal to unity. The corresponding transition rates are given by

$$T_{k,-1}(n) = n_k, \; T_{k,+1}(n) = NF\left(\sum_l w_{kl} n_l / N\right), \tag{5.32}$$

where w_{kl} is the effective synaptic weight distribution from the lth to the kth population. Equation (5.31) is supplemented by the boundary conditions $P(n,t) \equiv 0$ if $n_i = -1$ for some i. The master

equation preserves the normalization condition $\sum_{n_1\geq 0}\sum_{n_M\geq 0} P(n,t) = 1$ for all $t \geq 0$. Now introduce the rescaled variables $a_k = n_k/N$ and corresponding transition rates

$$\Omega_{k,-1}(a) = a_k,\ \Omega_{k,1}(a) = F\left(\sum_l w_{kl}a_l\right). \tag{5.33}$$

Carrying out a Kramers–Moyal expansion to second order then leads to the multivariate Fokker–Planck equation

$$\frac{\partial P(a,t)}{\partial t} = -\sum_{k=1}^{M}\frac{\partial}{\partial a_k}\left[V_k(a)P(a,t)\right] + \frac{\epsilon}{2}\sum_{k=1}^{M}\frac{\partial^2}{\partial a_k^2}\left[B_k(a)P(a,t)\right] \tag{5.34}$$

with $\epsilon = N^{-1}$,

$$V_k(a) = \Omega_{k,1}(a) - \Omega_{k,-1}(a), \quad B_k(a) = \Omega_{k,1}(a) + \Omega_{k,-1}(a). \tag{5.35}$$

The solution to the Fokker–Planck equation (5.34) determines the probability density function for a corresponding stochastic process $\mathbf{A}(t) = (A_1(t),\ldots,A_M(t))$, which evolves according to a neural Langevin equation of the form

$$dA_k = V_k(A)dt + \epsilon^{1/2}b_k(A)dW_k(t). \tag{5.36}$$

with $b_k(x)^2 = B_k(x)/2$. Here $W_k(t)$ denotes an independent Wiener process such that

$$\langle dW_k(t)\rangle = 0, \quad \langle dW_k(t)dW_l(s)\rangle = 2\delta_{k,l}\delta(t-s)dtds. \tag{5.37}$$

We can now take the continuum limit of the above Langevin equation along the lines outlined in [12]. Suppose that there is a uniform density ρ of neuronal populations distributed along the x-axis. We partition the x-axis into discrete intervals of length Δx within which there are $\rho\Delta x$ populations. Let us denote the set of populations in the interval $[m\Delta x,(m+1)\Delta x)$ by $\mathcal{N}(m\Delta x)$. As a further approximation, suppose that the weights w_{kl} are slowly varying on the length–scale Δx so that we can write $w_{kl} = w(m\Delta x, n\Delta x)$ for all $k \in \mathcal{N}(m\Delta x)$ and $l \in \mathcal{N}(n\Delta x)$. It follows that

$$\sum_l w_{kl}A_l = \sum_n \omega(m\Delta x, n\Delta x)\sum_{l\in\mathcal{N}(n\Delta x)} A_l. \tag{5.38}$$

Define the local spatially averaged activity variable $A(n\Delta x)$ according to

$$A(n\Delta x) = \langle A_l \rangle \equiv \frac{1}{\rho \Delta x} \sum_{l \in \mathcal{N}(n\Delta x)} A_l \tag{5.39}$$

where $\rho\Delta x$ is the number of populations in each set $\mathcal{N}(n\Delta x)$. Performing a local population averaging of the Langevin equation (5.36) with respect to $k \in \mathcal{N}(m\Delta x)$, and making the mean field approximation $\langle b_k(A)dW_k \rangle = b_k(\langle A \rangle)\langle dW_k \rangle$ then gives[1]

$$\begin{aligned} dA(m\Delta x,t) &= \left[-A(m\Delta x,t) + F\left(\rho \Delta x \sum_n w(m\Delta x, n\Delta x) A(n\Delta x) \right) \right] dt & (5.40) \\ &\quad + \varepsilon^{1/2} g_m[A] dW(m\Delta x,t), & (5.41) \end{aligned}$$

where

$$g_m[A] = \sqrt{A(m\Delta x,t) + F\left(\rho \Delta x \sum_n w(m\Delta x, n\Delta x) A(n\Delta x) \right)} \tag{5.42}$$

and $W(m\Delta x,t) = (\rho\Delta x)^{-1} \sum_{k \in \mathcal{N}(m\Delta x)} W_k(t)$. Thus, $\langle dW(m\Delta x,t) \rangle = 0$ and

$$\begin{aligned} \langle dW(m\Delta x,t) dW(n\Delta x,t) \rangle &= \frac{1}{(\rho\Delta x)^2} \sum_{k \in \mathcal{N}(m\Delta x)} \sum_{l \in \mathcal{N}(n\Delta x)} \langle dW_k(t) dW_l(s) \rangle \\ &= \frac{1}{\rho \Delta x} \delta_{m,n} \delta(t-s) dt ds. \end{aligned} \tag{5.43}$$

Finally, setting $x = m\Delta x, y = n\Delta x$ and taking the continuum limit $\Delta x \to 0$ with $\rho^{1/2} W(m\Delta x,t) \to W(x,t)$, $\rho w(m\Delta x, n\Delta x) \to w(x,y)$ and $A(m\Delta x,t) \to A(x,t)$, we obtain a neural field Langevin equation of the form (5.27), except that now the multiplicative noise term is nonlocal:

$$g_0 A(x,t) \to \rho^{-1/2} \sqrt{A(x,t) + F\left(\int_{-\infty}^{\infty} w(x,y) A(y,t) dy \right)}. \tag{5.44}$$

We conclude that under the Langevin and local mean field approximations, the master equation reduces to a stochastic neural field equation with nonlocal multiplicative noise, which in the thermodynamic limit $N \to \infty$ or $\varepsilon \to 0$ reduces to the deterministic neural field equation (5.1). Note, however, that in contrast to the previous examples, the multiplicative noise is Ito rather than Stratonovich.

[1] Note that equation (5.40) would be exact in the case of additive noise under the local homogeneity assumption for the synaptic weights. However, performing the local averaging with respect to $k \in \mathcal{N}(m\Delta x)$ in the case of multiplicative noise is nontrivial. At the very least, some form of perturbation expansion in ε would be needed in order to determine corrections to the mean field approximation. The issue of local population averaging has been addressed in some detail within the context of spatially discrete versions of equation (1.13) with additive noise, where the nonlinearity F appears inside the sum over weights [33].

Previously, Buice and Cowan [18] have used path integral methods and renormalization group theory to establish that a master equation formulation of neural field theory that evolves according to equation (5.1) in the deterministic limit belongs to the universality class of directed percolation, and consequently exhibits power law behaviour suggestive of many measurements of spontaneous cortical activity *in vitro* and *in vivo* [5, 61]. One crucial assumption of their theory is that the neural field supports a zero absorbing state, which holds provided that the rate function satisfies $F(0) = 0$. In light of our current study, we see that another feature of this master equation is that the underlying deterministic mean field equation (5.1) supports a propagating pulled front. Such a front is particularly sensitive to the effects of fluctuations in the leading edge of the front. This has important implications for front solutions of the underlying master equation, where discreteness effects (in space and in the number of active neurons) play a crucial role within the leading edge of the front. That is, there is a fundamental quantum of activity within a local population consisting of a single active neuron, that is, $A = 1/N$. In other words, there is an effective lower cut–off within the leading edge of the front. In the case of nonlinear reaction diffusion equations, such discreteness effects have been shown to have a significant effect on the asymptotic velocity of a pulled front [59]. It would be interesting to explore how such results carry over to neural field master equations with nonlocal interactions.

Chapter 6

Conclusions and Perspectives

In this thesis we have analysed neural field models of binocular rivalry waves in the primary visual cortex. In chapter 2 we introduced a deterministic continuum field model of binocular rivalry. Formulating the problem in this way allowed us to obtain several interesting results analytically. In particular, we showed that a symmetry breaking mechanism is necessary for wave propagation to occur, in that the neural fields for the left and right eye neurons have to be different on the time scales where a wave is propagating. We were also able to identify a possible biological substrate for this symmetry breaking in synaptic depression, though we would expect that other forms of slow adaptation such as spike frequency adaptation would also be sufficient. As a result of incorporating this symmetry breaking mechanism we were able to recover wave speeds similar to those seen in experiments. Furthermore, dependence between experimental variables such as wave speed and stimulus contrast was also exhibited by our model. However, it was not possible to analyse noise at this stage and it was necessary to rely on computer simulation to explore the effects of noise.

In order to better understand noise a one dimensional neural field equation with multiplicative noise was developed in chapter 3 using techniques adapted from PDE theory. We found that for a freely propagating front the wave position undergoes a drift-diffusion process with variance growing as t. On the other hand, noise affected a similar neural field equation whose input represented a moving stimulus in a qualitatively different manner. In this case, the position of the front was found to undergo an Ornstein-Uhlenbeck process where the variance saturates as $t \to \infty$ which could be seen as an example of biological robustness.

In chapter 4 a stochastic extension of the binocular rivalry model of chapter 2 was analysed using the techniques developed in chapter 3. It was possible to show that noise has a very significant

impact on wave propagation in the case of noisy activity variables, where once again they were found to undergo a drift-diffusion process. This implies that the first passage time for waves hitting a fixed barrier is inverse Gaussian. Moreover, a numerical study of noise in the adaptation variables found that the distribution is also inverse Gaussian. Thus the key result of this is a fairly general prediction which could be experimentally testable and lead to further refinements of the theory!

In future work on deterministic binocular rivalry it would be interesting to extend the model presented in chapter 2 to consider a more realistic topology of V1. As mentioned in the introduction V1 actually has neurons which respond to each possible orientation for every point in the visual field. Thus it would make sense to consider a model on $\mathbb{R} \times S^1$ where there is a circle of orientations for each point on a line. It would then be possible to consider questions such as how wave speed varies with orientation which is an experimentally observed variable [44, 45] and lead to further refinements of the model. There are also several stochastic variables in binocular rivalry which are as yet unexplained. Firstly it has been shown in experiment that there is an optimal trigger period which is most likely to induce a travelling wave using the experimental technique from section 1.1.2. This is a form of first passage time problem but not for the wave itself, rather for the probability of the depression variables being in an acceptable state. It is the author's opinion that it would likely require results for first passage times for a line of Ornstein-Uhlenbeck variables, given that the first passage time of a single Ornstein-Uhlenbeck process was only recently elucidated this is likely a complex and interesting problem. Second, experiments on travelling waves on oriented grating stimuli being able to cross a gap have shown that this is a stochastic variable and we would hope that it is possible to extend the analysis of chapter 3 to situations involving non-constant underlying orientation such as this one. Finally, travelling fronts are not the only form of travelling wave possible in neural systems though they are common in binocular rivalry. Studies of wave propagation on in-vitro disinhibited cortical slices find that the waves often take the form of pulses rather than fronts, so it is important for techniques to be developed to handle this kind of problem as well.

Bibliography

[1] L. F. Abbott, J. A. Varela, K. Sen, and S. B. Nelson. Synaptic depression and cortical gain control. *Science*, 275(5297):221–224, 1997.

[2] S. Amari. Dynamics of pattern formation in lateral-inhibition type neural fields. *Biological cybernetics*, 27(2):77–87, 1977.

[3] A. Angelucci, J. B. Levitt, E. J. S. Walton, J.-M Hupe, J. Bullier, and J. S. Lund. Circuits for local and global signal integration in primary visual cortex. *The Journal of Neuroscience*, 22(19):8633–8646, 2002.

[4] J. Armero, J. Casademunt, L. Ramirez-Piscina, and J. M. Sancho. Ballistic and diffusive corrections to front propagation in the presence of multiplicative noise. *Physical Review E*, 58(5):5494, 1998.

[5] J. M. Beggs and D. Plenz. Neuronal avalanches are diverse and precise activity patterns that are stable for many hours in cortical slice cultures. *The Journal of neuroscience*, 24(22):5216–5229, 2004.

[6] R. Ben-Yishai, R. L. Bar-Or, and H. Sompolinsky. Theory of orientation tuning in visual cortex. *Proceedings of the National Academy of Sciences*, 92(9):3844–3848, 1995.

[7] H. Berestycki, G. Nadin, B. Perthame, and L. Ryzhik. The non-local fisher–kpp equation: travelling waves and steady states. *Nonlinearity*, 22(12):2813, 2009.

[8] R. Blake and N. K. Logothetis. Visual competition. *Nature Reviews Neuroscience*, 3(1):13–21, 2002.

[9] G. G. Blasdel. Orientation selectivity, preference, and continuity in monkey striate cortex. *The Journal of Neuroscience*, 12(8):3139–3161, 1992.

[10] C. A. Brackley and M. S. Turner. Random fluctuations of the firing rate function in a continuum neural field model. *Physical Review E*, 75(4):041913, 2007.

[11] P. C. Bressloff. Traveling fronts and wave propagation failure in an inhomogeneous neural network. *Physica D: Nonlinear Phenomena*, 155(1):83–100, 2001.

[12] P. C. Bressloff. Stochastic neural field theory and the system-size expansion. *SIAM Journal on Applied Mathematics*, 70(5):1488–1521, 2009.

[13] P. C. Bressloff. Metastable states and quasicycles in a stochastic wilson-cowan model of neuronal population dynamics. *Physical Review E*, 82(5):051903, 2010.

[14] P. C. Bressloff. Spatiotemporal dynamics of continuum neural fields. *Journal of Physics A: Mathematical and Theoretical*, 45(3):033001, 2011.

[15] P. C. Bressloff, J. D. Cowan, M. Golubitsky, P. J. Thomas, and M. C. Wiener. Geometric visual hallucinations, euclidean symmetry and the functional architecture of striate cortex. *Philosophical Transactions of the Royal Society of London. Series B: Biological Sciences*, 356(1407):299–330, 2001.

[16] P. C. Bressloff and M. A. Webber. Front propagation in stochastic neural fields. *SIAM Journal on Applied Dynamical Systems*, 11(2):708–740, 2012.

[17] P. C. Bressloff and M. A. Webber. Neural field model of binocular rivalry waves. *Journal of computational neuroscience*, 32(2):233–252, 2012.

[18] M. A. Buice and J. D. Cowan. Field-theoretic approach to fluctuation effects in neural networks. *Physical Review E*, 75(5):051919, 2007.

[19] M. A. Buice, J. D. Cowan, and C. C. Chow. Systematic fluctuation expansion for neural network activity equations. *Neural computation*, 22(2):377–426, 2010.

[20] F. S. Chance, S. B. Nelson, and L. F. Abbott. Synaptic depression and the temporal response characteristics of v1 cells. *The Journal of neuroscience*, 18(12):4785–4799, 1998.

[21] S. Coombes. Waves, bumps, and patterns in neural field theories. *Biological Cybernetics*, 93(2):91–108, 2005.

[22] S. Coombes. Neural fields. *Scholarpedia*, 1(6):1373, 2006.

[23] S. Coombes and C. R. Laing. Pulsating fronts in periodically modulated neural field models. *Physical Review E*, 83(1):011912, 2011.

[24] S. Coombes, G. J. Lord, and M. R. Owen. Waves and bumps in neuronal networks with axo-dendritic synaptic interactions. *Physica D: Nonlinear Phenomena*, 178(3):219–241, 2003.

[25] S. Coombes and M. R. Owen. Evans functions for integral neural field equations with heaviside firing rate function. *SIAM Journal on Applied Dynamical Systems*, 3(4):574–600, 2004.

[26] F. de Pasquale, J. Gorecki, and J. Popielawski. On the stochastic correlations in a randomly perturbed chemical front. *Journal of Physics A: Mathematical and General*, 25(2):433, 1992.

[27] U. Ebert and W. van Saarloos. Front propagation into unstable states: universal algebraic convergence towards uniformly translating pulled fronts. *Physica D: Nonlinear Phenomena*, 146(1):1–99, 2000.

[28] G. B. Ermentrout. Neural networks as spatio-temporal pattern-forming systems. *Reports on progress in physics*, 61(4):353, 1998.

[29] G. B. Ermentrout, J. Z. Jalics, and J. E. Rubin. Stimulus-driven traveling solutions in continuum neuronal models with a general smooth firing rate function. *SIAM Journal on Applied Mathematics*, 70(8):3039–3064, 2010.

[30] G. B. Ermentrout and J. B. McLeod. Existence and uniqueness of travelling waves for a neural network. *Proceedings of the Royal Society of Edinburgh: Section A Mathematics*, 123(03):461–478, 1993.

[31] A. A. Faisal, L. P. J. Selen, and D. M. Wolpert. Noise in the nervous system. *Nature Reviews Neuroscience*, 9(4):292–303, 2008.

[32] C. P. Fall, T. J. Lewis, and J. Rinzel. Background-activity-dependent properties of a network model for working memory that incorporates cellular bistability. *Biological cybernetics*, 93(2):109–118, 2005.

[33] O. Faugeras, J. Touboul, and B. Cessac. A constructive mean-field analysis of multi-population neural networks with random synaptic weights and stochastic inputs. *Frontiers in computational neuroscience*, 3, 2009.

[34] D. Ferster and K. D. Miller. Neural mechanisms of orientation selectivity in the visual cortex. *Annual review of neuroscience*, 23(1):441–471, 2000.

[35] R. A. Fisher. The wave of advance of advantageous genes. *Annals of Eugenics*, 7(4):355–369, 1937.

[36] S. E. Folias and P. C. Bressloff. Stimulus-locked traveling waves and breathers in an excitatory neural network. *SIAM journal on Applied Mathematics*, 65(6):2067–2092, 2005.

[37] R. Fox and F. Rasche. Binocular rivalry and reciprocal inhibition. *Perception & Psychophysics*, 5(4):215–217, 1969.

[38] J. García-Ojalvo and J. M. Sancho. External fluctuations in a pattern-forming instability. *Physical Review E*, 53(6):5680, 1996.

[39] C. W. Gardiner. *Handbook of stochastic methods*. Springer Berlin, 1985.

[40] S. A. Gourley. Travelling front solutions of a nonlocal fisher equation. *Journal of mathematical biology*, 41(3):272–284, 2000.

[41] D. H. Hubel and T. N. Wiesel. Receptive fields, binocular interaction and functional architecture in the cat's visual cortex. *The Journal of physiology*, 160(1):106, 1962.

[42] D. H. Hubel and T. N. Wiesel. Functional architecture of macaque monkey visual cortex. In *Proc. R. Soc. Lond. B*, volume 198, pages 1–59, 1977.

[43] K. Jacobs. *Stochastic Processes for Physicists: Understanding Noisy Systems*. Cambridge University Press, 2010.

[44] M. Kang, D. J. Heeger, and R. Blake. Periodic perturbations producing phase-locked fluctuations in visual perception. *Journal of vision*, 9(2), 2009.

[45] M. Kang, S. Lee, J. Kim, D. J. Heeger, and R. Blake. Modulation of spatiotemporal dynamics of binocular rivalry by collinear facilitation and pattern-dependent adaptation. *Journal of vision*, 10(11), 2010.

[46] L. C. Katz, C. D. Gilbert, and T. N. Wiesel. Local circuits and ocular dominance columns in monkey striate cortex. *The Journal of Neuroscience*, 9(4):1389–1399, 1989.

[47] Z. P. Kilpatrick and P. C. Bressloff. Binocular rivalry in a competitive neural network with synaptic depression. *SIAM Journal on Applied Dynamical Systems*, 9(4):1303–1347, 2010.

[48] C. R. Laing and C. C. Chow. A spiking neuron model for binocular rivalry. *Journal of computational neuroscience*, 12(1):39–53, 2002.

[49] S. Lee and R. Blake. V1 activity is reduced during binocular rivalry. *Journal of Vision*, 2(9), 2002.

[50] S. Lee, R. Blake, and D. J. Heeger. Traveling waves of activity in primary visual cortex during binocular rivalry. *Nature neuroscience*, 8(1):22–23, 2004.

[51] D. A. Leopold and N. K. Logothetis. Activity changes in early visual cortex reflect monkeys' percepts during binocular rivalry. *Nature*, 379(6565):549–553, 1996.

[52] R. Llinas. Neuron. *Scholarpedia*, 3(8):1490, 2008.

[53] G. J. Lord and V. Thümmler. Computing stochastic traveling waves. *SIAM Journal on Scientific Computing*, 34(1):B24–B43, 2012.

[54] P. N. Loxley and P. A. Robinson. Soliton model of competitive neural dynamics during binocular rivalry. *Physical review letters*, 102(25):258701, 2009.

[55] A. S. Mikhailov, L. Schimansky-Geier, and W. Ebeling. Stochastic motion of the propagating front in bistable media. *Physics Letters A*, 96(9):453–456, 1983.

[56] E. A. Novikov. Functionals and the random-force method in turbulence theory. *Sov. Phys. JETP*, 20(5):1290–1294, 1965.

[57] P. L. Nunez. The brain wave equation: A model for the eeg. *Mathematical Biosciences*, 21(3):279–297, 1974.

[58] K. Pakdaman, M. Thieullen, and G. Wainrib. Fluid limit theorems for stochastic hybrid systems with application to neuron models. *Advances in Applied Probability*, 42(3):761–794, 2010.

[59] D. Panja. Effects of fluctuations on propagating fronts. *Physics Reports*, 393(2):87–174, 2004.

[60] D. J. Pinto and G. B. Ermentrout. Spatially structured activity in synaptically coupled neuronal networks: Ii. lateral inhibition and standing pulses. *SIAM Journal on Applied Mathematics*, 62(1):226–243, 2001.

[61] D. Plenz and T. C. Thiagarajan. The organizing principles of neuronal avalanches: cell assemblies in the cortex? *Trends in neurosciences*, 30(3):101–110, 2007.

[62] A. Polonsky, R. Blake, J. Braun, and D. J. Heeger. Neuronal activity in human primary visual cortex correlates with perception during binocular rivalry. *Nature neuroscience*, 3:1153–1159, 2000.

[63] A. Rocco, U. Ebert, and W. van Saarloos. Subdiffusive fluctuations of "pulled" fronts with multiplicative noise. *Physical Review E*, 62(1):R13, 2000.

[64] F. Sagués, J. M. Sancho, and J. García-Ojalvo. Spatiotemporal order out of noise. *Reviews of Modern Physics*, 79(3):829, 2007.

[65] B. Sandstede. Evans functions and nonlinear stability of traveling waves in neuronal network models. *International Journal of Bifurcation and Chaos*, 17(08):2693–2704, 2007.

[66] L. Schimansky-Geier, A. S. Mikhailov, and W. Ebeling. Effect of fluctuation on plane front propagation in bistable nonequilibrium systems. *Annalen der Physik*, 495(4-5):277–286, 1983.

[67] A. Shpiro, R. Curtu, J. Rinzel, and N. Rubin. Dynamical characteristics common to neuronal competition models. *Journal of neurophysiology*, 97(1):462–473, 2007.

[68] A. Shpiro, R. Moreno-Bote, N. Rubin, and J. Rinzel. Balance between noise and adaptation in competition models of perceptual bistability. *Journal of computational neuroscience*, 27(1):37–54, 2009.

[69] L. C. Sincich and G. G. Blasdel. Oriented axon projections in primary visual cortex of the monkey. *The Journal of Neuroscience*, 21(12):4416–4426, 2001.

[70] F. K. Skinner, N. Kopell, and E. Marder. Mechanisms for oscillation and frequency control in reciprocally inhibitory model neural networks. *Journal of computational neuroscience*, 1(1-2):69–87, 1994.

[71] W. R. Softky and C. Koch. The highly irregular firing of cortical cells is inconsistent with temporal integration of random epsps. *The Journal of Neuroscience*, 13(1):334–350, 1993.

[72] A. L. Taylor, G. W. Cottrell, and W. B. Kristan Jr. Analysis of oscillations in a reciprocally inhibitory network with synaptic depression. *Neural computation*, 14(3):561–581, 2002.

[73] F. Tong and S. A. Engel. Interocular rivalry revealed in the human cortical blind-spot representation. *Journal of Vision*, 1(3):130–130, 2001.

[74] F. Tong, K. Nakayama, J. T. Vaughan, and N. Kanwisher. Binocular rivalry and visual awareness in human extrastriate cortex. *Neuron*, 21(4):753–759, 1998.

[75] R. B. Tootell, M. S. Silverman, E. Switkes, and R. L. De Valois. Deoxyglucose analysis of retinotopic organization in primate striate cortex. *Science*, 218(4575):902–904, 1982.

[76] R. B. Tootell, E. Switkes, M. S. Silverman, and S. L. Hamilton. Functional anatomy of macaque striate cortex. ii. retinotopic organization. *The Journal of Neuroscience*, 8(5):1531–1568, 1988.

[77] J. Touboul. Propagation of chaos in neural fields. *arXiv preprint arXiv:1108.2414*, 2011.

[78] W. van Saarloos. Front propagation into unstable states. *Physics reports*, 386(2):29–222, 2003.

[79] J. A. Varela, K. Sen, J. Gibson, J. Fost, L. F. Abbott, and S. B. Nelson. A quantitative description of short-term plasticity at excitatory synapses in layer 2/3 of rat primary visual cortex. *The Journal of neuroscience*, 17(20):7926–7940, 1997.

[80] M. A. Webber and P. C. Bressloff. The effects of noise on binocular rivalry waves: a stochastic neural field model. *Journal of Statistical Mechanics: Theory and Experiment*, 2013(03):P03001, 2013.

[81] H. R. Wilson, R. Blake, and S. Lee. Dynamics of travelling waves in visual perception. *Nature*, 412(6850):907–910, 2001.

[82] H. R. Wilson and J. D. Cowan. A mathematical theory of the functional dynamics of cortical and thalamic nervous tissue. *Biological Cybernetics*, 13(2):55–80, 1973.

[83] L. Zhang. On stability of traveling wave solutions in synaptically coupled neuronal networks. *Differential and Integral Equations*, 16(5):513–536, 2003.